



leti
cea tech

TECHNOLOGY
RESEARCH
INSTITUTE

2017

Annual research report

OPTICS AND PHOTONICS



TECHNOLOGY
RESEARCH
INSTITUTE

Committed to Innovation, Leti Creates Differentiating Solutions for its Industrial Partners.

Leti is a research institute of CEA Tech and a recognized global leader in miniaturization technologies. Leti's teams are focused on developing solutions that will enable future information and communication technologies, health and wellness approaches, clean and safe energy production and recovery, sustainable transport, space exploration and cybersecurity.

For 50 years, the institute has built long-term relationships with its industrial partners, tailoring innovative and differentiating

solutions to their needs. Its entrepreneurship programs have sparked the creation of 64 start-ups. Leti and its industrial partners work together through bilateral projects, joint laboratories and collaborative research programs.

Leti maintains an excellent scientific level by working with the best research teams worldwide, establishing partnerships with major research technology organizations and academic institutions. Leti is also a member of the Carnot Institutes network*.

*Carnot Institutes network: French network of 34 institutes serving innovation in industry.



CEA Tech is the technology research branch of the French Alternative Energies and Atomic Energy Commission (CEA), a key player in research, development and innovation in defense & security, nuclear energy, technological research for industry and fundamental physical and life sciences.

www.cea.fr/english

Leti at a glance

€315
million budget

800
publications per year

ISO 9001
certified since 2000

Founded in

1967

Based in

France (Grenoble)
with offices in the

USA (Silicon Valley)
and **Japan** (Tokyo)

350
industrial partners

1,900
researchers

2,760
patents in portfolio

91,500
sq. ft. cleanroom space,
8" & 12" wafers

64
startups created



2017

Annual research report

OPTICS AND PHOTONICS



Within CEA Tech and Leti, Optics and Photonics activities are focused principally on big industrial markets of photonics: all-wavelength imaging (visible, infrared, THz), information displays, solid-state lighting, optical data communications, optical environmental sensors.

The R&D projects are performed with industrial and academic partners. The industrial partners of the Optics and Photonics division range from SME to large international companies. The projects are merging fundamental aspects with advanced technological and industrial developments; nano-sciences are interweaved with material sciences, optics, electronics and micro & nano-fabrication.



CONTENTS

EDITO	05
KEY FIGURES	06
SCIENTIFIC ACTIVITY	07
01 / Infra-red imaging: cooled detectors	09
02 / Infra-red imaging: room-t° detectors	15
03 / Visible imaging	21
04 / Silicon photonics	27
05 / Optical environmental sensors	35
06 / Solid-state lighting (LEDs)	41
07 / Display components	45
08 / Optics and Nanophotonics	53
09 / PhD Degrees awarded	57

ÉDITO



Ludovic POUPINET
Head of Optics and
Photonics Division

Optics and Photonics Division (DOPT) of Leti fosters employment in France and Europe by developing innovative photonic components.

We see miniaturization and integration as the main driving factors to reach this target. We help our industrial partners to decrease the cost, to improve the performances and to diversify the functionalities of their products.

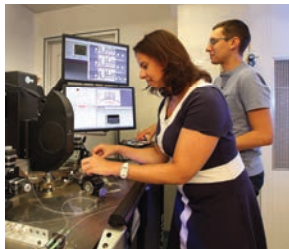
DOPT is focused on various topics such as visible, infrared and THz imaging sensors as well as integrated photonic components, optical gas sensors and light emitting arrays, displays and smart lighting. In each area, DOPT, with its 300 staff members, concentrates long-term expertise, up-to-date clean rooms and equipment and dedicated characterization benches. 90% of our funding is obtained through one-to-one or collaborative projects, both with academic and industrial partners. The high quality of our partners is also our strength.

Staying at the leading edge of applied photonic research requires a deep understanding of product and application needs in terms of performance, cost and functions, as well as an ability to introduce new concepts in our process flows. It also relies on our ability to set-up new optical benches for in depth characterization or for proof of concepts validation.

I hope that reading this report will make you want to know more about us, meet us at conferences, forums or Leti events, join us as a researcher or PhD student or, of course, build fruitful collaborations on research topics tackling the microscopic behavior of photons using state-of-the-art industry compatible facilities.

Have a nice reading!

Key figures



215 permanent researchers

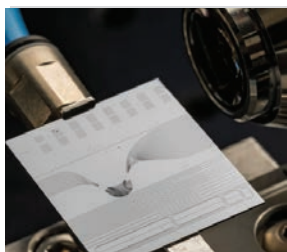
40 PhD students and Post-docs

50 CEA experts: with **4** directors of research
and **2** international experts



150 publications in 2017 including

65 papers in peer reviewed journals



90 patents filed in 2017

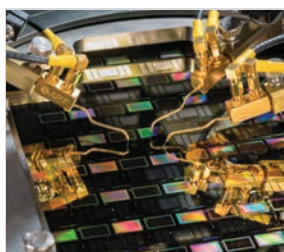
500 patents portfolio with about

20% under licensing contract



Dedicated clean rooms for III-V and II-VI materials on versatile substrate geometries up to 150 mm

Access to Leti clean rooms through numerous photonic fab processing modules in 200 and 300 mm format



Optics and opto-electronics characterization facilities

Advanced means of modeling and simulation

Scientific activity

Awards

François TEMPLIER received a “best paper award” of the Journal of the Society of Information Display (JSID) for “GaN-based emissive microdisplays: A very promising technology for compact, ultra-high brightness display systems”



Badhise BEN BAKIR and Thomas FERROTTI received a “best paper award” at the International Conference on Solid State Devices and Materials (SSDM), for the design and the tests of a 1,3 μ m hybrid III-V on Silicon Transmitter operating at 25Gb/s

Divya TANEJA received the “Student traveler award” at the Electronic Components and Technology Conference (ECTC 2017) for the paper « Cu-SnAg Interconnects Evaluation for the Assembly at 10 μ m and 5 μ m Pitch”

Conference and workshop organization

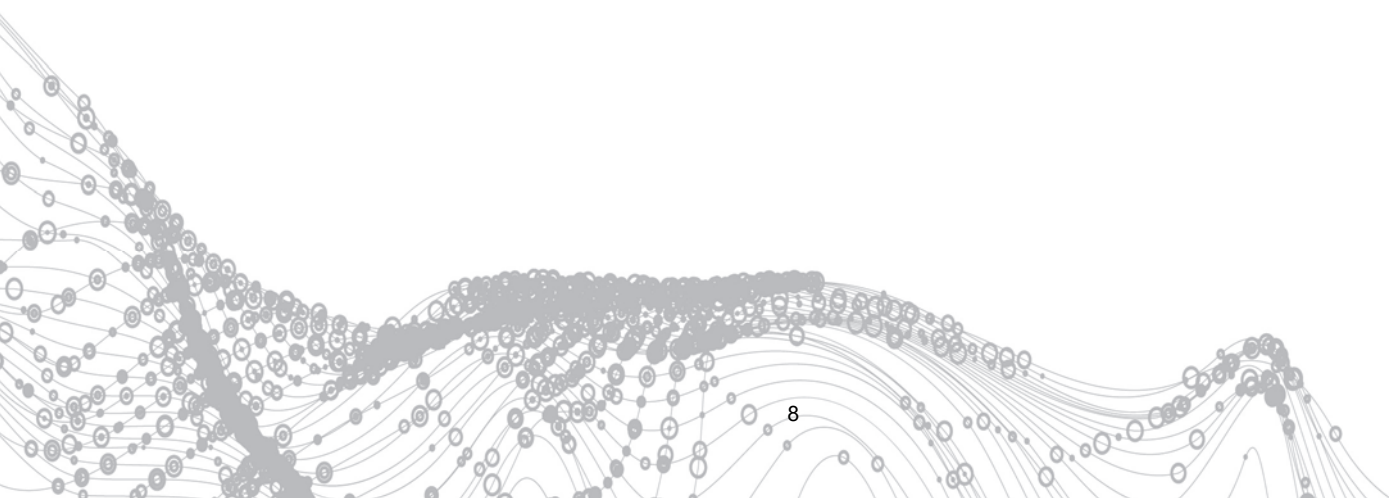
Tony MAINDRON: the RAFALD workshop on “Atomic Layer Deposition (ALD) techniques” (Montpellier, France)

Guy FEUILLET: at the “Int. Conference on Nitrides semiconductors” (ICNS, Strasbourg, France)

Book

Sylvie MENEZO: chapter of the book “Optical Interconnects for Data Centers », Woodhead Publishing Series in Electronic and Optical Materials, Elsevier







O1

IR IMAGING: COOLED

- **Internal strain in HgCdTe photodetectors**
- **Intensity-dependent photoluminescence decay in HgCdTe**
- **Dark current in HgCdTe photodetectors**

MICRO-LAUE INVESTIGATION OF INTERNAL STRAIN IN HgCdTe PHOTODIODES

AUTHORS:

A.Tuaz, P.Ballet, X.Biquard¹ and F.Rieutord (CEA INAC)

ABSTRACT:

White beam micro-Laue has been used at ESRF to investigate bi-axial strain profiles in HgCdTe/CdZnTe structures. In particular the effect of alloy composition variation induced lattice mismatch in multilayer stacks or diffused interfaces has been studied. Through two different examples we show that microLaue can be used to very accurately track small diffraction peak displacements allowing for extracting strain profiles with a very good precision and a 200nm in-depth resolution.

SCIENTIFIC COLLABORATIONS: ¹ CEA-INAC : Institute for Nanoscience and Cryogenics, Grenoble, France

Context and Challenges

Internal strain in HgCdTe photodiodes is generally considered as a prominent source of extended defects via lattice relaxation, and its origin can be multiple resulting from epitaxial misfit, annealing induced composition interdiffusion, or technological processing. While macroscopic manifestation of strain build-up can be related to device performance, its microscopic determination over the range of an interface and within large thickness layers or multilayer stacks requires the sub-micronic resolution of extremely focused white X-ray beams only available at synchrotron radiation facilities.

Main Results

Here we propose to demonstrate the ability of Laue micro-diffraction to resolve low strain gradients (in the 10^{-4} range) over large thickness layers with a spatial resolution of about 200nm. We have conducted Laue experiments with a 300nm diameter white beam probe using the micro-diffraction setup of the French CRG beamline BM32 at the European Synchrotron Radiation Facility (ESRF). We already demonstrated the ability of this setup to spatially resolve lattice deformation induced by processing steps in HgCdTe [1]. This time we focus our analysis on the extraction of biaxial strain along the growth direction in molecular beam epitaxy grown HgCdTe/CdZnTe structures, and we correlate our results with the evolution of the alloy fraction, either imposed by growth or induced by annealing.

The first example is the study of a diffused HgCdTe/CdZnTe interface after annealing at about 400°C. The measured strain deduced from the diffraction peak displacement when crossing the interface is displayed on Figure1 together with the calculation of this strain component based solely upon the lattice parameter variation due to alloy composition variation extracted from SIMS data.

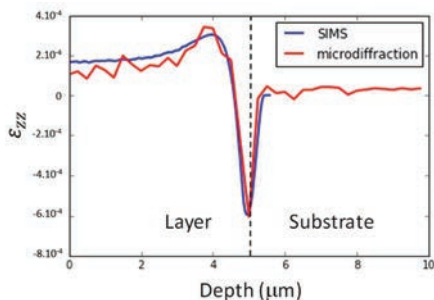


Figure 1: out-of-plane bi-axial stress extracted from microdiffraction measurements (red) compared to the expected value deduced from alloy composition diffusion at the interface diffusion (blue).

Microdiffraction and diffusion-derived strain data fully match over the substrate-layer interface demonstrating the ability of this technique to provide quantitative and spatially resolved strain values in quasi lattice-matched systems.

The second example is a more complex dual-band structure made of several HgCdTe layers of different alloy composition. The structural and compositional investigation is here made through energy dispersive X-ray (EDX) in scanning tunnelling electron microscopy mode (STEM) : Figure 2, showing in reddish contrast the localization of the cadmium-rich layers (substrate-barrier-cap) and the superposition of the extracted cadmium profile with the out-of-plane stress extracted from micro-Laue. Again, the correlation is striking, thus demonstrating that the strain is mostly related to lattice parameter variation induced by composition changes throughout the entire stack. Please note that we logically measure zero strain in the lowest cadmium concentration layer because the zinc content in the substrate has been set for lattice-matching to that particular layer.

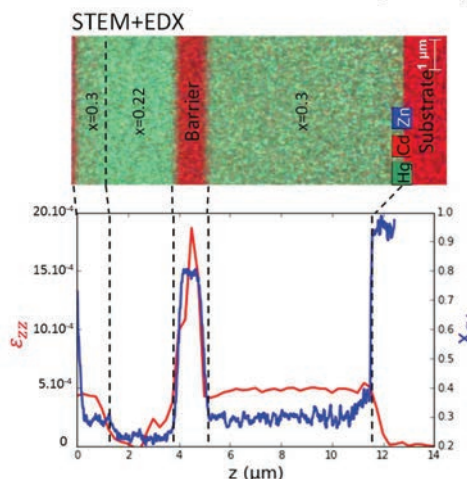


Figure 2: Top: STEM-EDX image of a dual-band stack, bottom: micro-Laue strain (red) and EDX derived cadmium fraction as a function of depth z.

Perspectives

This study demonstrates the validity of the micro-Laue extracted biaxial strain in quasi lattice-matched HgCdTe/CdZnTe structures with a 200nm spatial resolution thus offering the potential for investigating localized strain fields in HgCdTe photodiodes with possible correlation with device performance. Going further, a complete technological device combining epitaxial and processing sources for strain could be successfully investigated.

RELATED PUBLICATIONS:

[1] A.Tuaz, P.Ballet, X.Biquard and F.Rieutord, Micro-diffraction investigation of localized strain in mesa-etched HgCdTe photodiodes, J. Electron. Mater.46, 5442 (2017)

LIGHT INJECTION LEVEL DEPENDENT PHOTOLUMINESCENCE DECAY LIFETIME MEASUREMENTS IN SEMICONDUCTORS FOR IR DETECTION AND EMISSION

AUTHORS:

J. Rothman, B. Delacourt, P. Bleuett

ABSTRACT:

A photoluminescence decay (PLD) measurement set-up have been developed to measure the lifetime of minority carriers in small band-gap semi-conductors that are elaborated for infra-red applications. The set-up uses original HgCdTe avalanche photodiodes (APDs), manufactured CEA/Leti, to detect the temporal variation of the photoluminescence signal down to the low injection regime even in samples with low doping levels and up to wavelengths of 5.6 μm . This has enabled to study the PLD signal as a function of the injection level in small gap semiconductor. The analysis of this variation improve the separation of the different contributions to the recombination mechanism in the samples and our understanding of the fundamental limits in terms of dark current and operating temperature.

Context and Challenges

The understanding and quantitative calibration of the generation and recombination mechanisms, that govern the minority carrier lifetime, are essential for the optimization of the performance of semiconductor devices. In particular, a long lifetime at relatively high doping levels is essential to minimize the dark current and/or to increase the operating temperature in infrared photo-detectors, which is a main driver to reduce the cost, increases the reliability and reduce power consumption of the detectors.

The measurement of the lifetime in semiconductors is difficult as it require a high sensitivity to explore the temporal dependence of a small perturbation of the carrier density that is negligible to the doping level in the sample. This particularly relevant for PLD lifetime measurements in which the low level of emitted photons needs to be extracted from the sample and concentrated onto a fast photodetector. PLD measurement in the IR range is further impeded by the absence of commercially available high sensitivity and fast photodetectors in the IR range which have limited the full exploration of this measurement technique in the past.

Main Results

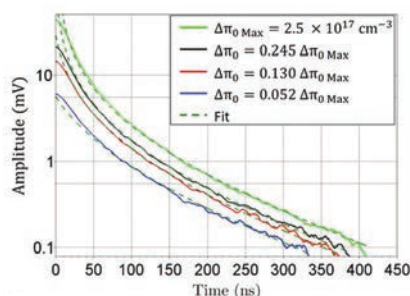


Figure 1: PLD signal at different initial light injection levels, measured on a mercury vacancy doped (V_{Hg}) $\text{Hg}_{0.7}\text{Cd}_{0.3}\text{Te}$ P-type sample with $p=5 \times 10^{15} \text{ cm}^{-3}$ at 80 K.

The development of high sensitivity time resolved HgCdTe APD photo detection modules [1] have allowed us to reach a new level of sensitivity for PLD measurement at IR wavelengths up

to 5.6 μm . This has enabled to explore the PL signals into the low injection regime and enable carrier lifetime measurement even in samples with low carrier densities. In addition, we have shown that the analysis of the evolution of the PLD signal from the high to low injection levels enables to quantitatively separate the Auger, radiative and Shockley-Read-Hall contributions to the carrier recombination by taking into account the expected variation of each contribution as a function of the excess carrier concentration [2]. Figure 1 shows a comparison between measured and calculated injection dependent PLD signal for different initial injection levels on a mercury vacancy (V_{Hg}) doped P-type $\text{Hg}_{0.7}\text{Cd}_{0.3}\text{Te}$. The corresponding variation of the estimated contributions are plotted as a function of temperature in Figure 2. The incertitude of the estimation is presently limited by our knowledge of the photon extraction efficiency in the samples and will be reduced with time. In this sample of more academic interest, the analysis has improved our understanding of the SRH lifetime limitations of the centers associated with V_{Hg} doping and improved our calibration of the Auger generation and recombination model in HgCdTe.

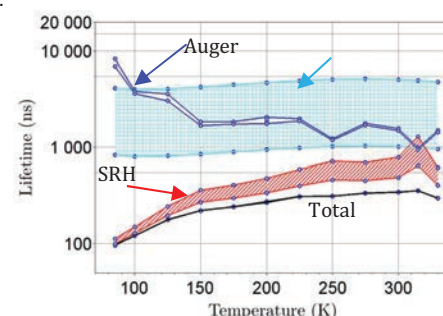


Figure 2: Variation of the estimated contributions to the lifetime in V_{Hg} doped $\text{Hg}_{0.7}\text{Cd}_{0.3}\text{Te}$

Perspectives

The PLD measurement set-up have recently been improved to map the lifetime on wafers during the processing of the photodiodes. It is presently used to optimize the diodes in all projects that aim to increase the operating temperature of the detectors. The set-up will be optimized to achieve spectral and sub-pixel spatial resolution. We also intend to explore its use for other applications of time resolved IR microscopy, such as biology or surface chemistry.

RELATED PUBLICATIONS:

- 1) J. Rothman, E. de Borniol, J. Abergel, G. Lasfargues, B. Delacourt, A. Dumas, F. Gibert, O. Boulade, X. Lefoule, "HgCdTe APDs for low-photon number IR detection", Proc. SPIE 10111, Quantum Sensing and Nano Electronics and Photonics XIV, 1011119, 27 January 2017
- 2) B. Delacourt, P. Ballet, F. Boulard, A. Ferron, L. Bonnefond, T. Pellerin, A. Kerlain, V. Destefanis and J. Rothman, "Temperature and injection dependence of photoluminescence decay in MWIR HgCdTe" *J. Electron. Mater.*, **46**, pp. 6817-6828, 2017

RULE 07 REVISITED FOR LW AND VLW IR DETECTORS

AUTHORS:

N. Baier, O. Gravrand, C. Lobre, O. Boulade, A. Kerlain (SOFRADIR), N. Péré-Laperne (SOFRADIR)

ABSTRACT:

Rule 07 heuristic law is very convenient to describe the dark current for *p-on-n* photodiodes processed on high quality HgCdTe materials. Easy to compute, it is used as a powerful tool for comparison and benchmarking for II-VI manufacturers and III-V compounds competitors but also for agencies to specify the requirements for next generation ground or space instruments. However, Rule 07 law is not based on physic considerations and outside the application range it shows its limits, especially in the LW and VLW bands. An improvement of this rule has been proposed, based on results obtained on detectors from CEA-LETI.

SCIENTIFIC COLLABORATIONS: CEA-IRFU, GIF SUR YVETTE, FRANCE, IPAG (CNRS/Université Grenoble Alpes, France, Centre National d'Etudes Spatiales (CNES) and the European Space Agency (ESA)

Context and Challenges

The hunt for exoplanets has become one of the major challenge for deep space observation within the last decade. For some candidates, further analysis could be performed and particularly on the content of their atmosphere. ECHO and ARIEL ESA missions have been designed to answer this question. But observing cold and faint objects at a long distance from Earth leads to strong requirements: long cutoff wavelength and low dark current, the last one calculated according to Rule 07 law. Improvements of the technological process have been introduced to meet these requirements at low temperature.

Main Results

Different detectors batches have been manufactured to improve a new technological heterojunction process based on HgCdTe liquid phase epitaxy and to verify the gain on performances. The results show that the dark current is in good agreement with Rule 07 law at 78K, but when the temperature decreases, the dark current decreases at a lower rate than Rule 07, following a pure diffusion law [1].

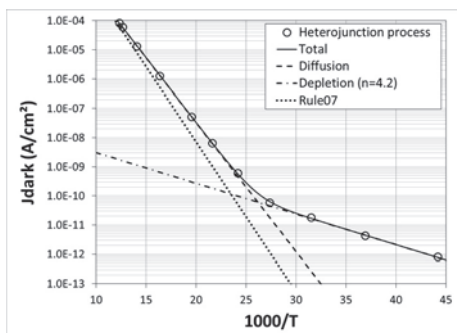


Figure 1: dark current density evolution as a function of temperature, compared with "Rule 07" law and a diffusion-depletion fit.

Despite the good performance of the tested detector, limited by diffusion dark current down to 40K, the requirements could not be reached by one order of magnitude. This underlines the drawback of the use of a convenient but simple law and moreover, outside its application range. It does not reflect the physical behavior of *p-on-n* photodiodes at low temperature.

RELATED PUBLICATIONS:

- [1] Baier N., Cervera C., Gravrand O., Mollard L., Lobre C., Destefanis G., Bourgeois G., Zanatta J.P., Boulade O., Moreau V.: "Latest developments in long-wavelength and very-long-wavelength infrared detection with *p-on-n* HgCdTe" Journal of Electronic Materials 44(9), 3144-3150 (2015).
[2] N. Baier, O. Gravrand, C. Lobre, O. Boulade, A. Kerlain, N. Péré-Laperne : "Rule 07 revisited for LW and VLW" to be published.

The origin of the difference relies in the expression of Rule 07:

$$J = J_0 \exp(C \times E_g(T)/kT)$$

where $C = -1.1624$ according to the reference paper, instead of -1 which corresponds to the physical law of the diffusion dark current. This rule appears to be very accurate to calculate the dark current at 78K on a large range of cutoff wavelengths, which was its main utility, and not the evolution of the dark current with temperature for a given HgCdTe compound.

Using the measurements performed at CEA-LETI and CEA-IRFU on various detectors of different cutoff wavelength, a new rule has been introduced to calculate the dark current of *p-on-n* photodiodes made of HgCdTe [2]. Even if it is partially inspired by the Rule 07, it allows to determine the dark current with a high reliability for a larger range of cutoff wavelength and operating temperature than Rule 07. This rule is less simple the Rule 07 but still easy to compute with only few parameters:

$$J_{diff}(T) = J_0 \exp(-29.936/\lambda_{c@78K}) \exp(-E_g(T)/kT)$$

Its accuracy has been verified on detector from CEA-LETI (with cutoff wavelength from 9.5 to 17.2 μm at 78K) and on measurements published on detectors from other manufacturers.

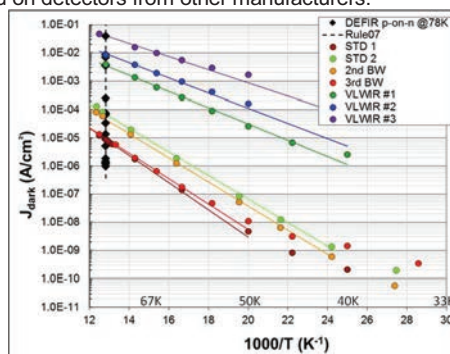
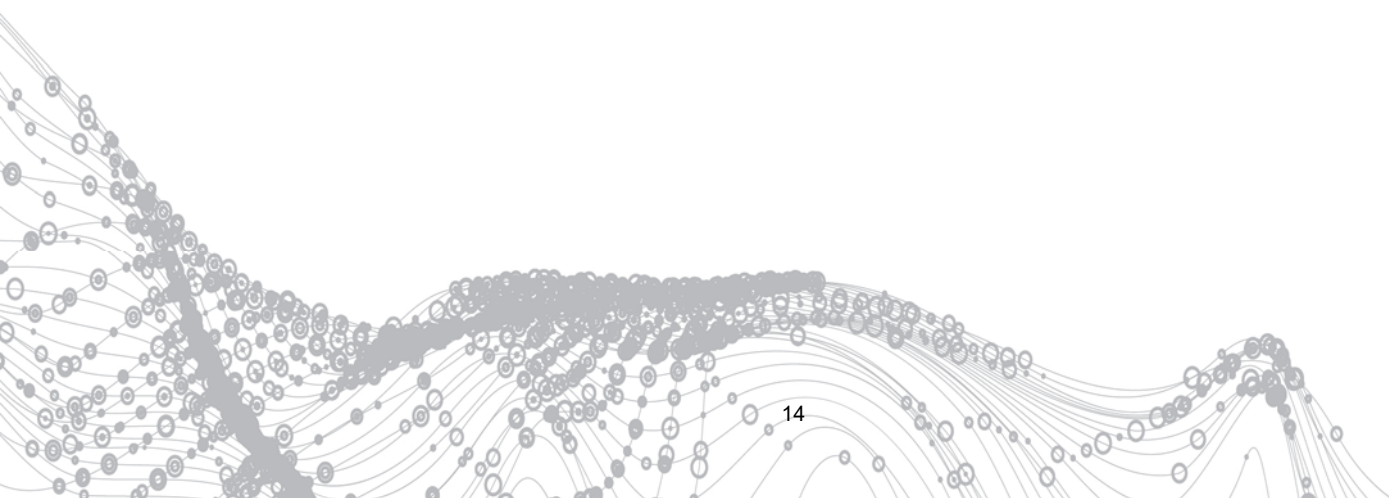
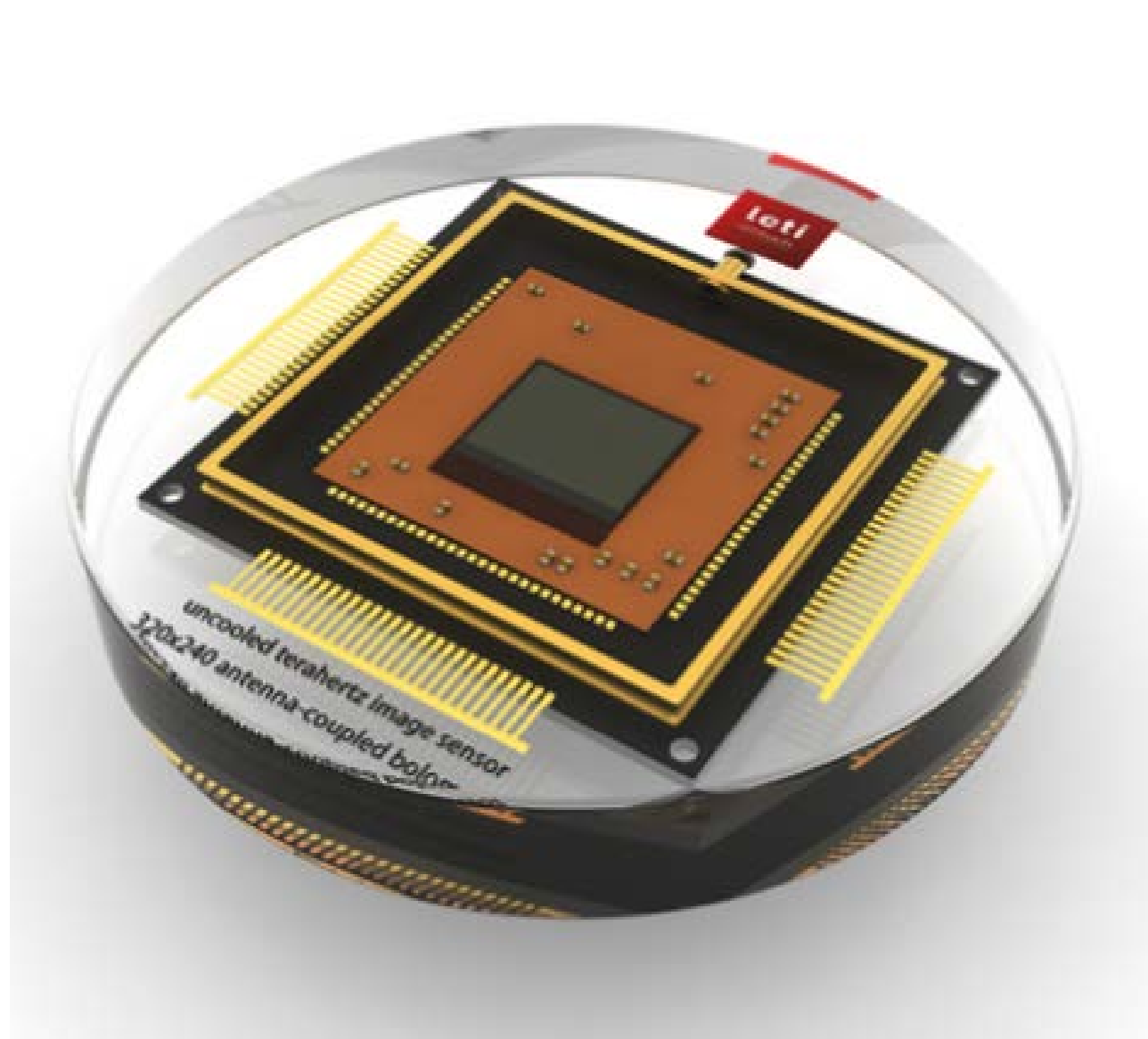


Figure 2: dark current density as a function of temperature for 8 detectors from CEA-LETI and comparison with the new dark current rule.

Perspectives

This new rule, based on measurements performed on detectors from CEA-LETI, brings to IR community a tool to calculate the dark current on a wide range of cutoff wavelengths and temperatures for state-of-the-art *p-on-n* HgCdTe technology.





O2

IR IMAGING: ROOM-T°

- **Electromechanical resonators as thermal imaging sensors**
- **Silicon bolometers as millimeter wave detectors**
- **THz spectroscopy for hydration monitoring of green plants**

12 μm -PITCH ELECTROMECHANICAL RESONATOR FOR THERMAL SENSING

AUTHORS: L. Laurent, J.-J. Yon, J.-S. Moulet (DCOS), M.L. Roukes (CalTech), L. Duraffourg

ABSTRACT:

We have demonstrated a 12 μm pitch nanoelectromechanical resonant infrared sensor with fully integrated capacitive transduction. Low temperature fabrication process was used to manufacture torsional resonators arrays. H-shape legs supporting pixel with 9 μm -long nano-rods and 250 nm \times 30 nm-cross section were designed to provide strong thermal response, with experimental values up to 1024 Hz/nW. A mechanical dynamic range of over 113 dB was obtained, which led to an unprecedented Allan deviation of $\sigma_A = 3 \times 10^{-7}$ at room temperature and 50 Hz noise-bandwidth ($\sigma_A = 1.5 \times 10^{-7}$ over 10 Hz). These features allowed to reach a sensitivity to the 8-12 μm radiations of 27 pW/ $\sqrt{\text{Hz}}$ leading to a noise equivalent temperature difference (NETD) of 2 K for a 50 Hz noise-bandwidth ($\text{NETD} = 1.5 \text{ K}$ at 10 Hz). By both improving the temperature coefficient of frequency of a factor 10 and using a readout electronics at the pixel level, these resonators will lead to a breakthrough for uncooled infrared detectors.

SCIENTIFIC COLLABORATIONS: KAVLI NANOSCIENCE INSTITUTE, CALIFORNIA INSTITUTE OF TECHNOLOGY

Context and Challenges

Over the last 20 years microbolometer has become the most prominent uncooled infrared technology. They operate by converting the radiation-induced heating of a thin membrane in a variation of electrical resistance. Such thermistors are commonly made of a thin film of semiconductor, using mostly Vanadium Oxide (VOX) or amorphous silicon ($\alpha\text{-Si}$). The induced heating effect is advantageously enhanced by achieving a high thermal insulation between the sensor and the substrate. Thermal insulation as high as 200 MK/W has been reported for microbolometers with 12 μm -pixel pitch [5]. Such devices currently exhibit 50mK-noise NETD (F/1 lens, 30Hz frame rate, 300K background) [1]. Nevertheless, in case of excessive radiant power the temperature of the sensing material can increase dramatically leading to a detrimental drift of the thermistor properties. To address this issue, we suggest unique pixel architecture whose arrangement calls for the replacement of the common thermistor by a mechanical nano-resonator designed to be highly sensitive to temperature.

Main Results

Contrary to NEMS approaches usually used to get stable nano resonators, we have chosen a low temperature fabrication process, which is inherited from classical bolometers [2]. The figure 1a) shows structures magnified by scanning electronic microscope (SEM). The microsystem is excited at its first torsion mode using an actuation electrode placed under the plate. An incident infrared electromagnetic wave is absorbed by a thin metallic layer deposited on top of the plate and causes its heating by free carriers Joule effect. Thereby, the temperature rise induces a variation of the torsional resonance frequency that is measured through capacitive signal between the detection electrode and the oscillating plate. A dedicated readout electronics board based on a trans impedance circuit was carefully developed for measuring the tiny capacitance variation ($\sim 30\text{aF}$) compared to both the capacitance at rest ($\sim 0.18\text{fF}$) and the parasitic capacitance ($\sim 1\text{pF}$). Typical electromechanical response with frequency and an AC-actuation voltage V_{AC} (at $V_{pol}=10\text{V}$) is plotted in FIG. 1b). The output voltage at resonance is clearly proportional to V_{AC}^2 [3], [4]. To perform the thermal characterizations, we embed the system in a down-mixed Phase Locked Loop (PLL) to track the resonance frequency change in real-time. The electronics

board with pixels were placed into a home-made vacuum chamber that were illuminated by a black body source.

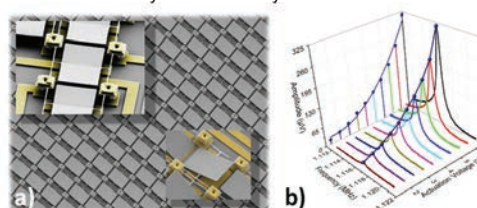


Figure 1. a) Scanning electron microscope (SEM) picture of typical matrix of micro electromechanical pixels - b) electromechanical response according to frequency and actuation voltage

The frequency response to IR incident pulses (26nW-peak) is presented in Fig. 2. A typical experimental thermal response $R_f=720 \text{ W}$ has been extracted from this measurement. From noise measurements, we have estimated a sensitivity to 8-12 μm radiation below 27nW/ $\sqrt{\text{Hz}}$ leading to a NETD of 2 K at 50Hz and NETD=1.5K at 100ms (with a sub-millisecond response time) [1].

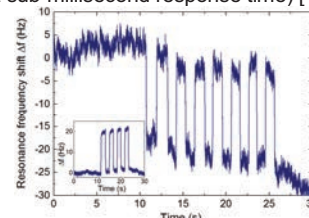


Figure 2. Frequency response. IR illumination corresponds to 26-nW incident power.

Perspectives

We have demonstrated the great potential of high frequency resonant sensor fabricated with a low temperature process dedicated to uncooled infrared imaging. A NEP of 190pW has been measured with our system at 50Hz-integration time. With a co-integrated electronics which reads 14 pixels in a 700 Hz-bandwidth through an above IC self-oscillating loop, the NEP should drop down to 165pW close to the anomalous phase noise of the resonant sensor. However, to surpass the bolometers below 12 μm -pitch the temperature sensitivity has to be increased at least by a factor 10. To this end, works based on first order phase transition material should allow to increase the frequency response through a large improvement of the TCF.

[1] L. Laurent, JJ Yon, JS Moulet, M Roukes, L Duraffourg, "12- μm -Pitch Electromechanical Resonator for Thermal Sensing", Physical Review Applied 9, 024016 (2018)

[2] L. Laurent, JJ Yon, JS Moulet, P Imperinetti, L Duraffourg, "Low noise torsional mechanical resonator for 12 μm microbolometers", and Applications VI 9974, 997407 (2016)

[3] L. Laurent, JJ Yon, JS Moulet, P Imperinetti, L Duraffourg, "Compensation of nonlinear hardening effect in a nanoelectromechanical torsional resonator Sensors and Actuators A 263, 326-331 (2017)

[4] L. Laurent, JJ Yon, JS Moulet, P Imperinetti, L Duraffourg, "Torsional nano-resonator: Characterization of a nonlinear hardening behavior and noise analysis SENSORS, 2016 IEEE (2016)

[5] S. Becker, P Imperinetti, JJ Yon, JL Ouvrier-Buffer, V Goudon, A Hamelin, C Vialle, A Arnaud, "Latest pixel size reduction of uncooled IR-FPA at CEA, LETI

DESIGN AND FABRICATION OF COOLED SILICON BOLOMETERS FOR mm WAVE DETECTION.

AUTHORS:

V. Goudon, A. Aliane, W. Rabaud, C. Vialle, S. Pocas, E. Baghe, L. Dussopt, P. Agnese, N. Lio Soon Shun, S. Becker, V. Reveret (IRFU), J.-L. Sauvageot (IRFU), L. Rodriguez (In-te Néel), M. Solana (In-te Néel), L. Saminadayar (In-te Néel)

ABSTRACT:

CEA has a long history of optoelectronic components development for space and astronomy applications. With this expertise, we are undertaking the development of cooled silicon bolometers for millimeter (mm) and sub-mm wave polarization detection addressing the needs of next generation radio-telescopes. The sensor presented in this work is optimized for the 1.5-mm band and operates around 100mK to reach a noise-equivalent power of a few $\text{aW/Hz}^{0.5}$. The bolometer is composed of doped-silicon thermometers suspended above an optical cavity and supporting superconducting thin film absorbers. 16×16 -pixel arrays with a pitch of 1.2 mm are fabricated in LETI's facilities on 200-mm CMOS read-out circuit wafers in an above-IC configuration.

SCIENTIFIC COLLABORATIONS: IRFU, CNRS (Néel Institute); This work has been partially supported by the LabEx FOCUS ANR-11-LABX-0013.

Context and Challenges

The development of large focal planes with high sensitivity cryogenic detectors is a strong need for the observation of the universe in sub-mm and mm-wave bands. The current state of the art includes several kinds of cooled detectors such as KIDs (kinetic inductance detectors), TES (transition edge sensors), and silicon bolometers. In contrast to KIDs and TES, silicon bolometer technology has been demonstrated successfully in space conditions through the Herschel mission. It benefits from a simple and low-power read-out circuit that can be integrated below the detector array in an above-IC (Integrated Circuit) integration scheme. The fabrication of large arrays of detectors, tuned in the mm-wave band, using standard microelectronic processes above a CMOS read-out IC is a key challenge addressed in these developments.

Main Results

A novel silicon bolometer pixel has been designed for radiation detection and polarization measurement at 1.5-mm wavelength. The fabrication is made in LETI's clean room facilities on 200mm CMOS readout circuit wafers (figure 1). Each array is composed of 16×16 pixels with a pitch of 1.2 mm; the pixel structure is composed of active and reference thermometers arranged in four half-bridge circuits to enhance the sensitivity (figure 2). Thermometers are made of ion-doped and diffused silicon meandered arms suspended above a thick oxide layer and a metal reflector forming an optical cavity. The absorption of the incident radiation is made by a superconducting bi-layer Ti/TiN thin film deposited on the silicon thermometer.

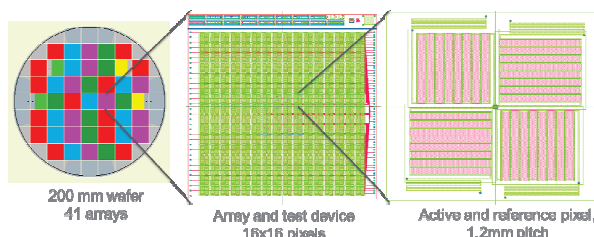


Figure 1: Illustration of the collective manufacturing on a 200mm wafer.

The silicon thermometers are $1.5 \mu\text{m}$ thick and doped with phosphorus and boron species. Doping and diffusion have been optimized to achieve an uniform doping profile through the thermometer thickness and to have a 3D variable range hopping (VRH) conduction with a weak $1/f$ noise at low temperature. Simplified thermometer test structures have been characterized at low temperature, typically in the range of 40-200 mK, and showed a good accordance to an Efros law. A sensitivity ($S = -T/R \cdot dR/dT$) of -6.5 was measured at 100 mK and can be further increased by lowering the working temperature.

Superconducting absorbers made of Ti/TiN bi-layers were developed as well and tuned in critical temperature T_c and electrical impedance [1]. A thickness of 100/5 nm was selected with a critical temperature of about 750 mK.

Based on these experimental results, the electrical, thermal and optical performances of the pixel have been simulated. An optical absorption of about 95% at 1.5 mm wavelength is obtained (figure 2) and a Noise Equivalent Power (NEP) of a few $\text{aW/Hz}^{0.5}$ at 100 mK is expected.

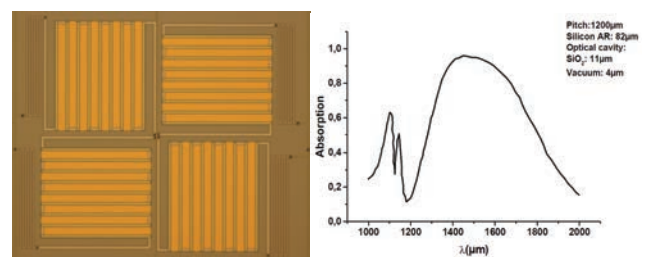


Figure 2: Photograph of the fabricated pixel with a pitch of 1.2mm and simulated absorption as a function of wavelengths.

Perspectives

First wafers of silicon bolometer arrays without read-out circuit have been fabricated in LETI's clean room facilities and are currently under characterizations. The experimental results will be used to improve electrical and thermal models for the design of next-generation focal plane arrays for mm wave detection.

RELATED PUBLICATIONS:

[1] A. Aliane, M. Solana, W. Rabaud, L. Saminadayar, P. Agnese, V. Goudon, L. Dussopt, C. Vialle, E. Baghe, S. Pocas, L. Carle, N. Lio Soon Shun, S. Becker, V. Reveret, L. Rodriguez, A. Hamelin, A. Poglitsch, S. Bounissou, O. Adami, "Superconducting Ti/TiN thin films for mm wave absorption", Journal of low temperature physics, <https://doi.org/10.1007/s10909-018-1919-y>, 2018

HIGH PRECISION MONITORING OF PLANT WATER STATUS USING THZ TIME-DOMAIN SPECTROSCOPY

AUTHORS:

M. Hamdi, J. Oden, J. Meilhan, F. Simoens, and B. Genty (CNRS, Univ. Aix-Marseille, UMR7265)

ABSTRACT:

THz time-domain spectroscopy (TDS) is a promising method for drought stress monitoring in plants. Hence, the absorption coefficient of water in this part of the electromagnetic spectrum is remarkably high and can be used as a vital indicator for the physiological monitoring of plants. In this study, we analyzed the THz transmission through ivy leaves and a realistic multilayer model was developed to improve the estimation of the water content as compared to commonly used single layer models. Experimental results were obtained with less than 2% of residual error as compared to a reference gravimetric measurement.

Context and Challenges

Efficient irrigation is crucial to optimize the productivity and the use of water resources in agriculture. Plant water status can be used as a reliable indicator for irrigation schedule. For this purpose, the non-destructive monitoring of leaves/plants water content has gained major interest since existing techniques like gravimetric method, distillation method and pressure chambers are mainly time-consuming and destructive.

The THz spectrum range appears to be well suited for continuous non-invasive contactless water content monitoring.

One of the unique properties of the THz radiation is the strong absorption by polar liquids like water, which can be considered as a reliable indicator for leaf water content [1]. In this work, we focus on mild water stress for physiological leaf water contents which range between full turgor and turgor loss point. In addition, we take a closer look at the physical modeling of the leaf by using a more realistic multilayers approach.

Main Results

Experiments were performed on Ivy leaves (*Hedera helix*). Gravimetric and THz measurements were carried out simultaneously on a single leaf disc dehydrating in the ambient atmosphere. The THz measurements were carried out using a fiber-coupled THz TDS system in transmission mode employing a collimated beam. The THz and gravimetric measurements were done at the sampling rate of 15 Hz and 5 Hz, respectively.

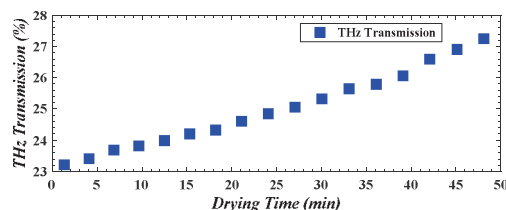


Figure 1. THz transmission at 200 GHz as a function of dehydration time.

Figure 1 presents the transmission coefficient at a frequency

of 200 GHz as a function of dehydration time. The results show a clear increase in transmission as the leaves loose water, which demonstrates the high sensitivity of THz spectroscopy even at high water content.

The first leaf model used in this study was a simple heterogeneous layer made up of water, air, and dried leaf tissue. We noticed a significant deviation between the relative water content (RWC) derived from the gravimetric and THz measurements; the relative error is up to 5%, which prevents a reliable evaluation of leaf water content from THz measurement.

Typical leaf anatomy shows that distinct tissue layers compose the leaf and makes it a complex medium. We modeled the leaf by a new multilayer stack composed of distinct layers mimicking the different tissues and we developed a dedicated root finding algorithm based on latent variables for the inverse problem extraction process.

Figure 2 shows a good agreement between the RWC derived from the gravimetric and THz measurements. In this case, we obtained a residual error less than 2 %.

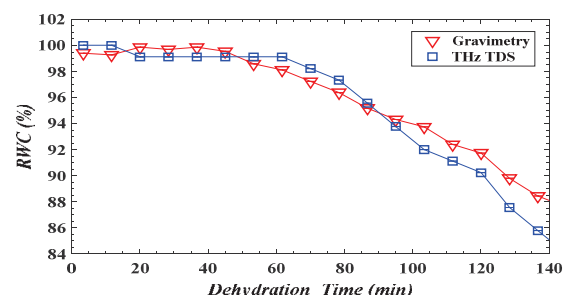


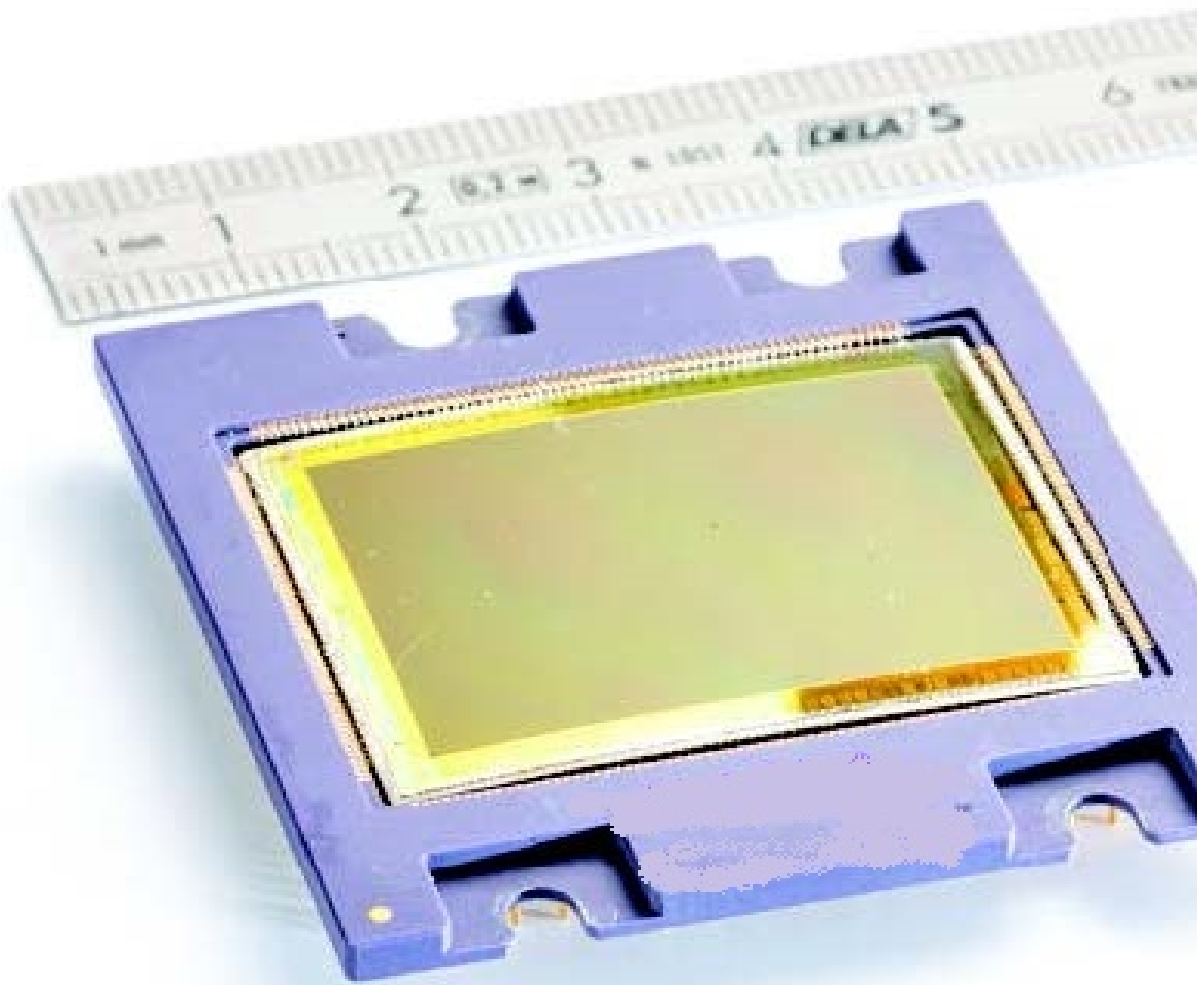
Figure 2. Comparison of gravimetric (triangles) and THz (squares) measurements of the RCW of ivy leaves.

Perspectives

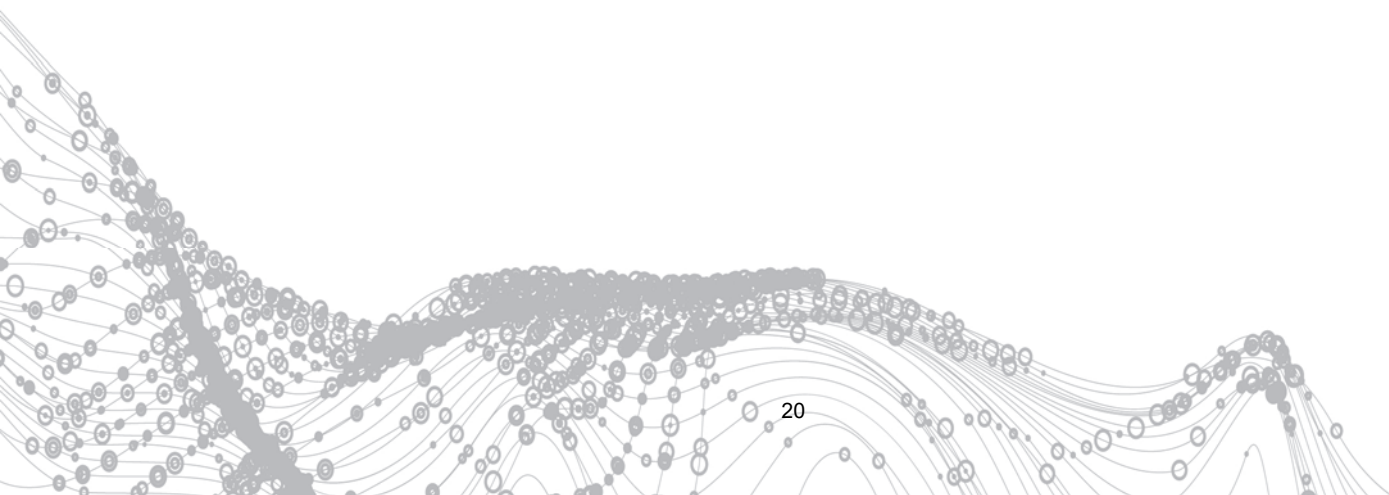
Future works will include the experimental validation on new plant species and more statistical analysis of the root-finding algorithm for the inverse problem extraction process with refined models.

[1]. M. Hamdi, J. Oden, J. Meilhan, F. Simoens, and B. Genty, "Enhanced Plant Water Status Measurement using THz Time-Domain Spectroscopy", THz Days, 12-15 June 2017 — Dunkerque, France.

[2]. M. Hamdi, J. Oden, J. Meilhan, F. Simoens, B. Genty, "High precision monitoring of plant water status using THz time-domain spectroscopy", Conference on Infrared, Millimeter, and Terahertz Waves (IRMMW-THz), 2017, DOI: 10.1109/IRMMW-THz.2017.8067150



CEA-Leti_Denis Morel





O3

VISIBLE IMAGING

- **CMOS-integrated interference optical filters**
- **Depth imaging with indirect time-of-flight**
- **Curved CMOS sensors**

TRANSMISSION MEASUREMENTS OF MULTILAYER INTERFERENCE FILTERS DEVELOPED FOR A FULL INTEGRATION ON CMOS CHIP

AUTHORS:

L. Masarotto, L. Frey, M.-L. Charles, J.-B. Mancini, A. Roule, G. Rodriguez (DTSi), R. Souil (DTSi), V. Larrey (DTSi), C. Morales (DTSi)

ABSTRACT:

We describe a method to measure the transmission spectra of thin multilayers optical filters in order to be fully integrated on various types of CMOS image sensors (ambient light sensors, proximity detection, red green blue colour imaging, etc.). As the filters have to be deposited on top of a CMOS device, a promising approach in order to evaluate with accuracy their response on chip is (i) first to achieve the stacks on Si wafers (ii) then to perform a direct bonding of the structures on glass wafers (iii) in the end to remove the entire bulk silicon. In this way, we show the measured spectral responses of interference filters and can check particularly the agreement of transmission peaks with the simulations and their reproducibility wafer to wafer. It enables to optimize the filters designs and to check that the optical responses fulfill typical CMOS requirements of integration and reliability.

Context and Challenges

The spectral signatures of integrated multilayers filters on CMOS chip are observed in quantum efficiency measurements but do not show a perfect agreement in magnitude and in wavelength compared to simulated curves. As it is complex to differentiate the errors resulting from filters stacks and CMOS stacks, carrying out transmissions measurements becomes essential with a view to optimize the filters designs. Thus we show the possibility of bonding filters stacks on glass substrates and removing the Si initial bulk with chemical/mechanical thinning down in order to obtain the measured spectral transmittance of multilayers stacks made in similar conditions to the integration on CMOS chips

Main Results

In this study, we design and make bandpass filters using single or multiple Fabry-Perot cavities. In the prospect to integrate ambient light and presence detection on CMOS chip, we investigate filters with Cu/dielectrics and a-Si/SiO₂ multilayer stacks for respectively the ALS and NIR functions. At first, the entire filters were deposited on 200mm Si wafers with polished and cleaned top PECVD oxides. The Cu and SiN films of ALS stacks were developed at ambient temperature using DC magnetron sputtering. The SiO₂ and a-Si layers of NIR stacks were processed at 400°C by the PECVD technique. As shown in Fig. 1, both process techniques were adjusted to lower deposition rates to achieve a high control on the layer thicknesses and uniformities. The various stacks were carried out in different chambers of same tool without breaking the vacuum between the depositions in order to have clean interfaces without impurities or residual oxidations.

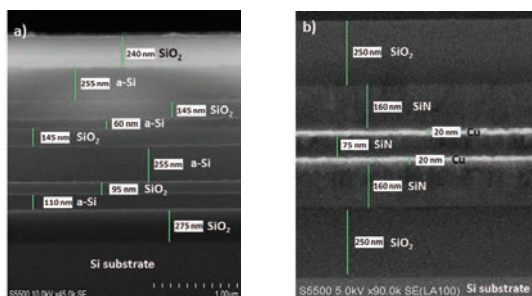


Figure 1: SEM images of the multilayer stacks deposited on Si wafer (a) a-Si/SiO₂ stack (b) Cu/dielectrics stack

RELATED PUBLICATIONS:

[1] L. Masarotto, L. Frey, M.-L. Charles, A. Roule, G. Rodriguez, R. Souil, C. Morales, V. Larrey, "Transmission measurements of multilayer interference filters developed for a full integration on Complementary Metal Oxide Semiconductors chips", Thin Solid Films, vol. 631, pp. 23-28, June 2017.

Then face-to-face direct bondings were performed on glass 200mm wafers and followed with a 400°C annealing for 2H. Finally, using successive mechanical and chemical thinning down processes, the sacrificial Si bulk were removed. Transfer process of multi-layers stacks shows a change of optical systems support without deteriorating or modifying the morphological properties. It enables the optical measurements in transmission of optical systems processed on Si bulk. The optical measurements of the multilayer have been performed by spectrophotometry. The measured and calculated spectral transmittances of the a-Si/SiO₂ and Cu/dielectrics multilayer filters are presented in Fig. 2. Each filter was measured several times with distinct wafers to check the structures reproducibility. We observe for both studied designs an excellent agreement between measured and simulated data with regard to the transmission peak wavelength and magnitude. The reproducibility of filter responses is moreover very satisfactory meaning the achieved processes are stable with standard deviation much better than the specified dispersion (5%) for the used tools. These results confirm that this method is a reliable way to optimize the designs and responses of the filters.

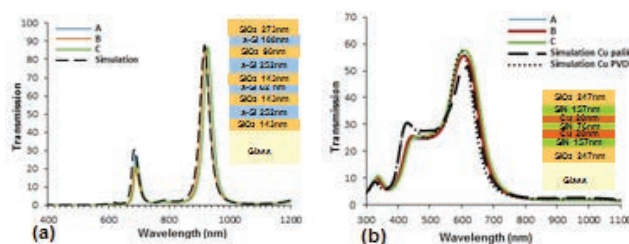


Figure 2: Comparison between the simulated and measured spectral responses of (a) NIR a-Si/SiO₂ filters (b) ALS Cu/dielectrics filters

Perspectives

This paper presents a novel method to measure the spectral transmittance of filters on opaque Si wafers by carrying out the transfer of multilayer stacks on glass wafer via direct molecular bonding. The transfer process did not impair the morphological and optical properties of the thin multilayers stacks and a good agreement between simulated and measured spectral responses is observed for both ALS and NIR interference filters with an excellent reproducibility. The bonding of multilayers stacks on glass substrates appears as a useful and efficient technique in order to measure the spectral transmittance and can be used for the optimization of filter designs and check precisely the predictions of optical responses in view of an integration on CMOS chips.

DEPTHMAP IMAGE OBTAINED FROM INDIRECT TOF (TIME OF FLIGHT) PIXELS WITH FAST TRANSFER GATES

AUTHORS:

B. Rodrigues(ST), M.Guillon, N.Billon-Pierron, J.B.Mancini, O.Saxod, B.Giffard, Y.Cazaux, P.Malinge (ST), P.Waltz (ST), A.Ngoua (ST), Y.Kerleguer (ST), A.Taluy (ST), S.Kuster (ST), S.Joblot (ST), F.Roy (ST), G.N.Lu (INL)

ABSTRACT:

We developed a time of flight (TOF) pixel with implementation of 3-tap phase-shifting technique [1]. The pixel integrates a pinned photodiode (PPD) and 3 charge-transfer paths. Each path is delimited by deep trenches and integrates a fully depleted memory (storage site) enabling Correlated Double Sampling (CDS) and a low-noise buried-channel Transfer Gate (TG). In order to achieve fast and efficient charge transfer. The pixel was designed in a size of $6.2\mu\text{m} \times 6.2\mu\text{m}$, and an image sensor chip was fabricated. Testing results show a dark current of 30 e-/s @ 60°C , readout noise of 3.2e- and a demodulation contrast (DC) of 73% @110 MHz using a 930nm light source.

SCIENTIFIC COLLABORATIONS: *Institut des Nanotechnologies de Lyon, Univ. C.Bernard Lyon1, 69622 Villeurbanne, France*

Context and Challenges

Several methods based on Time-of-flight (TOF) can be realized for acquiring a depth image : one of them is based on a continuous wave (CW) modulation with implementation of a multi-tap approach. The proposed pixel integrates a pinned photodiode (PPD) and 3 fully depleted memories as storage sites. It also integrates low-noise buried-channel to optimize charge collection and transfer efficiency from PPD to the 3 storage sites. The achieved pixel size is $6.2\mu\text{m} \times 6.2\mu\text{m}$, integrated in a QVGA image sensor chip which was fabricated and tested.

Main Results

To measure the distance, the scene is illuminated by a modulated near infra-red light source and the reflected light with delay is detected by the PPD of the pixel. Photo-generated electrons are then successively sampled at high frequency, typ. 10 to 130MHz, and stored in 3 different memory sites. An additional fourth path is also included for anti-blooming (AB) purpose. Fig. 1. When TG is ON, photo-generated electrons from PPD are temporarily stored beneath its gate. When TG is OFF, the electrons are transferred into the memory (storage site). After a succession of switching TG with charge transfer, when the integration period is over, the whole sampled signal in charges is stored in the memory. For signal reading, the stored charges can be transferred into the FD node by turning Tx gate ON. This architecture allows CDS (before and after charge transfer through Tx gate), which eliminates kTC noise and rejects most $1/f$ noise. The phase difference between the emitted light signal and the received one by reflection is easily calculated and the distance is then determined:

$$\varphi = \arctan(\sqrt{3} \cdot \frac{C_2 - C_1}{(C_1 - C_0) + (C_2 - C_0)}) \quad \& \quad D = \frac{c_{light}}{4\pi f} \varphi$$

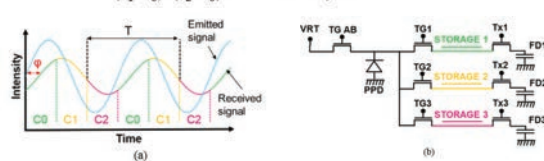


Figure 1: (a) 3-sample phase-shifting (3-tap) technique for distance measurement (b) Our 3D TOF pixel scheme

RELATED PUBLICATIONS:

[1] B. Rodrigues, M. Guillon, N. Billon-Pierron, J-B. Mancini, O. Saxod, B. Giffard, Y. Cazaux, P. Malinge, P. Waltz, A. Ngoua, Y. Kerleguer, A. Taluy, S. Kuster, S. Joblot, F. Roy, G-N. Lu, "Indirect ToF Pixel integrating fast buried-channel transfer gates and gradual epitaxy, and enabling CDS", <http://imagesensors.org/2017-papers/>, International Image Sensor Workshop, 30th May-2nd June 2017, Hiroshima, Japan

The designed 464×197 pixel (QVGA) test chip was fabricated and a "burst characterization" was performed to evaluate charge-draining capability of the TGs, consisting in synchronizing a received laser pulse with one TG's opening time during integration. Then the sampled signal (in charge packet) stored in the corresponding memory (after integration time) was compared to the sum of the stored charges in all memories. The results show that more than 70% of photo-generated electrons go to the desired storage site and the charge-draining via TG control is efficient for opening time down to a few ns. The demodulation contrast (DC): $DC = (A-B)/(A+B)$, where A and B correspond to the maximum and minimum of the charge ratio respectively, reaches 75% at 50 MHz and 73% at 110 MHz (3ns of corresponding sampling period) @ 930nm illumination signal. Table 1 presents a summary of our pixel's characteristics, in comparison with recently reported studies. Our achievements include high demodulation contrast ratio, low dark current, and low readout noise. Fig. 2 shows an acquired 3D image from the (QVGA) test chip, illuminated by a 25MHz 870nm LED.

Parameter	Our pixel	A. Payne et al.	E. Tadmor et al.
Pixel size	$6.2\mu\text{m} \times 6.2\mu\text{m}$	$10\mu\text{m} \times 10\mu\text{m}$	$6.7\mu\text{m} \times 6.7\mu\text{m}$
Array resolution	464×197	512×424	360×180
Conversion Gain	$62 \mu\text{V/e-}$	$26 \mu\text{V/e-}$	$64 \mu\text{V/e-}$
FWC	$3 \times 12 \text{ ke-}$	100 ke-	$4 \times 9.5 \text{ ke-}$
Read out Noise	3.2e-	12.3e-	7.5e-
Dark current	30 e-/s @ 60°C	-	30000 e-/s @ 50°C
Demodulation Contrast	75%/73% @930nm	58%/57% @860nm	98% @850nm
QE	6% @50MHz/130MHz	6% @50MHz/130MHz	10% @100MHz
Voltage swing	2.5V	3.3V	7V
Max Frequency	160MHz	130MHz	>100MHz

Table 1: compared measured characteristics

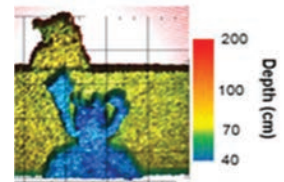


Figure 2: acquired depthmap

Perspectives

This paper presents a novel pixel structure for depth map acquisition. We developed $6.2\mu\text{m}$ 3D-TOF pixel using pinned photodiode, fully depleted memories and operating with a 4T reading architecture. Integration of buried-channel TGs built on a doping-profile-controlled epitaxial layer improves charge-transfer efficiency and speed, which lead to high demodulation contrast. Due to its compatibility with common imaging process and voltage supply, the proposed pixel can be applied to the ultimate goal which is the integration of depth and color pixel in the same die. the standalone RGBZ camera.

CURVED CMOS SENSORS: TOWARDS MORE COMPACT OPTICAL SYSTEMS

AUTHORS:

B. Chambion, Chr. Gaschet, Th. Behaghel (LAM), A. Vandeneynde, S. Caplet, S. Gétin, D. Henry, E. Hugot (LAM), W. Jahn (LAM), S. Lombardo (LAM), M. Ferrari (LAM)

ABSTRACT:

In this paper, we first describe advantages of curved sensor and associated packaging process applied on a 1/1.8" format 1.3Mpx global shutter CMOS sensor (Teledyne EV76C560) into its standard ceramic package with a spherical radius of curvature $R_c=65\text{mm}$ and 55mm. The mechanical limits of the die are discussed (Finite Element Modelling and experimental), and electro-optical performances are investigated. Then, based on the monocentric optical architecture, we propose new design, compact and with a high resolution, developed specifically for a curved image sensor including optical optimization, tolerances, assembly and optical tests. Finally, a functional prototype is presented with same performances and a x2.5 reduction of length compared to a commercial one. The finality of this work was a functional prototype demonstration on the CEA-LETI during Photonics West 2018 conference.

SCIENTIFIC COLLABORATIONS: Astrophysical Laboratory of Marseille (LAM), France.

Context and Challenges

Curved sensors help the correction of off-axis aberrations, such as Petzval Field Curvature, astigmatism, and bring significant optical and size benefits for imaging systems. There are already several developments on the fabrication of curved sensors. For the monolithic approach, the fabrication has been demonstrated on uncooled and cooled infrared sensors, for very compact high-performance camera [1], Charge Couple Device (CCD) (ex.: <http://www.andanta.de>), or Complementary Metal Oxide Semiconductor (CMOS) (Itonaga, K. et al., *Sony R&D Platform, Atsugi, Japan. Symposium on VLSI Technology, 2014 and Guenter, B. et al., Optics Express 25, no. 12, 2017*). None is in industrial production. In 2017, two optical systems prototypes equipped with curved sensor have been realized and tested. One is dedicated to professional photography and the other one for machine vision (discussed in this paper). These demonstrations were possible with mechanical and optical modelling, curved CMOS sensor packaging, electro-optical tests, and optical characterization.

Main Results

In order to implement a spherically shaped CMOS sensor, changes are required to adapt this standard structure. First, the sensor is thinned with a grinding equipment to a targeted thickness in order to make the sensor mechanically "flexible". It can be followed by a Chemical Mechanical Polishing (CMP). In this work, the targeted thickness is $100\mu\text{m}$. Mechanical models (ANSYS software) help us to define curving limits of the dies. Then, that thinned chip is glued (structural attachment) onto a curved substrate. The CMOS final shape is drove by the substrate. Wire bonding process, developed for electrical connections, is also optimized in order to prevent damages on thinned dies.

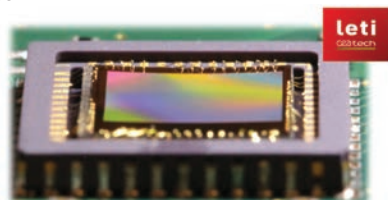


Figure 1: Curved Teledyne EV76C560 sensor with CEA-LETI

process ($R=65\text{mm}$).

Figure 1 shows a global view of the final packaging, curved into its commercial packaging. The radius of curvature is $R=65\text{mm}$.

Effects of tensile or compressive stresses applied on the CMOS active layers have to be studied in order to know if curved sensors keep good performances.

Results on curved sensor show a standard response compared to flat sensor (standard) and we can confirm that within (+inf.; 55mm) radius of curvature range, curving process has no significant impact on the Teledyne EV76C560.

The step forward is the optical design. Thanks to Zemax software, monocentric architecture (system which combines compactness, wide field of view, high resolution, large light collection, and highly curved focal plane) has been implemented and optimized according to mechanical limits of the CMOS sensor. After tolerances, assembly, optical tests, and using our curved technology, we demonstrate an impressive simplification of the optical system (~40% of lenses) and a huge reduction of the total length by 2.5 time for the same optical performances compared to an equivalent commercial system (figure 2).

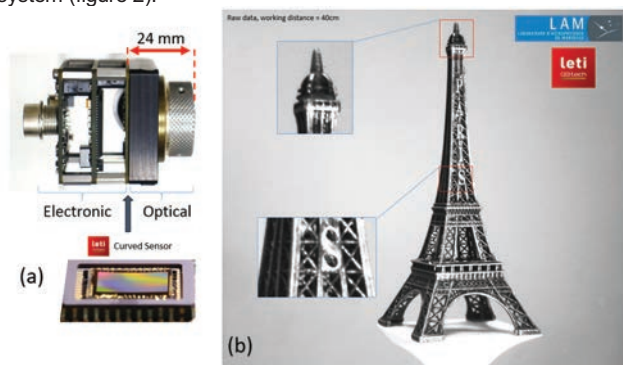
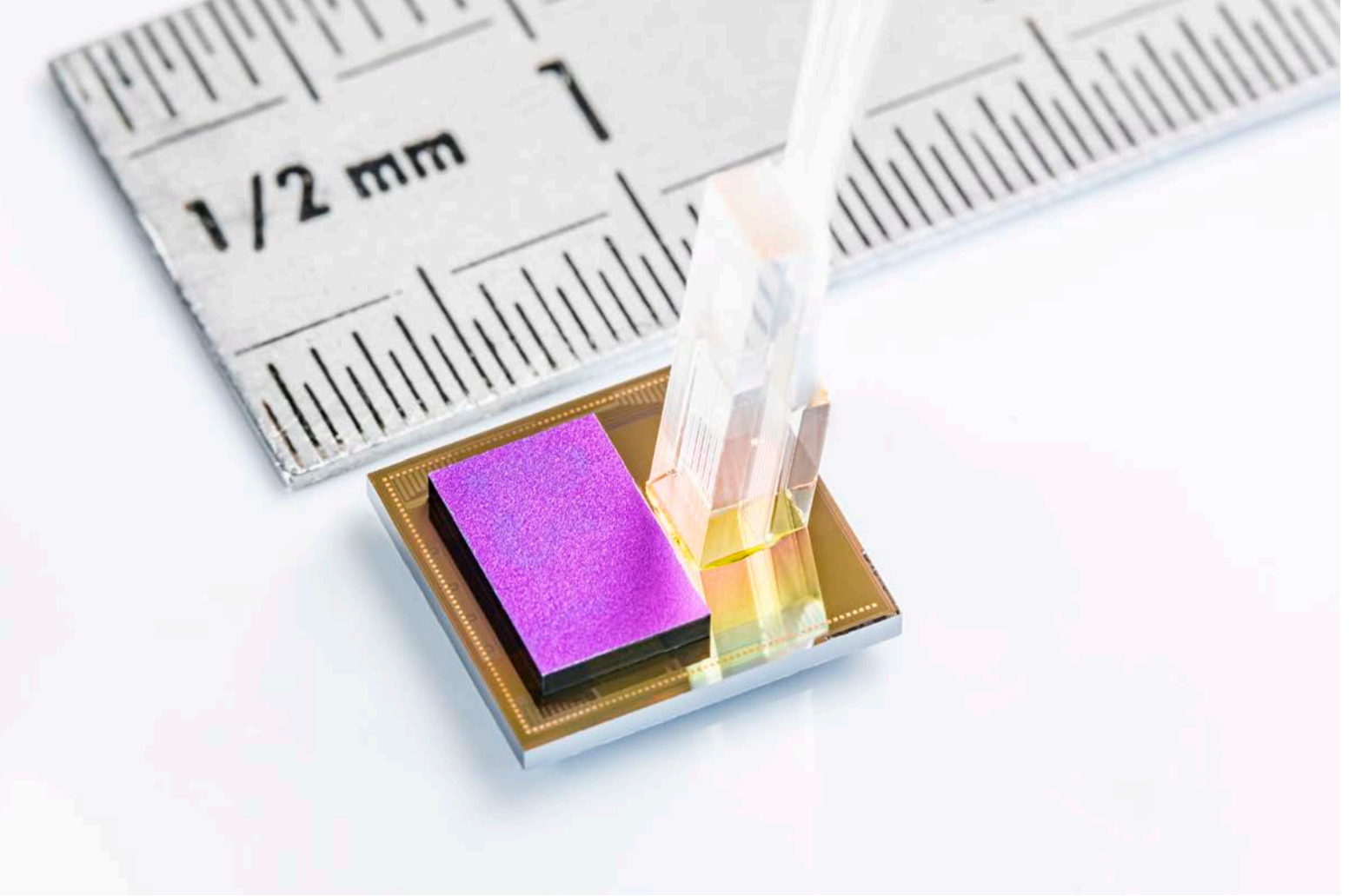


Figure 2: a) LETI prototype equipped with curved sensor. b) Image from this prototype (working distance 40 cm).

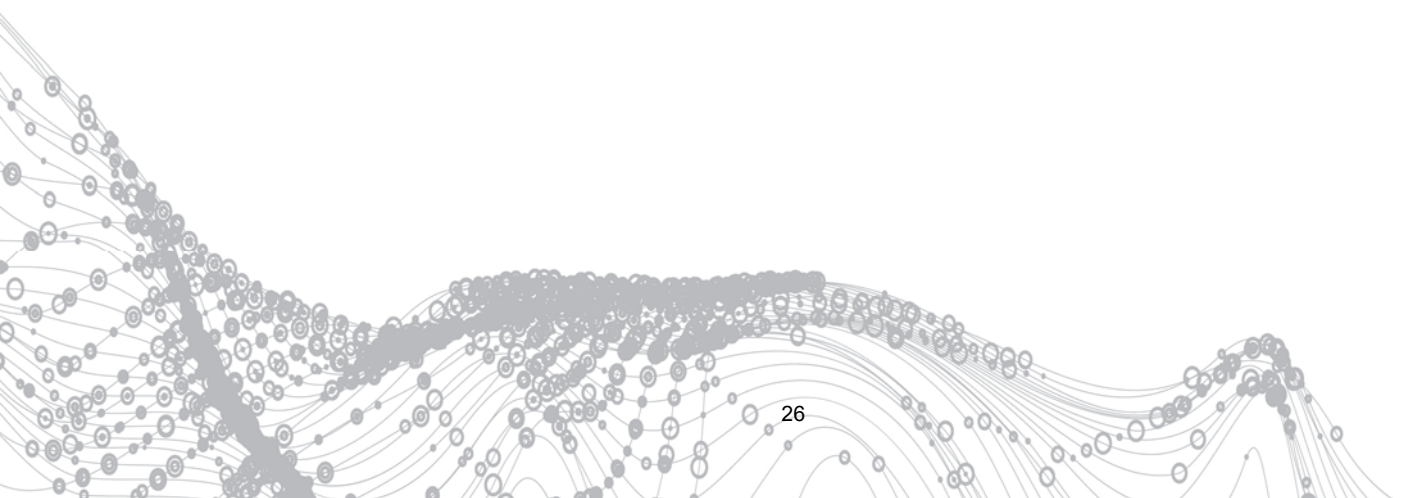
Perspectives

Curved sensor technology is a disruptive approach to bring innovations in optical systems. Using curved sensors, we demonstrate the opportunity to drastically reduce the complexity of existing solutions. Our bending process is scalable to any die size. Further developments are in progress for cost effective, large-scale manufacturing processes.

[1] D. Dumas, M. Fendler, N. Baier, J. Primot, and E. Le Coarer, "Curved focal plane detector array for wide field cameras," *Applied Optics* 51, no. 22, pp. 5419-5424 (2012).



CEA-Leti/Denis Morel





O4

SILICON PHOTONICS

- **Sol+SiN platform for t° -insensitive CWDM transceivers**
- **Frequency-combs with Si_3N_4**
- **GeSn lasers**
- **200 mm CMOS-compatible III-V/Si DFB lasers**
- **Micro-ring modulators integrated with III-V/Si lasers**
- **Reflective FTTH/PON unit**

SOI-SiN PHOTONIC PLATFORM FOR TEMPERATURE-INSENSITIVE CWDM OPTICAL TRANSCEIVERS.

AUTHORS:

Q. Wilmar, C. Sciancalepore, D. Fowler, H. El Dirani, K. Hassan, S. Garcia, L. Adelmini, D. Robin-Brosse (DCOS), K. Louv (ST Microelectronics), J.-A. Dallery (ST Microelectronics), J. Bustos (ST Microelectronics), C. Socquet-Clerc (DTSi), S. Malhouitre, and S. Olivier.

ABSTRACT:

Within the framework of the H2020 European project COSMICC, we report on the integration of a SiN photonic layer in the LETI's 200 mm silicon photonics platform. This enhanced platform targets energy-efficient optical transceivers for datacom applications by taking advantage of the low temperature sensitivity of SiN. Wafer-level characterizations of low-loss SiN waveguides in the O-band confirm the superior passive properties of SiN. Furthermore, we demonstrate a temperature quasi-insensitive SiN multiplexer as well as broadband hybrid Si-SiN grating fiber couplers and Si-SiN interlayer transition.

Context and Challenges

The constantly growing network traffic in data centres requires low cost, high speed and energy efficient transmission solutions. This challenge can be met by Silicon photonics. In the near future, using CMOS compatible manufacturing process opens the way to large volume and low cost fabrication of on-chip photonic transmitters or receivers [1]. Looking toward integrated photonic systems, and targeting data center applications, an attractive solution to expand the data rate of transceivers is coarse wavelength division multiplexing (CWDM). This standard provides a large enough channel spacing of 20 nm to avoid an energy-consuming temperature control of the lasers but it requires broadband and low temperature sensitivity optical devices. In this respect, Silicon Nitride (SiN) is an appealing material for photonics: it is CMOS-compatible, its lower optical index offers a better robustness to fabrication imperfections, lower propagation losses and above all, its thermo-optics coefficient, 10-fold lower than Silicon's, allows the development of temperature quasi-insensitive devices.

Main Results

We successfully demonstrated the integration of SiN in the LETI's silicon photonic platform [2] (see Fig. 1.a). Notably, the SiN is deposited at a low enough temperature (300 °C) to allow compatibility with Si or Ge implanted active devices such as modulators and photodetectors.

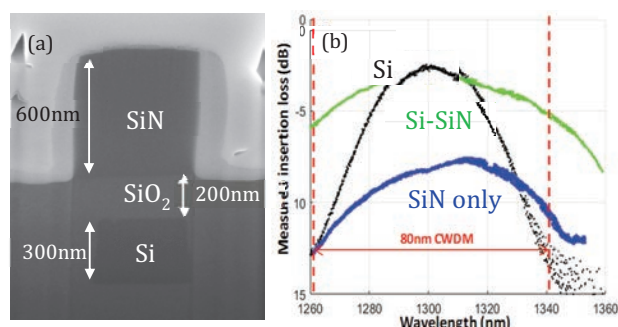


Figure 1: (a) SEM image of the platform cross section. (b) Insertion loss of the Si-SiN grating coupler (green line) compared with Si and SiN only couplers (black and blue lines).

SiN monomode strip waveguides show reduced propagation losses (0.8 dB/cm) compared to Si strip and ring waveguides

(3.6 and 1.5 dB/cm respectively). Furthermore, the SiN thermo-optics coefficient is measured at $1.7 \times 10^{-5} \text{ K}^{-1}$, which is one order of magnitude lower than Si and lower than most previously reported SiN platforms.

In order to be able to manipulate light in both layers, interlayer Si-SiN transitions are designed and measured, showing a great efficiency with losses below 0.1 dB all over the O-band. Taking advantage of the new platform, we designed and measured a bi-layer Si-SiN grating fiber coupler showing a large bandwidth enhancement compared to its pure Si counterpart, as shown in Fig. 1.b. This will prove particularly useful to test CWDM components for which the bandwidth extends over 80 nm.

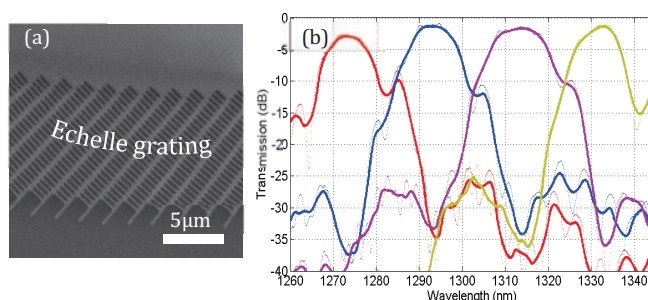


Figure 2: (a) SEM image of the 400nm-period grating of the SiN Echelle multiplexer. (b) Transmission spectrum of the 20 nm-spaced 4-channels SiN Echelle multiplexer for CWDM applications.

Finally, we report on design, fabrication and test of SiN echelle grating (de-)multiplexer for CWDM [3] (see Fig. 2). It exhibits low average insertion loss (1.5 dB), high inter-channel isolation (~ 30 dB), and a -1 dB channel bandwidth above 8 nm. Moreover, the device shows a very low temperature sensitivity, measured below $13 \text{ pm}^\circ\text{C}$, thus constituting an ideal candidate for high-performing wavelength de-multiplexing operation in radically different thermal environments.

Perspectives

We have demonstrated a 200 mm Si-SiN platform with passive components; the next step will be to demonstrate the SiN integration with Si active components, such as modulators, and hybrid III-V/Si lasers to develop full transmitter circuits, and to enhance the Leti's device library with SiN polarization management devices for receiver circuits. SiN is also intended to be used for other applications and will be included in a future 300 mm photonic platform.

RELATED PUBLICATIONS:

- [1] B. Szilag, B. Blampey, T. Ferrotti, V. Reboud, K. Hassan, S. Malhouitre, G. Grand, D. Fowler, S. Brision, T. Bria, G. Rabillé, P. Brianceau, J.M. Hartmann, V. Hugues, A. Myko, F. Elleboode, F. Gays, J.M. Fédéli, C. Kopp, "Multiple wavelength silicon photonic 200 mm R+D platform for 25Gb/s and above applications," Proc. SPIE 9891, Silicon Photonics and Photonic Integrated Circuits V, 98911C (13 May 2016);
- [2] Q. Wilmar, D. Fowler, C. Sciancalepore, K. Hassan, S. Plantier, L. Adelmini, S. Garcia, D. Robin-Brosse, S. Malhouitre, S. Olivier, "A hybrid SOI/SiN photonic platform for high-speed and temperature-insensitive CWDM optical transceivers," Proc. SPIE 10537, Silicon Photonics XIII, 1053709 (22 February 2018);
- [3] C. Sciancalepore, Q. Wilmar, D. Robin-Brosse, L. Adelmini, S. Malhouitre and S. Olivier, "O-band CWDM Echelle Grating Demultiplexers on SiNOI Exhibiting Quasi-absolute Thermal Insensitiveness", Proc. SSDM (September 2017).

ANNEALING-FREE Si_3N_4 FREQUENCY COMBS FOR MONOLITHIC INTEGRATION WITH SI PHOTONICS

AUTHORS:

H. El Dirani, M. Casale, S. Kerdiles (DTSi), P. Brianceau (DTSi), C. Socquet-Clerc (DTSi), C. Sciancalepore, C. Monat (INL), A. N. Kamel (DTU), L. K. Oxenlowe (DTU), and K. Yvind (DTU)

ABSTRACT:

We report on the fabrication and testing of Si_3N_4 nonlinear photonic circuits for CMOS-compatible monolithic co-integration with silicon-based optoelectronics. In particular, a novel process has been developed to fabricate annealing- and crack-free Si_3N_4 750-nm-thick films for Kerr-based nonlinear functions featuring full thermal budget compatibility with front-end CMOS and Silicon photonics. Frequency comb generation in microring resonators based on such annealing-free silicon nitride films is demonstrated spanning 800 nm (1300 nm - 2100 nm) and counting almost 250 newly generated frequencies. Such milestone paves the way to low-threshold power-efficient Kerr-based broadband sources featuring full thermal processing compatibility with Si photonic integrated circuits (Si-PICs).

SCIENTIFIC COLLABORATIONS: CNRS / Lyon Institute of Nanotechnology (INL), France; Technological University of Denmark (DTU), Denmark

Context and Challenges

Silicon-based photonic integrated circuits (Si-PICs) pave the way towards a brand-new optoelectronics featuring a significant integration potential with cost-effective complementary metal-oxide-semiconductor (CMOS) technology and micro-nano-electronics circuits and nodes.

A paradigm shift in optical transmission can be however constituted by exploiting the full potential of χ^3 nonlinear optical processes to generate Kerr-based optical frequency combs (OFCs). In this way, tens or even hundreds of optical channels can be obtained thus substituting an equal amount of III-V on Si individual laser diodes to be integrated on a chip as illustrated in Fig. 1. However, *all prior works* based on stoichiometric Si_3N_4 -based OPOs made use of high-temperature annealing ($\sim 1200^\circ\text{C}$) of the nitride film and silica uppercladding used to break N-H bonds otherwise causing absorption in the C-band, otherwise severely degrading its nonlinear functionality. As well as that, substrate preparation made by etching crack-limiting trenches in the SiO_2 undercladding has been also used to prevent the propagation of tensile strain-related cracks in the nitride film which would deteriorate dramatically the optical quality of the material. Indeed, the use of such annealing is *intrinsically incompatible* for a monolithic cointegration of such nonlinear circuits on existing Si-based photonics and optoelectronics as, for instance, extreme annealing would destroy the Silicon optical layer underneath along with its functions (modulation, photodetection, etc...). To prevent the aforementioned drawbacks, a novel annealing-free crack-free process has been developed to deposit such thick nitride-based films for nonlinear optics applications exhibiting front-end process compatibility with CMOS and Silicon photonics integrated circuits (Si-PICs). Such generated broadband sources can be able to provide sufficient aggregate data transmission bandwidth to reach 100's of Tbit/s and beyond.

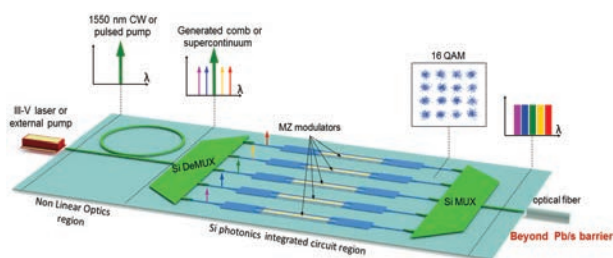


Figure 1: Principle of ultra-high speed rate communications with Kerr frequency combs. Artistic view of a future ultra-high rate transmitter, leveraging a Kerr frequency comb source onto a Silicon optoelectronic chip.

RELATED PUBLICATIONS:

- [1] H. El Dirani, M. Casale, S. Kerdiles, C. Socquet-Clerc, X. Letartre, C. Monat, and C. Sciancalepore, "Crack-Free Silicon-Nitride-on-Insulator Nonlinear Circuits for Continuum Generation in the C-Band," in *IEEE Photonics Technology Letters*, vol. 30, no. 4, pp. 355-358, Feb. 15, 15 2018. doi: 10.1109/LPT.2018.27
- [2] A. N. Kamel, H. E. Dirani, M. Casale, S. Kerdiles, C. Socquet-Clerc, M. Pu, L. K. Oxenlowe, K. Yvind, and C. Sciancalepore, "Frequency comb generation in crack-free Si-photonics compatible Si_3N_4 microresonator chip," *IEEE/OSA Conference on Lasers and Electro-Optics (CLEO)*, San Jose, USA, May 2018
- [3] H. E. Dirani, et al., "Annealing-free Si_3N_4 frequency combs for monolithic integration with Si photonics", submitted to *APL photonics*

Main Results

Optical frequency comb generation. The silicon nitride microresonators based on the annealing-free CMOS-compatible process are shown in Fig. 2. The chips were then continuous-wave pumped via an external C-band EDFA laser + amplifier at 1569 nm wavelength. Quality factors of the microring exceed 600,000, allowing to reach optical parametric oscillation threshold at 80 mW pumping power. Cascaded four-wave mixing (FWM) processes and parametric gain via anomalous-dispersion-engineered waveguide constituting the microring allow to generate a native-line-spaced optical frequency comb counting almost 250 new generated frequencies over a wavelength span of nearly 800 nm (1300 nm - 2100 nm). Its optical spectrum is reported in Fig. 3. Via such demonstration, we claim the *first-time realization* of annealing-free silicon nitride frequency comb microresonators, following a tailored deposition method, minimizing the hydrogen content. Our annealing-free and crack-free fabrication process provides our devices with the right specification (microring GVD and characteristics) to underpin Kerr frequency combs, thus representing a significant step toward the full compatibility of Si_3N_4 -based Kerr-comb sources with the thermal budgets of front-end CMOS and Si photonics processing.

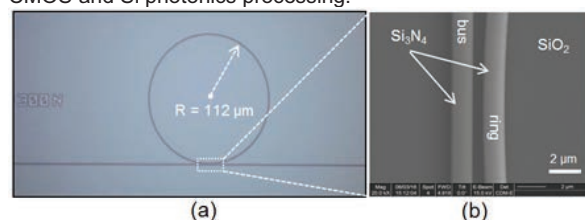


Figure 2: SiN-based waveguides and microresonators for nonlinear parametric amplification.

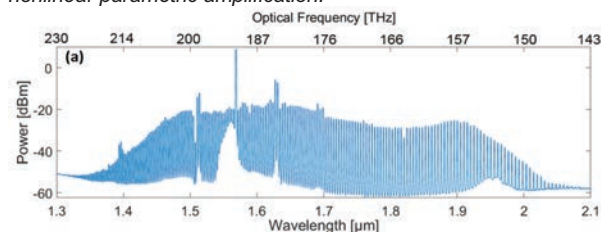


Figure 3 : Kerr-based frequency comb generation spanning 1300 nm - 2100 nm in front-end CMOS-compatible Si_3N_4 rings.

Perspectives

Current research is focused on both material and technology optimization to reduce the parametric threshold power dramatically.

LASING IN OPTICALLY PUMPED GeSn PHOTONIC CRYSTALS

AUTHORS:

V. Reboud, Q.M. Thai (INAC), M. Bertrand, N. Pauc (INAC), J. Chrétien (INAC), J. Aubin (DTSi), R. Khazaka (DTSi), A. Tchelnokov, J.M. Hartmann (DTSi), V. Calvo (INAC)

ABSTRACT:

Germanium based materials can overcome some limits inherent to standard Silicon Photonics devices and be used notably in Mid-Infrared sensing applications and Network-On-Chip applications. One of the main challenges in this field is to transform the indirect group-IV semiconductor bandgap to a direct one using high tensile strains or by alloying germanium with tin. We lately demonstrate lasing in optically pumped GeSn photonic crystal membrane with 16% Sn content. The active $\text{Ge}_{0.84}\text{Sn}_{0.16}$ layer is grown on a step-graded GeSn buffer, thus limiting the density of the misfit dislocations. Obtained thresholds (227 kW/cm^2 at 15 K to 340 kW/cm^2 at 60 K) are comparable to our previous works indicating the robustness of GeSn optical gain.

Context and Challenges

Si photonics is advantaged by its full compatibility with the current massively produced Si complementary metal-oxide semiconductor (CMOS) technology. Lately, germanium (Ge) based materials appeared to be a good candidate to tackle the current limitations of Si, since it is also fully CMOS compatible. Recent progresses in Chemical Vapor Deposition (CVD) allowed to grow in LETI high Sn content in the Ge crystalline matrix. A direct bandgap can be obtained in GeSn if the Sn content is high enough and the residual compressive strain low enough (when grown on Ge). The low thermal stability of GeSn alloys requires a careful selection of process parameters during epitaxy. Recent studies have demonstrated lasing in optical cavities made with $\text{Ge}_{1-x}\text{Sn}_x$ alloys. So far, lasing were reported in Fabry-Perot cavity [1] and in micro-disk cavity [2].

Main Results

We investigated the benefit of using photonic crystals structures that contain some guided modes with group velocities approaching zero. The slowing down of the light propagation enhances light-matter interaction, which a favourable condition to achieve lasing effect. This effect is known in literature as band-edge lasers.

The GeSn layers were grown in a 200 mm Epi Centura 5200 Reduced Pressure-Chemical Vapor Deposition (RP-CVD) cluster from Applied Materials. The growth was carried at reduced temperatures – between 300°C and 350°C . The optically active layer was grown on top of a thick Ge strain relaxed buffer, with Ge_2H_6 and SnCl_4 flux ratio modified during the process to create discrete concentration ramp– referred here as “GeSn step-graded buffer”– before reaching the target concentration of Sn (16%). This method helps to relax partially the compression in the GeSn layer, while capturing misfit dislocations at the interfaces inside the graded buffer (instead of propagating them towards the surface), thus preserving the crystalline quality of the partially relaxed $\text{Ge}_{0.84}\text{Sn}_{0.16}$ optical layer [3].

We developed processes on (i) GeSn anisotropic etching and (ii) isotropic selective etching of Ge versus GeSn to get suspended photonic crystals structures (Figure 1). Highly selective under etching was achieved even for GeSn with a Sn content as low as 6% (selectivity of 57 for 6% Sn layers, and 433 for layers with 8%) [4].

RELATED PUBLICATIONS:

- [1] S. Wirths, R. Geiger, N. von den Driesch, G. Mussler, T. Stoica, S. Mantl, Z. Ikonik, M. Luysberg, S. Chiussi, J. M. Hartmann et al, Nature Photonics 9,88 (2015).
- [2] V. Reboud, A. Gassenq, N. Pauc, J. Aubin, L. Milord, Q. M. Thai, M. Bertrand, K. Guillo, D. Rouchon, J. Rothman, T. Zabel, F. Armand Pilon, H. Sigg, A. Chelnokov, J.M. Hartmann, V. Calvo, Optically pumped GeSn micro-disks with 16 % Sn lasing at $3.1 \mu\text{m}$ up to 180K, <http://arxiv.org/abs/1704.06436>
- [3] J. Aubin, J.M. Hartmann, A. Gassenq, J.L. Rouvière, E. Robin, V. Delaye, D. Cooper, N. Mollard, V. Reboud, V. Calvo, Semicond. Sci. Technol., vol. 32, 2017.
- [4] L. Milord, J. Aubin, A. Gassenq, S. Tardif, K. Guillo, N. Pauc, J. Rothman, A. Chelnokov, J.M. Hartmann, V. Calvo, V. Reboud, Proc. SPIE 10108, Silicon
- [5] Q.M. Thai, N. Pauc, J. Aubin, M. Bertrand, J. Chrétien, R. Khazaka, A. Chelnokov, J.M. Hartmann, V. Reboud, V. Calvo, submitted.

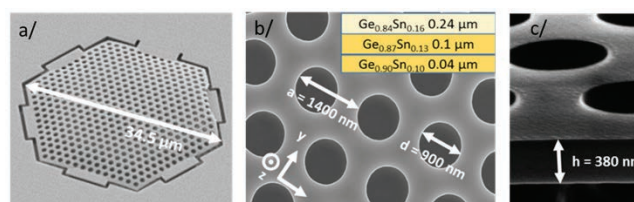


Figure 1: a/ SEM image of the GeSn photonic crystal membrane, b/ Top-view of the photonic crystal showing its critical dimension, c/ Cross-section of the suspended band-edge laser.

The structures were optically pumped with a 1064 nm pulsed laser. Fourier transform infrared (FTIR) spectroscopy was used to study the photoluminescence of these samples. To identify the nature of the lasing mode, 3D plane wave expansion method was used to simulate the band-structure of the photonic crystal membranes. The simulated band-structure, alongside the experimental spectra (15 K) at the threshold value, are shown in figure 2a. Good agreement is found between experimental and calculated reduced band-edge mode frequencies of the photonic crystal. Lasing is shown on Figure 2b using $P_{\text{in}} - P_{\text{out}}$ light emission curves at 15 K, 35 K and 60 K. Thresholds were measured at 227 kW/cm^2 at 15 K to 340 kW/cm^2 at 60 K [5].

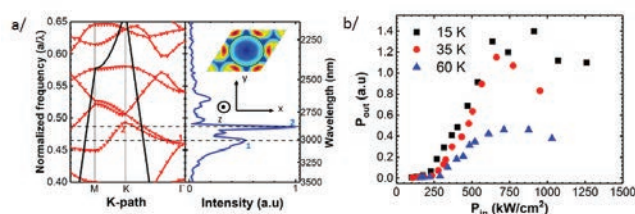


Figure 2: a/ TE-like band structure (left) of the hexagonal photonic crystal. The spectra at the threshold excitation is plotted at the right side to compare with the simulation results. Leaky band-edge mode is denoted 1, while guided band edge mode below the light lines (lasing mode) is denoted 2, b/ $P_{\text{in}} - P_{\text{out}}$ characteristics of our PC membrane at 15 K (black), 35 K (red) and 60 K (blue).

Perspectives

Our results confirm the robustness of GeSn optical gain for lasing applications, despite a high surface/volume ratio of the photonic crystal membrane. Surface passivation and carrier confinement using SiGeSn/GeSn heterointerfaces and/or multi-layer structures will be later used to enhance the $\text{Ge}_{1-x}\text{Sn}_x$ radiative recombination efficiency.

HYBRID III-V/Si DFB LASER INTEGRATION ON A 200 MM FULLY CMOS-COMPATIBLE SILICON PHOTONICS PLATFORM

AUTHORS:

B. Szelag, K. Hassan, L. Adelmini, E. Ghegin, Ph. Rodriguez (DTSi), S. Bensalem (ST Microelectronics), F. Nemouchi (DTSi), T. Bria, M. Brihoum (ST Microelectronics), P. Brianceau (DTSi), E. Vermande (DTSi), O. Pesenti (DTSi), A. Schembri (DTSi), R. Crochemore (DTSi), S. Dominguez (DTSi), M.C. Roure (DTSi), B. Montmayeul (DTSi), L. Sanchez (DTSi), C. Jany

ABSTRACT:

In this work we demonstrate the first integration of a hybrid III-V/Si laser in a fully CMOS compatible 200mm technology. Device with SMSR up to 50 dB and a maximum output power of 4mW coupled in the waveguide have been measured. The fabrication flow is fully planar and compatible with large scale integration silicon photonics circuit. The conventional Au-based contacts used in III-V laser are replaced by Ni-based alloyed contact with no penalties on the series resistance

Context and Challenges

Silicon photonics platforms are becoming more and more mature with competitive devices suitable for increasing needs of HPC (High Performance Computing) systems and datacenters. However, compared to bulk III-V technologies, Si photonics technologies are suffering from the lack of integrated light source. Several works have been done in the past years to integrate laser on silicon using III-V direct bonding on top of patterned silicon. Although, these demonstrations relied on CMOS-compatible process for the silicon part, all the process steps following the introduction of the III-V material were carried out with small wafer diameter III-V fabrication lines [1]. With such integrations, the cost advantage of silicon photonics based on the use of CMOS platforms and large wafer format is no more valid. It is therefore necessary to propose the same kind of III-V on silicon hybrid device integration using CMOS compatible technology on 200 or 300mm wafer.

Main Results

In this work we present, to the best of our knowledge, the first monolithic integration of a fully CMOS compatible hybrid DFB laser on a 200mm silicon photonics platform is demonstrated. A damascene process is used to locally increase the silicon thickness in order to have the 500nm thick silicon layer needed for the hybrid laser. This approach leads to a modular integration scheme, the laser being really an optional device of the overall platform, keeping the same silicon substrate with or without laser integration. The novelty here also relies on the use of innovative laser electrical contacts which do not contain any noble metals such as gold and for which integration "lift-off" based process are prohibited [2]. Thanks to these properties, the contacts are using a planarized BEOL and are CMOS-compatible both in terms of composition and integration scheme. Figure 1 is showing a tilted SEM picture of the device before encapsulation and an optical top view of the device under test.

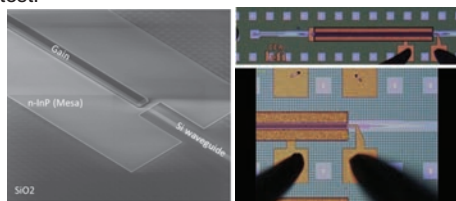


Figure 1: Tilted SEM view of the III-V/Si DFB laser after the III-V patterning steps (left). Optical microscope views of the Hybrid III-V/Si DFB laser under test probe (right)

A typical laser spectrum is shown in Fig. 2 reflecting its single-wavelength laser operation. A Side Mode Suppression Ratio (SMSR) of 50 dB has been measured, proving the good spectral purity of this laser. The laser central wavelength is 1300nm, slightly shifted vs. the optimum of the output grating coupler (see insert of Fig 2) which add a noticeable power penalty to the fiber.

The typical output power measured in the single-mode fiber is in the range of 150μW (maximum 400μW). Taking into account the grating coupler loss, it corresponds to a typical output power of 1.5mW coupled in the silicon waveguide (maximum 4mW). The lasing threshold current is stable between 50mA and 65mA. The series resistances are in the range of 10Ω which is in line with device fabricated with non-CMOS compatible process and materials. These results therefore validate the integration and the choice of fully CMOS-compatible Ni-based alloys as III-V metallization.

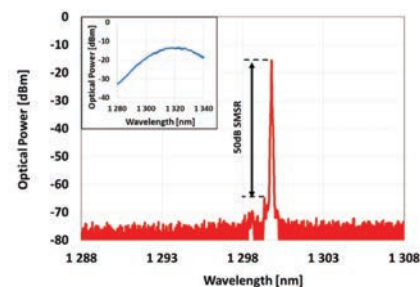


Figure 2: Laser spectrum at 160 mA injection currents. In insert is the transmission test of the grating couplers used as output of the laser. Peak wave length is at 1320nm. Around 10 dB loss per grating are measured at 1300nm

Perspectives

The monolithic integration of a fully CMOS compatible hybrid DFB laser on a 200mm silicon photonics platform is demonstrated. Only CMOS compatible process are used resulting in a fully planarized technology on which a multi metal level BEOL can be fabricated for large scale integration. The conventional Au-based contacts used in III-V laser are replaced by Ni-based alloyed contact with no penalties on the series resistance. Future works will concern the implementation of optimized designs taking into account the use the amorphous silicon to improve the emitted power level. Two metal levels routing will also be used to improve the current driving capabilities and reduce furthermore the series resistance.

Acknowledgment

The research leading to these results has received funding from the French national program 'programme d'Investissements d'Avenir, IRT Nanoelec' ANR-10-AIRT-05

RELATED PUBLICATIONS:

- [1] H. Duprez et al, Optic Express Vol. 23, Issue 7, pp. 8489-8497 (2015)
- [2] E. Ghegin et al, IEEE ITC/AMC conference, May 2016

DIRECT MODULATION ENHANCEMENT OF HYBRID III-V ON SILICON LASERS WITH SILICON RING FILTERS FOR CHIRP MANAGEMENT

AUTHORS:

K. Hassan, S. Malhouitre, S. Olivier
V. Cristofori, F. Da Ros, Y. Ding, L. K. Oxenløwe (DTU)
O. Ozolins, X. Pang (NETLAB)
M. E. Chaibi, L. Bramerie, Chr. Peucheret (FOTON)
A. Shen, A. Gallet, G.-H. Duan (III-V Lab)

S. Popov, G. Jacobsen (KTH)

ABSTRACT:

The use of a micro-ring resonator (MRR) to enhance the modulation extinction ratio and dispersion tolerance of a directly modulated laser is experimentally investigated with a bit rate of 25 Gb/s as proposed for the next generation data center communications. The investigated system combines a 11-GHz 1.55- μm directly modulated hybrid III-V/SOI DFB laser realized by bonding III-V materials (InGaAlAs) on a silicon-on insulator (SOI) wafer and a silicon MRR also fabricated on SOI. Such a transmitter enables error-free transmission (BER < 10⁻⁹) at 25 Gb/s data rate over 2.5-km standard single mode fiber without dispersion compensation nor forward error correction.

SCIENTIFIC COLLABORATIONS: DTU, NETLAB, FOTON, III-V LAB, KTH

Context and Challenges

The traffic in data centers has been steadily growing to fulfill the ever increasing customer demand and this has pushed research towards finding energy- and cost-effective solutions capable of reaching modulation speeds higher than the current standard of 10 Gb/s [1]. Transmission at 25 Gb/s over standard single mode fiber (SSMF) has been proposed as next target to be included in the IEEE 802.3 standard. In this perspective, directly modulated lasers (DMLs) have been recognized as good candidates to address these needs. We show in this work the enhancement of modulation speed of DMLs obtained with a silicon ring resonator filters.

Main Results

We report on an all-on-silicon transmitter operating at the target bit rate of 25 Gb/s. This is achieved by combining a directly modulating III-V/Si hybrid DFB laser and an optimized silicon MRR filter [2].

The hybrid III-V on silicon laser was fabricated on a 200-mm CMOS line starting with SOI wafers having a silicon top layer thickness of typically 440 nm. A patterning of the silicon is performed in order to define all the passive circuitry, including Bragg gratings used to realize an hybrid distributed feedback laser (DFB) cavity. In parallel, a 2" InP wafer containing multiple quantum well layers is grown. Next this III-V gain material is subsequently bonded onto the silicon wafer through molecular bonding, prior to the III-V patterning (gain, mesa, and electrical contacts). The fabricated laser is ready for wafer level probe testing using silicon vertical grating coupler as access for the optical probe. For this demonstration, a silicon micro-ring resonator (MRR) was realized on a second chip, as depicted in the Figure 1. The MRR parameters were optimized numerically in order to maximize the optical modulation amplitude (OMA) of a 25-Gb/s signal affected by transient and adiabatic chirp after filtering it, with free spectral range (FSR) of 100 GHz. The FSR value was chosen to potentially allow for simultaneous filtering of multiple FSR spaced WDM channel in a $N \times 25$ Gb/s laser array.

The dynamic characterization setup is shown in Fig. 1. The hybrid III-V/Si DFB laser was biased at 138 mA and directly modulated at 25 Gb/s with a 27 -1 non-return-to-zero (NRZ) pseudo-random binary sequence (PRBS) generated by a bit pattern generator with a peak-to-peak voltage of 3.4 V.

After direct modulation, the optical signal was coupled to the silicon MRR for ER enhancement through optical filtering. The laser bias current was adjusted to match the MRR resonance for suppression of the low-frequency content of the modulated optical spectrum.

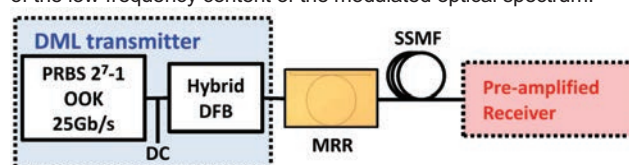


Figure 1: Experimental setup for dynamic characterization of the DFB laser at 25 Gb/s.

After ER enhancement by the MRR, the optical signal was transmitted over up to 2.5 km of SSMF and received by a standard preamplified receiver connected to an error analyzer for bit-error ratio (BER) measurements and to a sampling oscilloscope for eye diagram monitoring. The recorded eye diagrams are shown in Fig. 2. Considering first the back-to-back (B2B) scenario, it is possible to observe how the modulation ER is enhanced by the suppression of the signal '0' level by the MRR. The '0' level decreases getting closer to the yellow dashed line showing the oscilloscope ground level. This corresponds to an enhanced eye opening and an improvement in the ER from 3.8 dB to 6.8 dB.

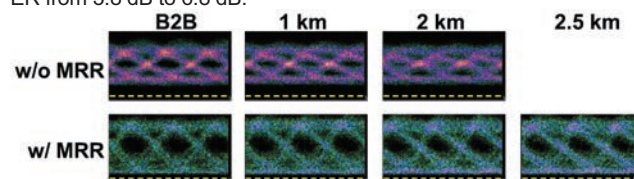


Figure 2: Eye diagrams of the 25 Gb/s signal for back-to-back and after transmission over 1, 2 and 2.5 km of SSMF with and without MRR filtering.

It is clear how the MRR filtering also enhances the signal dispersion tolerance. In fact, even if the dispersion effects are visible in all the eye diagrams, for the MRR filtered signal the eye remains open for a transmission distance up to 2.5 km

Perspectives

As both DFB laser and MRR have been fabricated on the SOI platform, combining the two devices can provide a compact all-silicon transmitter suitable for data center applications [3].

RELATED PUBLICATIONS:

- [1] V. Cristofori et al., "1.5- μm Directly Modulated Transmission over 66km of SMF with an Integrated Hybrid III-V/SOI DFB Laser", in Proc. of Group IV Photonics (GFP), 2017 IEEE 14th International Conference on.
- [2] V. Cristofori et al., "25-Gb/s Transmission Over 2.5-km SSMF by Silicon MRR Enhanced 1.55- μm III-V/SOI DML," IEEE PHOTONICS TECHNOL. LETT. **29**(12), June 2017
- [3] A. Gallet et al., "Hybrid III-V on Silicon Integrated Distributed Feedback Laser and Ring Resonator for 25Gb/s Future Access Networks", IEEE JLT **36**(8), April 2018

DEMONSTRATION OF A SILICON PHOTONICS BASED OPTICAL NETWORK UNIT FOR FTTH/PON

AUTHORS:

S. Bernabé, B. Charbonnier, S. Menezo, S. Bernabé, M. Fournier, B. Blampey, S. Straullu (ISMB, Torino), E. Temporiti (STMicroelectronics), J. Lee (Tyndall UCC), R. Gaudino (ISMB, Torino), S. Abrate (ISMB, Torino)

ABSTRACT:

Within the European project FABULOUS, we achieved the transmission experiments of a self-coherent reflective PON (Passive Optical Network), demonstrating 500 Mbps per user with a power budget of 24 dB in off-line processing and 21 dB in real-time. The transceiver module, aiming at being implemented in a Fiber To The Home (FTTH) Optical Network Unit (ONU), integrates a Silicon Photonics Circuit with a dedicated driver Electronic chip.

SCIENTIFIC COLLABORATIONS: Instituto Superiore Mario Boella, Torino, Italy ; Dipartimento di Elettronica e Telecomunicazioni, Politecnico di Torino, Torino, Italy ; Tyndall National Institute, Cork, Ireland; Università degli Studi di Pavia, Pavia, Italy

Context and Challenges

Fiber-To-The-Home (FTTH) Networks are among the most challenging applications for optoelectronic modules in term of integration and mass manufacturability. The FABULOUS European Project proposes a novel Optical Network Unit (ONU) for such Networks, relying on Silicon Photonics (SiPho) Circuits and dedicated driving CMOS electronics hybrid Integration, using flip-chip.

The architecture has already demonstrated, with discrete optical components and the off-line processing approach, to be capable of granting an aggregate capacity of 32 Gbps per wavelength compatible with new standards like XG-PON ODN class N2. Within the FABULOUS project, an integrated SiPho module has been demonstrated.

Main Results

The tested demonstrator is made of a Silicon Photonics circuit with a Reflective Modulator, enabling Frequency Division Multiple Access (FDMA) transmission. The required CMOS driver has been designed and manufactured by ST Microelectronics, while the SiPho Circuit has been designed and manufactured by CEA-LETI's 200nm Silicon Photonics platform, using SOI (Silicon-On-Insulator) wafers. It is made of a Reflective Mach Zehnder Modulator (R-MZM) with segmented electrodes, exhibiting a V_{π} -L π of 2 V·cm and an E/O bandwidth of 20 GHz when biased at -1 V [1].

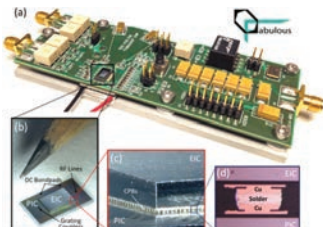


Figure 1: the packaged FABULOUS module (a), with Zoom-in of the optical engine (b), Further zoom-in showing the many discrete copper pillar bumps used to interconnect the driver to the SiPho circuit (c), and Microscope image of the copper pillar cross section (d)

RELATED PUBLICATIONS:

- [1] S. Menezo et al., "Transmitter Made up of a Silicon Photonic IC and its Flip-Chipped CMOS IC Driver Targeting Implementation in FDMA-PON", *J. Lightw. Technol.*, vol. 34, no. 10, pp. 2391–2397, May 2016..
- [2] S. Straullu et al., "Demonstration of a Partially Integrated Silicon Photonics ONU in a Self-Coherent Reflective FDMA PON," *Journal of Lightwave Technology*, vol. 35, no. 7, pp. 1307–1312, 2017.

The SiPho circuit was hybrid assembled with the driver using a flip-chip assembly method with interconnects made of Copper pillars. The resulting optical engine has been packaged by UCC Tyndall to form a testable module, made of a PCB with front-end electronics, and with temperature stabilization provided by a thermo-electric cooler (Figure 1). Optical Fibers have been aligned and glued to the SiPho circuit to enable system level tests (Figure 2), with two FPGA emulating a Central Office and a Network User.

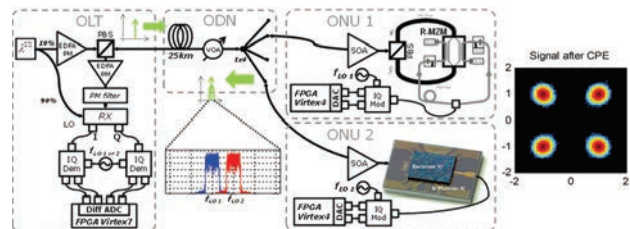


Figure 2: FABULOUS real-time experimental setup (left), with the measured constellation at 300MBd QPSK (right)

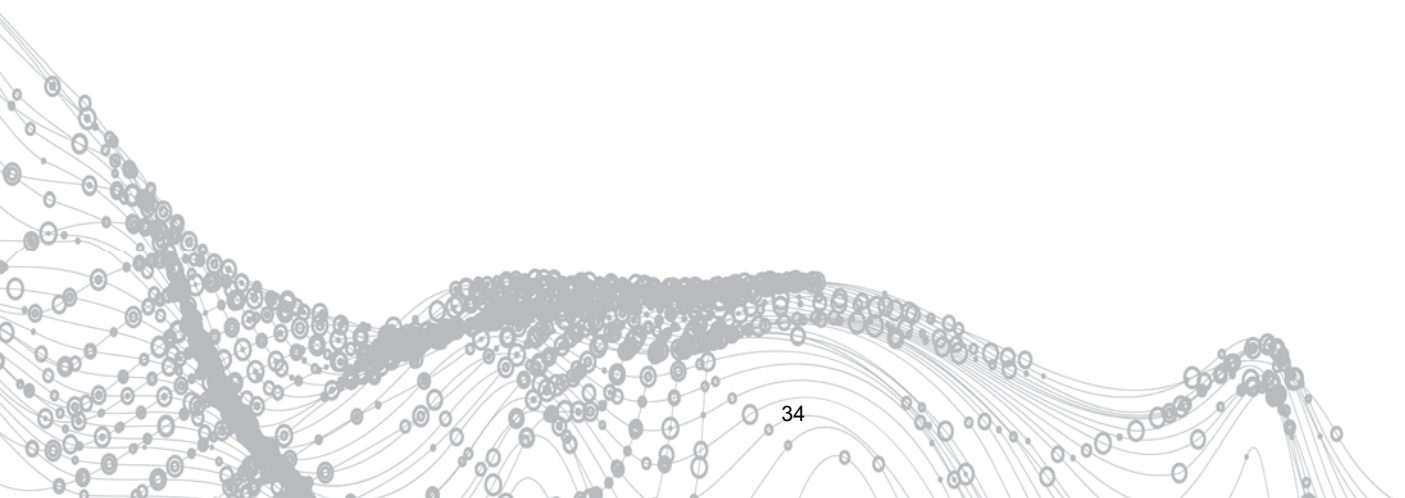
We demonstrated the feasibility of a reflective ONU with an unprecedented level of optical integration, achieving 300 MBaud QPSK transmission [2] leading to a useful resulting bit-rate of 500 Mbps per user. The use of QPSK provides more robustness with respect to the laser linewidth, which can be a sensitive parameter in this system.

Perspectives

For the first time, an integrated Silicon MZM is operated in real time over the FDMA PON proving that the different important features demonstrated with discrete components (reflective polarization insensitive carrier suppressed modulation) can be obtained at low cost and high production volume with a fully integrated silicon ONU. This experiment assesses Silicon Photonics as a promising technology, for next generation Passive Optical Networks, especially future standards requiring higher bandwidth and data rate per user (e.g. 25 Gbps PON) and also for future Central Office to Base Station optical interconnects in 5G Networks.



CEA-Leti/Denis Morel





O5

OPTICAL SENSORS

- **Si nanostructured μ -hotplates**
- **Si photoacoustic cell analyze multiple gases**
- **Mid-infrared photonic integrated circuits**

NANOSTRUCTURATION OF A SUSPENDED HOTPLATE: IR-EMISSION EFFICIENCY MULTIPLIED BY 2.

AUTHORS:

P. Barritault, E. Lorent, S. Boutami, A. Lefebvre

ABSTRACT:

In this letter, we present an IR emitter based on a freestanding hotplate coated with an array of tungsten nanostructures. The characterization of this hotplate, which follows its manufacturing in Leti's facilities, demonstrates a two-fold gain in the electrical to optical efficiency at the target wavelength of 4.26 μm . This IR emitter, when used as the μSource of a CO₂ NDIR based sensor, greatly helps reducing the power consumption of the sensor. This is of key importance in order to obtain the autonomous sensors required in Air Quality Monitoring. We are further developing this type of solution for the startup eLichens our joint lab partner.

SCIENTIFIC COLLABORATIONS: this work was supported by the National Research Agency (ANR) via project IDEE.

Context and Challenges

In the field of Air Quality control, a common solution to monitor certain gas, such as CO₂, is based on the measurement of IR gas absorption; the so-called Non Dispersive Infra-Red (NDIR) Sensors. These sensors need to be autonomous, and thus to have a low power consumption. Most often, the IR source used, a black body, has the biggest contribution in terms of power consumption, and therefore, increasing the IR source efficiency is particularly relevant to obtain an autonomous sensor. We present below a μSource IR emitter, developed at Leti [1], with an improved efficiency.

Main Results

This μSource is a freestanding hotplate, consisting in a micro-structured conductive track sandwiched between two dielectric layers. By applying a current through the track, Joule effect heats the membrane at a typical temperature of 650 °C thus enabling IR emission.

More recently, we were able to improve significantly the efficiency of the source by only adding a few steps to the standard μSource process. We have implemented on top of the μSource an array of tungsten squares (width 700 nm, thickness 100 nm and pitch 2.5 μm). This stack forms a so-called Metal-Insulator-Metal (MIM) resonant structure. The μSource when heating will emit light more specifically at a resonant wavelength, which in our case corresponds to the CO₂ maximum absorption: 4.26 μm .

We manufactured the nanostructured $\mu\text{Sources}$ in Leti's facilities on 200mm wafers. In Figure 1, we present a photography of the μSource along with a MEB image of the W-nanostructures.

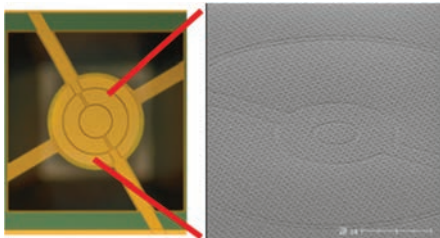


Fig. 1: μSource released (left) and W nanostructurations (right)

The $\mu\text{Sources}$ IR emission spectra were then measured showing the MIM resonance effect (see Figure 2): for the same input electrical power, a two-fold gain, at 4.26 μm , is obtained for nanostructured sources as compared to non-nanostructured ones.

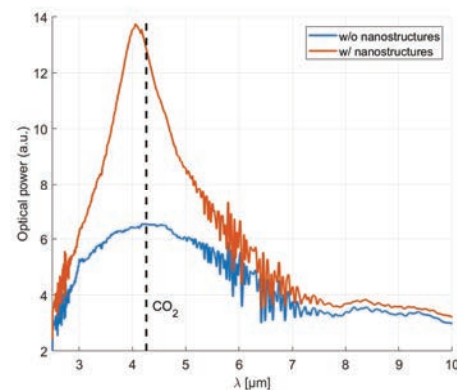


Fig. 2: Infrared spectrum of $\mu\text{Sources}$

Let us add that it is possible to tune the resonance wavelength or enlarge its width by modifying the dimensions of the nanostructures. Finally, in order to evaluate the dispersion over a wafer, we measured the electrical and optical (@ 4.26 μm) characteristics of the $\mu\text{Sources}$ on an automatic prober. The fab yield measured is over 90% and the dispersion on optical power is below 10%. This last point is encouraging since it shows that the dispersion on the W-dots width, inherent to technological process, has a limited impact on the optical properties of the source.

Perspectives

We are currently pursuing this work through our joint lab with the start-up elichens [2]. The goal is to increase the process maturity before transferring it to a foundry. The next step will be to process nanostructured $\mu\text{Sources}$ along with a Vacuum Wafer Level Packaging (WLP). This will reduce by 20-folds the electrical consumption of the source, for the same output optical power.

RELATED PUBLICATIONS:

- [1] A. Lefebvre et al., "CMOS compatible metal-insulator-metal plasmonic perfect absorbers," Optical Materials Express, vol. 6, no. 7, p. 2389, Jul. 2016.
- [2] <http://www.elichens.com/fr/>

PHOTOACOUSTIC CELL ON SILICON FOR MID-INFRARED QCL BASED MULTIGAS SPECTROSCOPIC ANALYSIS

AUTHORS:

J.-G.Coutard, A.Gliere, J.-M.Fedeli, O.Lartigue, J.Skubich, L.Duraffourg, G.Aoust (mirSense), M.Carras (mirSense)

ABSTRACT:

Photoacoustic cells are one type of optical sensors that can be used to detect gas traces. The photoacoustic spectroscopy technique is based on the absorption of photons by the molecules of interest and the subsequent creation of acoustic waves. Our new miniature silicon-based photo-acoustic cell combined with a quantum cascade laser exhibited high performance sensitivity. This new generation of photoacoustic cell open the gate to a cost effective sensor and mass production market.

Context and Challenges

PhotoAcoustic Spectroscopy (PAS) is one of the most sensitive techniques used to monitor chemical emission or to detect gas traces (A. Miklós, *et al.*, *Rev. Sci. Instrum.*, vol. 72, no. 4, pp. 1937–1955, Apr. 2001). In particular, in the Mid InfraRed (MIR), many gases of interest have their strongest absorption lines. We have demonstrated [1, 2] our centimetric PA-device can compete with bulky systems for multi-gas sensing without any compromises on performances. Today we have bring this technology on silicon enabling dramatic cost reduction and extreme integration of this high performance gas sensor.

Main Results

First, a complete new design has been achieved using Finite Element Modeling. Our acoustic model based on the Navier-Stokes equation taking in account the losses (surface, volume), enables to set the dimensions of the photoacoustic cell for maximizing performances.

The cells have been fabricated using our 200mm pilot line using standard processes (see figure 1).

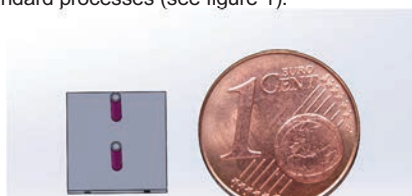


Figure 1: Scale of the miniPA cell

Several wafers have been released. We have tested single chips on our reference CO₂ test bench facility. The photoacoustic cells feature a very good matching with the simulation regarding the resonance frequency response (see figure 2).

Moreover the miniPA cell on silicon exhibits a sensitivity down to the ppm level in a gas flow.

RELATED PUBLICATIONS:

- [1] Coutard, J.G, Rouxel J. / Brun M. / Lartigue O. / Nicoletti S. / Badets F. / Carras M. / Gliere A. DEVELOPMENT OF A HIGH PERFORMANCE MINIATURIZED PHOTOACOUSTIC GAS SENSOR Laser Applications to Chemical, Security and Environmental Analysis (LACSEA)
[2] Rouxel, J., Coutard, J.-G., Gidon, S., Lartigue, O., Nicoletti, S., Parvite, B., Vallon, R., Zéninari, V., Glière, A. Miniaturized differential Helmholtz resonators for photoacoustic trace gas detection Sensors and Actuators, B: Chemical 236

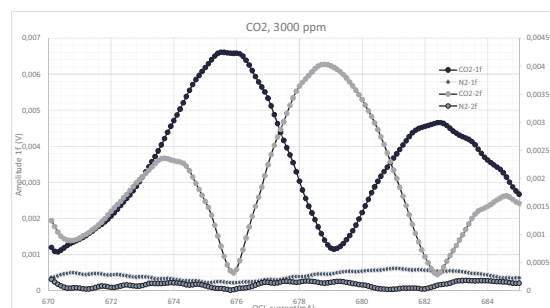


Figure 2: Photoacoustic wavelength modulation absorption spectroscopy with 1f and 2f detection on CO₂ absorption line at 2302 cm⁻¹.

Perspectives

The miniPA concept is being extended to an integrated multigas detector achieved in collaboration with the start-up mirSense (www.mirsense.com) under a joint laboratory (the multigas sensor from mirSense is shown in figure 3). We are focusing our development on the TRL improvement of this ultra-small cell assessing various conditions (temperature, hygrometric, aggressive gas, etc...).

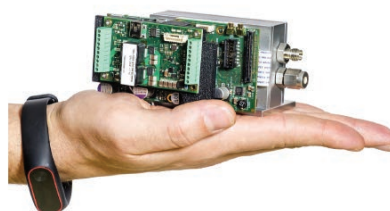


Figure 3: Picture of the compact QCL based sensor multiSense from mirSense

MID INFRARED PHOTONIC INTEGRATED CIRCUITS

AUTHORS:

J-M Fedeli, P Labeye, A Marchant, O Lartigue, M Fournier, J-M Hartmann (DTSi)

ABSTRACT:

For small gas system systems based on QCL arrays, we have developed two technology platforms for the fabrication of AWG with more than 35 inputs in the bands $3\mu\text{m}$ - $8\mu\text{m}$ and 8 - $12\mu\text{m}$ with SiGe₄₀ core clad with Si or Ge core clad with SiGe₂₀

Context and Challenges

Gas analysis in the Mid-Infra-Red wavelength region, also called the fingerprint region, allows to address a unique combination of fundamental absorption bands that are of orders of magnitude stronger than in the near IR. This feature enables highly selective, highly sensitive unequivocal identification of chemicals. Indeed, many molecules have strong and distinct absorption lines in the Mid-IR giving much interest to spectroscopic detection. With the recent progress in Quantum Cascade Laser (QCL) and Interband Cascade Laser (ICL) technologies, compact and reliable Mid-IR light sources are becoming available. In particular, specific emission wavelengths can be selected through Distributed FeedBack (DFB) QCLs in order to target the chemicals of interest.

Main Results

In this approach, the spectroscopic analysis uses a Mid-IR multi-wavelength source formed by an array of QCL lasers coupled to the multiplexer. This Photonic Integrated Circuit (PIC) is used to deliver each wavelength on a specific output. In order to address the 3 - $12\mu\text{m}$ QCL spectral range, our group developed two silicon photonics technologies. We designed Arrayed Wave Guide (AWG) type multiplexers using a fast design tool based on a Gaussian approximation of waveguide fundamental mode and Fourier diffraction optics. Dimension fluctuations were taken into account in order to guarantee a good fabrication reproducibility.

For the 3 - $8\mu\text{m}$ band, we selected a SiGe 40% core waveguide surrounded by Si. Basic passive devices (lines, bends, and splitters with Multi-Mode Interferometers) were first characterized in order to verify the quality of fabrication and to calibrate the testing apparatus. An ultra-low waveguide loss was estimated by the spirals method at 0.3 dB/cm . The Arrayed Wave Guide (AWG) presented a low loss normalized transmission (-1.6 dB) with a cross talk below -12 dB [1].

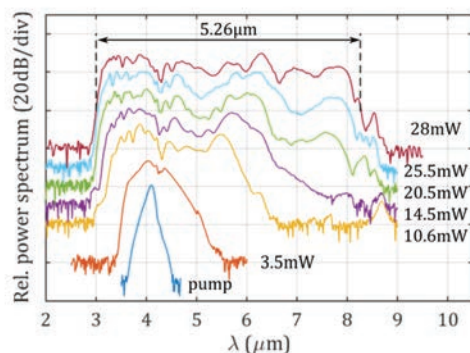


Figure 1: Output spectra measured at different coupled power of a SiGe/Si waveguide

In collaboration with the Institut des Nanotechnologies de Lyon (INL), excellent nonlinear properties have been measured, with the demonstration of an extended supercontinuum [2] (see Fig 1).

For the 8 - $12\mu\text{m}$ band, we chose a pure Ge core waveguide surrounded by SiGe 20%. As test device, we designed a 67 inputs multiplexer working close to $9.5\mu\text{m}$ (1050 - 1250 cm^{-1} range, with a spacing of 3 cm^{-1}) (see figure 2). The core layer of the waveguide is made of a $2.5\mu\text{m}$ thick Ge layer grown by RP-CVD on top of a thick SiGe 20% layer, which was deposited on a Si wafer. The definition of all the passive functions was performed by DUV 248nm photolithography. The Ge core layer was etched down to the SiGe layer underneath by deep reactive ion etching (DRIE) without any scalloping. To complete the fabrication, the Ge waveguides were fully embedded in $6\mu\text{m}$ thick epitaxial SiGe 20% layers. Input and output facets for the butt coupling of QCL were etched collectively on the wafers by DRIE. The spectral characteristics reported in figure 3 showed operation close to the simulation and adapted to the coupling to QCL laser arrays [3].



Figure 2: Image of an Ge AWG

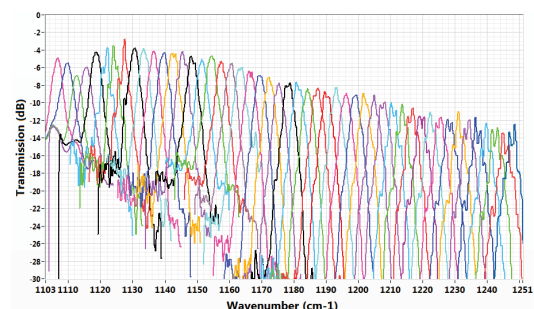


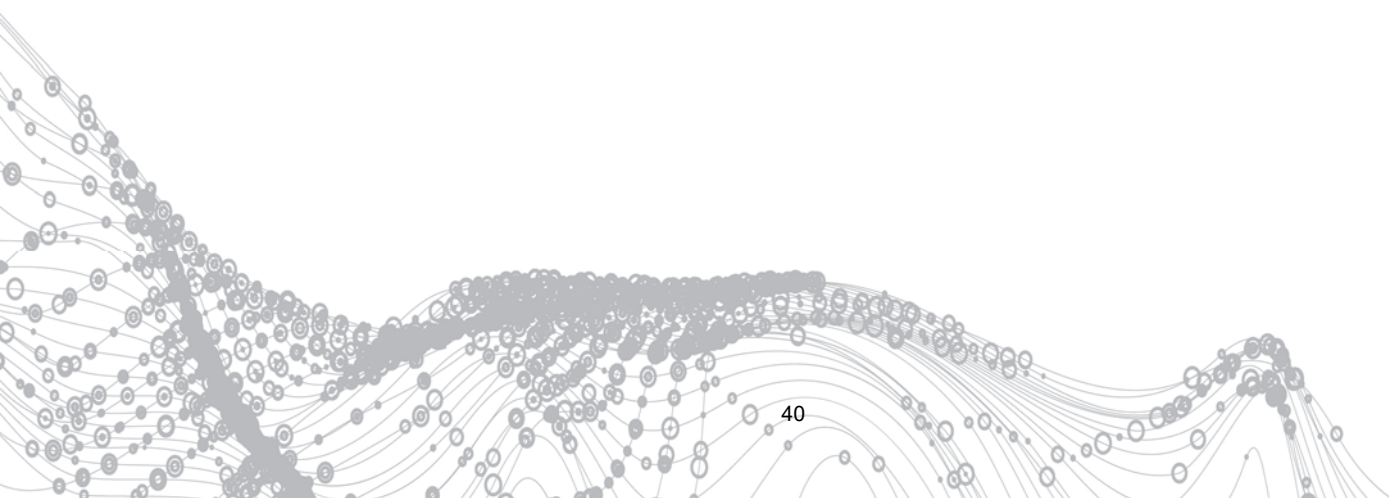
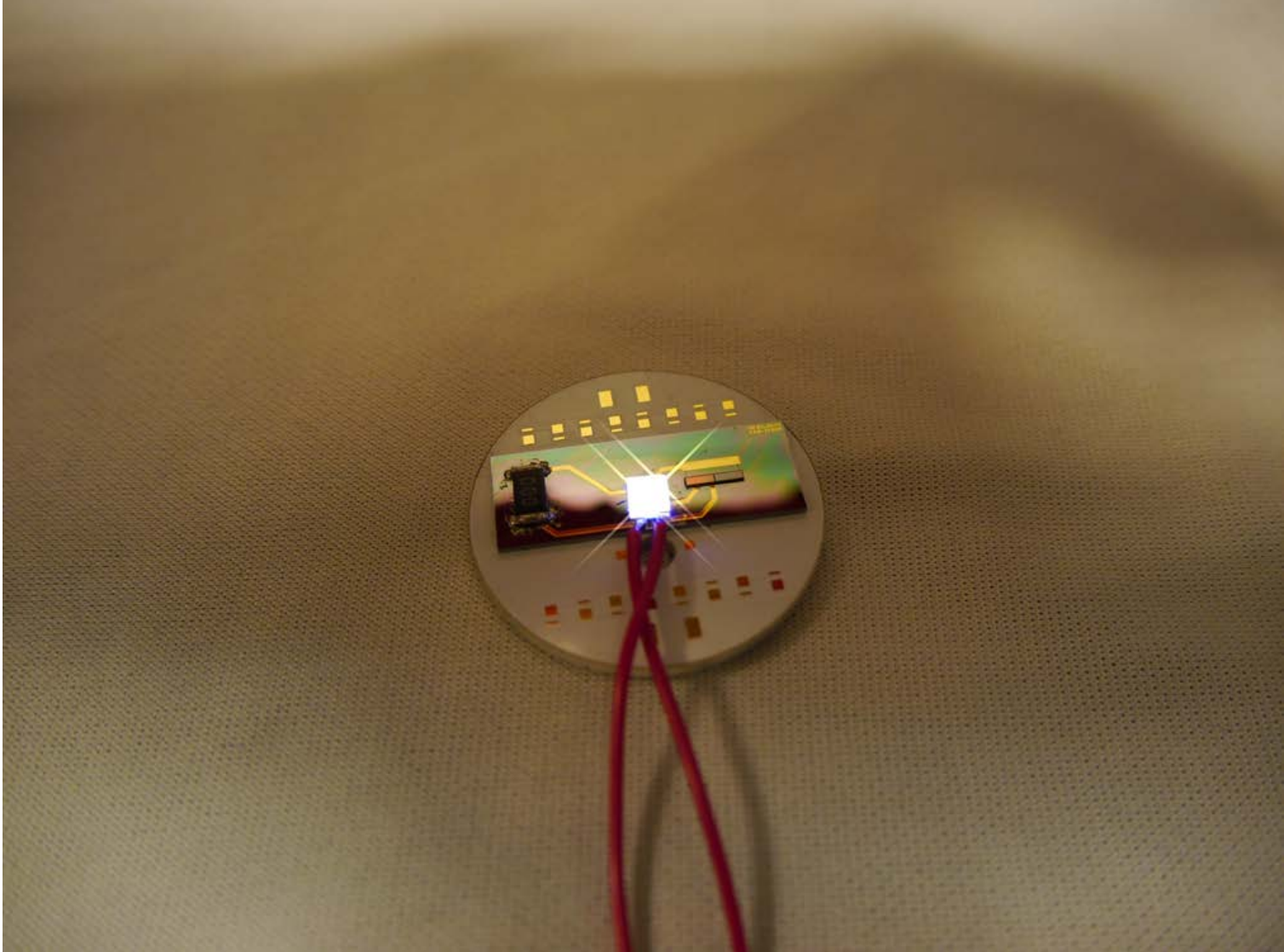
Figure 3: Partial spectral characteristic of the Ge AWG

Perspectives

These technologies are now offered to customer via the MIRPHAB pilot line [4]. Under new projects, more integrated devices will be searched as well as high performance non-linear ones.

RELATED PUBLICATIONS:

- [1] J. Favreau, J.-M. Hartmann, P. Labeye, J.-M. Fedeli, "Development of a SiGe Arrayed Waveguide Grating in the 2185 - 2285 cm^{-1} range" ECIO2017.
- [2] Milan Sinobad, Christelle Monat, Barry Luther-davies, Pan Ma, Stephen Madden, David J. Moss, Arnan Mitchell, David Allieux, Regis Orobitchouk, Salim Boutami, Jean-Michel Hartmann, Jean-Marc Fedeli, and Christian Grillet, "Mid-infrared octave spanning supercontinuum generation to $8.5\mu\text{m}$ in silicon-germanium waveguides," Optica 5, 360-366 (2018)
- [3] J.-M. Fedeli, P. Labeye, A. Marchant, O. Lartigue, M. Fournier, JM Hartmann, "Ge/SiGe photonic devices for the long mid-infrared", Proc. SPIE Photonics Europe paper 10686-21 (April, 2018)
- [4] MIRPHAB pilot line: <http://www.mirphab.eu/>





O6

SOLID-STATE LIGHTING

- **Size governs non-radiative losses in pixelated LEDs**
- **3D-stacked pixelated wireLEDs**

SHOCKLEY-READ-HALL AND AUGER NON-RADIATIVE RECOMBINATION IN GAN BASED LEDS: A SIZE EFFECT STUDY

AUTHORS:

F. Olivier, A. Daami, C.Licitra (DTSi), and F. Templier

ABSTRACT:

We investigate in this study the LED size influence on the radiative and non-radiative recombination [1]. The standard ABC model has been widely used to describe the efficiency of GaN based LEDs. Using this model, we extract A, B and C coefficients for various LED sizes showing how the competition between radiative and non-radiative recombination processes varies with LED geometry. Time-resolved photoluminescence allows us to determine coefficient B, related to radiative recombination. Through current-voltage-luminance characterizations we determine parameters A and C related to Shockley-Read-Hall (SRH) and Auger recombination. We find that coefficient A is strongly dependent on LED size, indicating a drastic effect of sidewall defects on the performances of LEDs. On the other hand, coefficient C is independent of LED size. This latter result demonstrates that efficiency droop does not depend on LED size.

Context and Challenges

GaN-based light-emitting diodes (LEDs) are very promising light sources for lighting and display applications. The growing interest for wearable devices and their numerous applications (augmented reality, head-up displays, etc.) have highlighted the need for high-performance micro-displays. Today's smaller pixel pitch in LED micro-displays is typically $10\mu\text{m}$ [2]. As a result, the comprehension of the relationship between size and performances of a LED is an important subject to tackle. LED efficiency is a competition between radiative and non-radiative recombinations. A common method to modelize such effects is known as the ABC model. In this work, we propose an extraction method to determine A, B and C coefficients, allowing the analysis of GaN-based LEDs efficiency, for different sizes ranging from 500×500 to $4\times 4\mu\text{m}^2$.

Main Results

According to the ABC model, the internal quantum efficiency (IQE) is expressed in terms of coefficients A, B, C and the carrier concentration n as:

$$\text{IQE} = \frac{B \cdot n^2}{A + B \cdot n^2 + C \cdot n^3} \quad (1)$$

while current density J is expressed as:

$$J = q \cdot w \cdot (A + B \cdot n^2 + C \cdot n^3) \quad (2)$$

where w is the total quantum wells thickness; and q is the elementary charge.

We here assume that Auger recombination is the cause of the efficiency droop. First, B has been calculated by plotting the normalized TRPL intensity decay curve at 5K. After extraction, we obtained a value of $B = 1 \times 10^{-11} \text{ cm}^3 \cdot \text{s}^{-1}$ which is in good agreement with literature values.

In order to extract coefficients A and C, we have performed IVL characterizations for various LED sizes, which allows to determine the external quantum efficiency (EQE), defined as:

$$\text{EQE} = \frac{P_{\text{opt}}}{P_{\text{in}}} = \frac{P_{\text{opt}}}{J \cdot A} = \text{IQE} \cdot \text{LEE}$$

where LEE is light extraction efficiency. We have determined a value of 14% for LEE for our structures. From above equation we can calculate the IQE for all measured devices.

Using expressions (1) and (2), we can express the carrier density n as:

$$n = \sqrt{\frac{(\text{IQE} \cdot J)}{(q \cdot w \cdot B)}}$$

Putting, $Y = 1/\text{IQE}$, $X = \sqrt{(\text{IQE} \cdot J)/(q \cdot w)}$, $\alpha = C/B^{3/2}$, and $\beta = A/B^{1/2}$ we obtain a simplified expression of IQE written as:

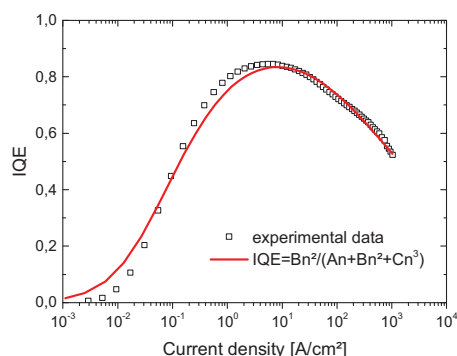
$Y = \alpha X + \beta/X + 1$. This equation implicitly shows that coefficient A (hence β), respectively C (hence α), will have an important effect at lower, respectively higher, current densities. Therefore the extraction of parameters A and C can easily be undertaken under different current density ranges by neglecting in equation

(6) one parameter or the other, which finally gives us two adjusting simple equations:

$$Y_{\alpha} = \alpha \cdot X_{\alpha} + 1 \quad \text{and} \quad Y_{\beta} = \beta/X_{\beta} + 1 \quad \text{where } \alpha \text{ and } \beta \text{ are related to high, respectively low, current densities.}$$

Following the adjustment with above equations we can determine coefficients A and C. We have determined values of $A = 3.7 \times 10^6 \text{ s}^{-1}$ and $C = 2.6 \times 10^{-31} \text{ cm}^6 \cdot \text{s}^{-1}$, for a typical LED size of $100 \times 100 \mu\text{m}^2$. These extracted values are in good agreement with those published for InGaN/GaN blue LEDs for both A and C values

We plot on the figure below the experimental IQE data of the $100 \times 100 \mu\text{m}^2$ sized LED and its adjustment by the ABC model after determining all coefficients. We obtain a good fit of all data in all current ranges. At low current density, the small mismatch between experimental data is mainly attributed to the experimental error in the measurement of very low optical power mainly due to intrinsic dark current of the measuring photodiode.



With parameters A, B and C fixed, we can now get back to the carrier concentration at each current density level, using equation (5). This gives us values ranging from $6 \times 10^{15} \text{ cm}^{-3}$ to $3 \times 10^{19} \text{ cm}^{-3}$, which is in accordance with typical values of carrier density in GaN LEDs

Perspectives

In summary, we have determined recombination coefficients of the ABC model on different LED sizes by IVL and TRPL measurements. Parameter B is calculated from time resolved photoluminescence decay through the measurement of carrier lifetime at 5K, while parameters A and C are determined by a simple extraction method based on IVL characterization. This model is particularly well suited for the study of GaN-based LEDs size effect. We have shown that non radiative SRH-like recombination is related to the LED perimeter and intensifies as LED size decreases. Meanwhile, coefficient C generally related to Auger effect, has been found to be a constant whatever the pixel size is, proving that efficiency droop is mostly related to the quality of the InGaN/GaN epitaxy

RELATED PUBLICATIONS:

[1] Francois Olivier, Anis Daami, Christophe Licitra, and Francois Templier, "Shockley-Read-Hall and Auger non-radiative recombination in GaN based LEDs: a size effect study", Appl. Phys. Lett. 111, 022104 (2017); doi: 10.1063/1.4993741,

[2] F. Templier, "GaN-based emissive microdisplays: A very promising technology for compact, ultra-high brightness display systems," J. Soc. Inf. Disp., vol. 24, no.

11, pp. 669–675, 2016

3D STACK HIGH VOLTAGE WIRELEDS : INVESTIGATIONS ON THERMAL, PROCESS DEVICE AND PACKAGING ISSUES

AUTHORS:

B. Chambion, B. Bouillard, A. Gasse, A. Vandeneynde, N. Ait-Mani, A. Gueugnot, B. Bouillard, M. Volpert, B. Soulier, D. Henry, F. Mercier (ALEDIA), P. Rueda (ALEDIA), V. Beix (ALEDIA), T. Lacave (ALEDIA)

ABSTRACT:

A 3D-stacked pixelated wireLED flip chip bonded onto a dedicated ASiC is proposed to target a direct high voltage AC LED. A vehicle test has been first fabricated to study the thermal impact of the bumping pattern with both finite element modelling and IR measurements. The experimental results were compared to the modelling and proved the reliability of the model. Finally a functional wireLED device based on the same vehicle test has been produced, in which lines of wireLED pixels may be driven separately in series. This work pave the way to enable efficient and compact 230V direct AC LEDs

Context and Challenges

Solid State Lighting systems need compact and reliable packaging technologies to be implemented. A 3D-stacked pixelated wireLED flip chip bonded onto a dedicated ASiC is proposed to target a direct high voltage AC LED. The high voltage wireLED is flip chip bonded on a dedicated ASiC. With this we reach a high level of packaging integration into a 6.7*3.9*1 mm package, directly pluggable on 230 volts AC power supply. However in this configuration the thermal management of the package becomes crucial

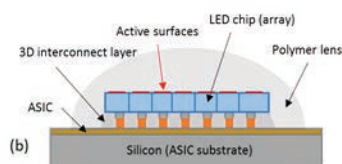


Figure 1: 3D-stacked pixelated LED array on ASiC

In this work, we present the major thermal management issues with thermal modelling and experimental characterizations on a dedicated vehicle test [1]. Flip chip interconnection has been implemented as well and a functional lighting demonstrator has been obtained [2].

Main Results

For the thermal study, we have tested various solder bumping patterns with a dummy thinned silicon die (thermal load) on a dedicated readout circuit.

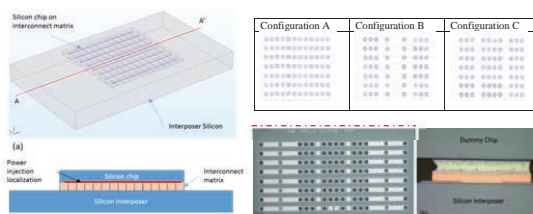


Figure 2: Vehicle test architecture (left) and Si interposer top view in bump configuration C with cross section view of a macro copper SnAg solder pillar (right).

RELATED PUBLICATIONS:

- [1] B. Chambion, B. Bouillard, A. Gasse, A. Vandeneynde, N. Ait-Mani, A. Gueugnot, D. Henry, F. Mercier, P. Rueda, *Experimental and modelling thermal study of a 3D-stacked silicon based LEDs array concept*, 23rd International Workshop on Thermal Investigations of ICs and Systems (THERMINIC), 27-29 SEPTEMBER 2017, AMSTERDAM.
- [2] A. Aitmani, B. Bouillard, A. Gasse, M. Volpert, B. Soulier, D. Henry, A. Vandeneynde, B. Chambion, F. Mercier, P. Rueda, V. Beix, T. Lacave, *High Voltage WireLED powered directly by mains 230 Volts*, EMPC 2017, 10-13 September 2017, Warsaw University of Technology, Poland.

Along the red line (figure above) are some pixels with and without bumps, which strongly impacts thermal dissipation. Comparing finite element modelling with IR measurement, we exhibit a good agreement with only 11 % difference located in the "no bump" area.

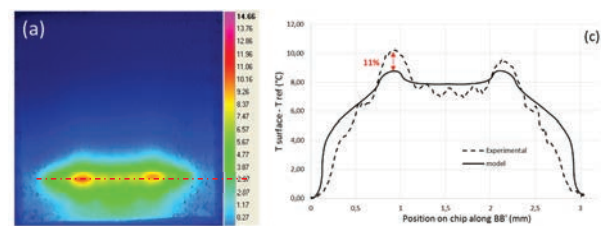


Figure 3: Comparison between IR measurement and simulation

We have also implemented wireLEDs on the same vehicle test where pixel LEDs line can be driven separately or in series to target 230 V.

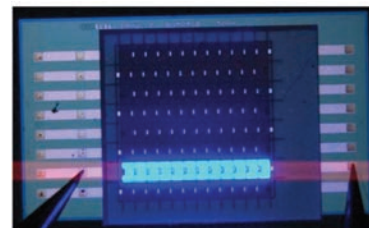
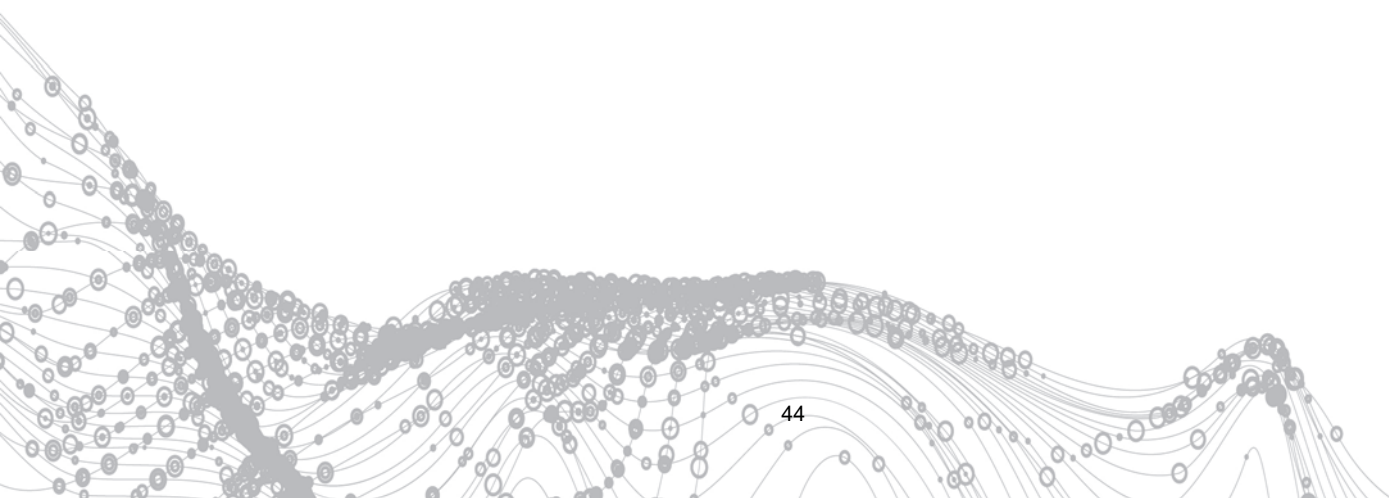
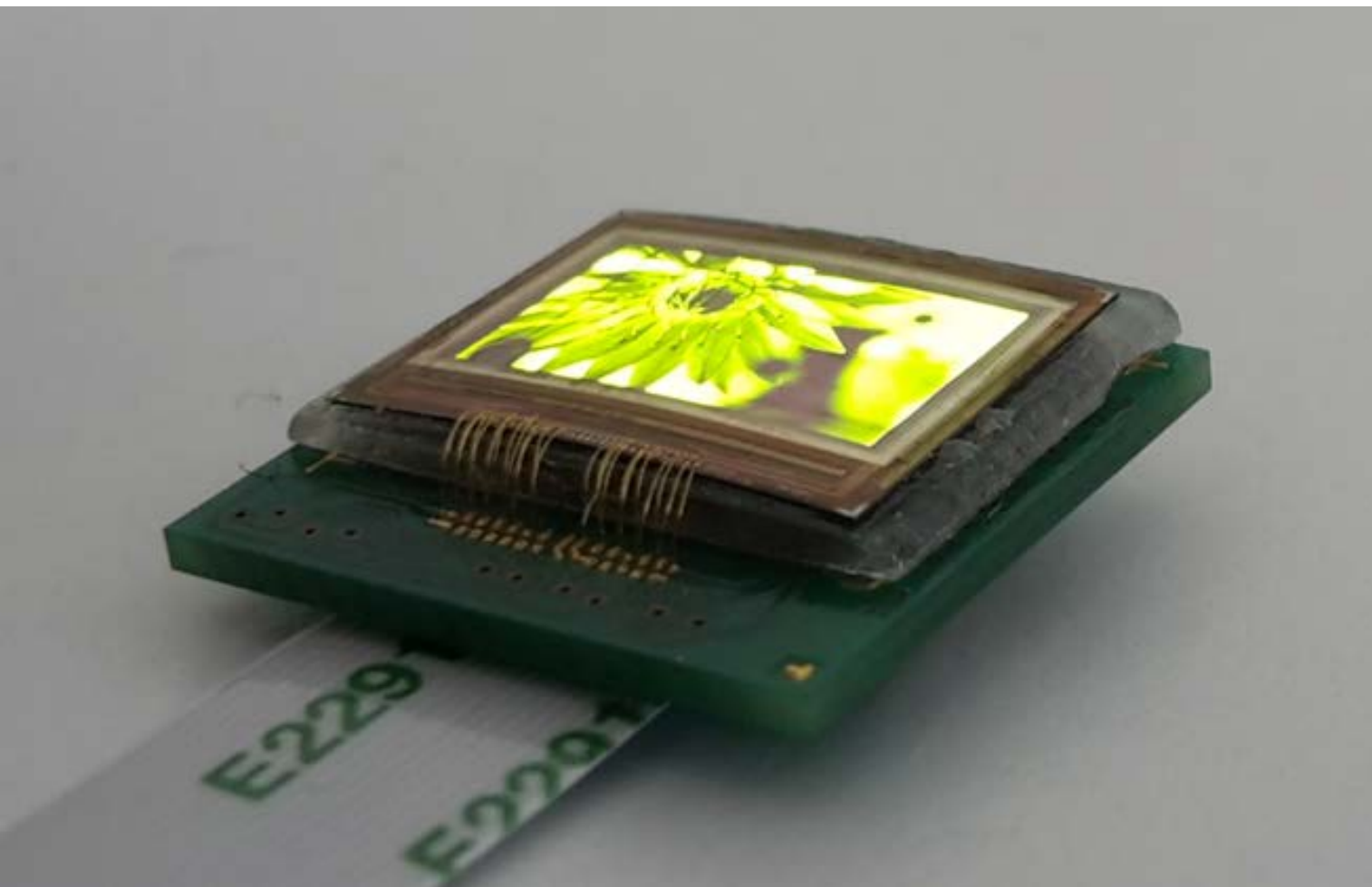


Figure 4 : Probe testing of a functional wireLEDs pixel line on a 3D stack

Perspectives

Next to this reliable thermal modelling of a 3D stack and first wireLEDs lighting demonstration, we will transfer the process to a dedicated ASiC enabling to drive the LED pixel lines in accordance with a 230V direct AC.





O7

DISPLAY COMPONENTS

- Intraocular projection display
- High-resolution GaN LED μ -display
- Thin-film packaging of OLED μ -displays
- Curved OLED μ -displays
- In-plane-switching liquid-crystal modulator matrix

HOLOGRAPHIC RECORDING SETUP FOR INTEGRATED SEE-THROUGH NEAR-EYE DISPLAY EVALUATION

AUTHORS:

Chr. Martinez, V. Krotov, D. Fowler

ABSTRACT:

We present a design of a hologram recording setup used to evaluate a concept of near to eye see through display. Our goal is to record a set of hologram element distributions related to a given image pixel orientation sequence. The recovery of the hologram should project a static image into the eye by a self-focusing effect.

Context and Challenges

Holographic optical Elements (HOE) are often used in see through devices due to the spectral selectivity of the hologram. Bragg selectivity allows the coding of optical function at a specific wavelength without jeopardizing the device transparency on the remaining visible spectrum. Various schemes have been developed for Augmented Reality displays based on holography (C. Jang et al., *Appl. Opt.* 55, A71-A85 (2016)).

The concept we propose is based on a coherent integral imaging scheme and on the use of 2D waveguides. The role of the hologram is to produce a distribution of emissive points that direct a wave front at a specific angle towards the eye. The image is then formed by a self-focusing effect into the eye [1]. As a general problem in holographic devices, the recording set up has to be carefully designed in order to produce the required interference distribution in a configuration as close as possible to the real device implementation.

We have designed a free space holographic set up to validate the concept of a multiple holographic element (hoel) distribution. The goal is to manufacture a sampled hologram that could project an image directly into the eye when addressed by the appropriate reference beam sequence.

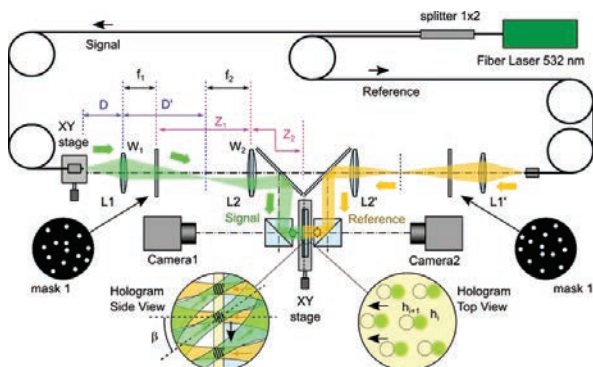


Figure 1: Description of the hologram recording set-up.

Figure 1 describes the holographic recording setup. A fiber laser is separated into signal and reference arms. The signal arm encodes the viewing direction of each image pixel with a fiber extremity moved in front of lens 1. The signal goes through a mask imaged on the hologram by an imaging lens 2. This

mask settles the hoel distribution on the hologram as shown on the top view and side view zoom. For each fiber position, the hologram is moved in order to cover the whole hologram surface in a spatial multiplexing scheme. The reference arm of the setup is symmetrical to the signal arm with a static fiber extremity.

Main Results

First studies have been dedicated to the choice of the optical elements of the recording set-up [2]. We have shown that a compromise is necessary between the size of the hologram and the viewing angle of the hologram. A first set of lens parameters led to the combination of 14 mm for the hologram diameter and 14° for the viewing angle.

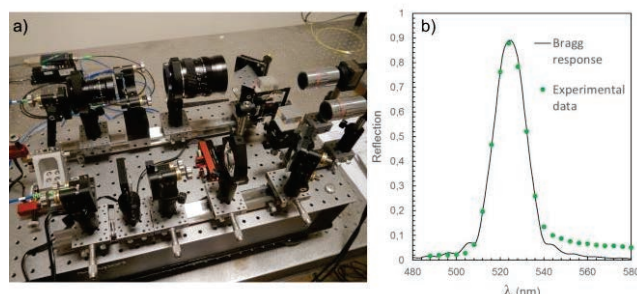


Figure 2: a) photograph of the hologram recording set-up currently built on the laboratory, b) reflection spectra of a hologram recorded in the laboratory (thickness 9 μm , index change amplitude 3.2 10^{-2}).

The recording setup has been recently built and will integrate soon all the motion control elements to implement our hoel distribution concept (figure 2a). A collaborative contract has been established with Holoconcept, a French holographic material supplier. A set of holograms has been recorded on our set-up with this material. First results show a good material response in terms of efficiency (> 90%, figure 2b).

Perspectives

Our next developments concern the implementation of the hoel segmentation on the holographic material. This will allow us to evaluate experimentally at short term the self-focusing effect in a device similar to the near-eye display we investigate. At midterm the holographic recording process will be implemented in conjunction with our 2D waveguide design to evaluate the physical interaction between guided-mode and holographic free space propagation.

In a more general perspective the holographic recording set-up will be used to investigate innovative HOE designs for a large variety of applications.

[1] C. Martinez et al. 'Holographic Lens-Free Near-Eye Retinal Projection Display: Concept for See-Through Applications', submitted to publication (2018)
 [2] C. Martinez et al. "Holographic Recording Setup for Integrated See-Through Near-Eye Display Evaluation," in *Imaging and Applied Optics 2017*, paper JTU5A.36

A NOVEL PROCESS FOR FABRICATING HIGH-RESOLUTION AND VERY SMALL PIXEL-PITCH GaN LED MICRODISPLAYS.

AUTHORS:

F. Templier, L. Benaïssa, B. Aventurier, Chr. Di Nardo, M. Charles, A. Daami, F. Henry, L. Dupré

ABSTRACT:

A new approach for fabricating very-small pixel pitch GaN microdisplays is proposed. It is based on the principle to bond directly an epilayer onto a CMOS wafer. MicroLEDs are then directly patterned on the wafer using the high-precision silicon line tools. Using this approach, we have demonstrated that MicroLEDs obtained from silicon grown epi GaN layers exhibit performances comparable to those obtained on classical sapphire templates. This technology shows very great promises in the fabrication of high brightness, ultra-high-resolution microdisplays required for augmented reality systems

SCIENTIFIC COLLABORATIONS: III-V Lab

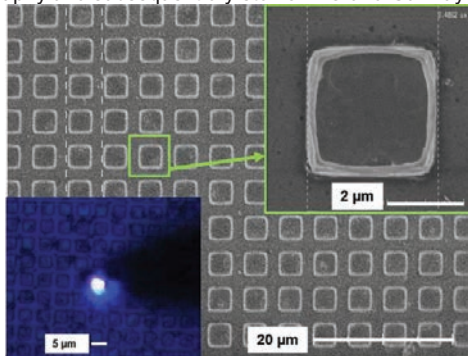
Context and Challenges

The growing interest for wearable devices has highlighted the need for high-performance microdisplays. To address this demand, inorganic GaN LED based arrays appear as a promising technological option [1]. Such microdisplays can be fabricated using hybridization of a GaN array on sapphire with CMOS active matrix. It has been already demonstrated that using microtube hybridization technology it is possible to reduce the pitch down to $10\ \mu\text{m}$ [1]. However, for high-brightness LED microdisplays, there is a need for a much smaller pixel pitch, typically $5\ \mu\text{m}$ or even $2\ \mu\text{m}$. Therefore, a new integration strategy for fabricating these GaN LED microdisplays is required. Recently, we have proposed a new approach for the fabrication of high-brightness LED [2], and here we report new results on this promising approach [3].

Main Results

On a first series of wafers, matrices of GaN microLEDs with different size and spacing were patterned using classical lithography and dry etching. No post-metallization has been applied. Arrays of MicroLEDs as small as $2\ \mu\text{m}$ with a spacing of $1\ \mu\text{m}$ were fabricated and operated successfully [2]. However, the lack of top-metal limited the On-current at higher voltages. Therefore it was decided to fabricate new devices with an n-contact metallization.

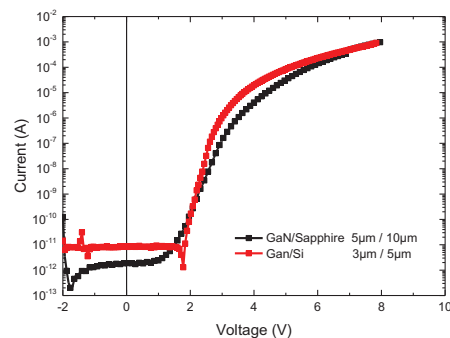
On a second series of wafers, Indium Tin Oxide (ITO) was deposited on top of the structures to provide an n-type contact. The transparency of ITO is well suited to permit the top-emission of structure by ensuring a wide current spreading without affecting the light emission. GaN microLEDs with different size and spacing were then patterned using standard lithography and subsequent dry etch of ITO and GaN layers.



On these arrays the microLEDs have a size of $3\ \mu\text{m}$ and a pixel pitch of $5\ \mu\text{m}$ (figure above). Light is emitted when a voltage is applied between the top electrode of each microLED as shown in inset of the above figure, and the common anode (not

shown).

Figure below shows the current-voltage characteristics of a microLED ($3\ \mu\text{m}$ size) fabricated using this new approach (GaN/Si) with ITO as the contact layer on N-type GaN. We compare it to a reference pixel ($5\ \mu\text{m}$ size) fabricated directly on sapphire and having both n and p-type metallizations.



The GaN/Si microLED shows a comparable turn-on voltage of about 2V, and comparable current levels to the GaN/sapphire microLED up to 1mA. This important result is mainly due to the contribution of the ITO layer on top of the n-type GaN. However, the GaN/Si $3\ \mu\text{m}$ microLED exhibits a slightly higher leakage current, which is interpreted as peripheral leakage due to the absence of passivation of the pixel mesa sidewalls in these first generation devices.

Perspectives

This work demonstrates the feasibility and improvement of high-resolution and very-small pixel pitch high-brightness GaN microdisplays. It highlights the feasibility of very small pixel pitch ($3\ \mu\text{m}$) microLED arrays from GaN epi layers grown on silicon wafers. Not only these are the smallest pitch microLEDs arrays achieved in the world to our knowledge, but these devices exhibit performances at least equivalent to those fabricated directly on sapphire. Furthermore, using this novel process integration, the devices are entirely fabricated using a CMOS line, which simplifies significantly the supply chain and paves the way for future low cost, mass production of GaN-based microdisplays. This technology is very promising for fabricating high-brightness, ultra-high-resolution microdisplays, which are necessary for new applications such as wearable devices, advanced Head-up display (HUD) systems and compact projectors.



RELATED PUBLICATIONS:

- [1] F. Templier, J-M. Bethoux, B. Aventurier, F. Marion, S. Tirano, M. Lacroix, M. Marra, V. Verney, L. Dupré, F. Olivier, F. Berger, W. Ben Naceur, A. Sanchot, I-C Robin, "Blue and Green $10\text{-}\mu\text{m}$ pixel pitch GaN LED Arrays with very high brightness", International Display Workshops 2015, Dec. 8-11 2015, Otsu, Japan (2015),
- [2] F. Templier, L. Benaïssa, I. Degirmencioglu, M. Charles and S. Tirano, "A new Approach for Fabricating High-Brightness GaN LED Microdisplays with High Resolution and Very Small Pixel-pitch", The 23rd International Display Workshops 2016 (IDW'16), December 7-9th 2016, Fukuoka, Japan (2016).
- [3] F. Templier, L. Benaïssa, B. Aventurier, C. Di Nardo, M. Charles, A. Daami, F. Henry, L. Dupré, "A Novel Process for Fabricating High-Resolution and Very Small Pixel-pitch GaN LED Microdisplays" Invited paper, Proc. Of Society for Information Display Conference 2017, Los Angeles, 21-26 May 2017, p. 268 (2017)

UV-CURABLE THIN-FILM PACKAGING FOR OLED-BASED MICRODISPLAYS

AUTHORS:

M. Provost, T. Maindron, A. Suhm, K. Raulin (Polyrise SAS), V. Gaud (Polyrise SAS)

ABSTRACT:

A thin-film Hard-Coat (HC) layer was investigated for the collective encapsulation and mechanical protection of top-emission OLED micro displays on wafer-scale and as an alternative solution to individual glass-lid protection. The HC is fabricated by UV-curing process from a silica-based hybrid polymer synthesized by sol-gel process.

Context and Challenges

It is widely known that organic light emitting diodes (OLEDs) are highly sensitive to moisture and oxygen ingress and require high barrier encapsulation. Moreover, a specific protection needs to be added to protect the device from mechanical failure. Depending on the application, various options from glass lids to flexible barriers have been developed. However, the former offers high mechanical protection but suffers from long implementation processes, while the later typically exhibits low hardness and poor wear resistance. This work aims to develop an alternative collective packaging solution using a thin-film HC layer directly processed onto OLED displays by photolithography [1].

Main Results

After the deposition of our HC protective layer at the wafer scale, the silicon wafer is diced under constant cooling water stream to obtain individual OLED chips. No major degradation such as scratches or stuck silicon residues can be observed. It turns out that the HC efficiently protects the ALD encapsulation layer from mechanical failures. Moreover, the HC shows a full chemical resistance to organic solvents used for surface cleaning. No solid residues were found surrounding the pattern. As a result, the hybrid encapsulation allows the easy electrical contact bonding of the display, using probes and wire bonding process.

Preliminary electro-optical characterizations were performed on white-emitting OLEDs. The HC slightly appears to impact the optical properties. The luminance does not change but a slight reduction of the emission in green region is observed, leading to a decrease of the OLED efficiency. It is expected that thin-film packaging allows a dramatic increase of image contrast especially at high brightness levels over the glued glass-lid packaging by removing the internal reflections on the glass and in the glue layer.

Enhancement of the performances of the HC layer can be obtained by optimizing the balance between organic and inorganic parts of the sol-gel formulation and by controlling the structure of the hybrid. The wear resistance of the HC appears to be sufficient for the dicing, cleaning and also the handling of


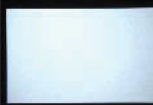
the silicon substrates. The HC shows improved flexibility and resilience compared to pure inorganic layers, leading to a less brittle coating (Fig. 1)

Table 1 Mechanical properties of the hybrid thin-film.

	PMMA 4-40 μm	Hybrid HC 3,5 μm	SiO ₂ 1 μm
Hardness (GPa)	0,13 [7]	0,19	0,34
Young Modulus (GPa)	2,75 [7]	4,5	6
Abrasion ISO9211-0104	19 %	6 %	0 %
Adhesion on ALD layer	low	medium	high

The fillers contained in the hybrid enhance the gas barrier properties of polymer matrices by increasing the diffusion pathway. The intrinsic properties of the composite cannot reach the requirement for OLED encapsulation but can be combined with a single alumina layer by Atomic Layer Deposition and exhibit high-barrier properties [2]. Accelerated aging tests were performed: no swelling or delamination were observed on the HC layer due to thermal choc or moisture ingress over the 300 hours of aging. In ambient conditions, regardless of the initial luminance, the samples exhibit systematically similar behaviors for as for standard OLED encapsulation.

Table 2 Picture of white emitting OLEDs before and after the storage test (60°C, 90%HR).

	LETI encapsulation [3]	ALD - HC
Aged 300 h		

Perspectives

Thin-film alternatives to the glass lid are developed and promote environmental as well as mechanical resistance. These packaging scenarios also opens up the possibilities for the use of flexible or conformable substrate.

Acknowledgment

This study is funded by the French Defense Procurement Agency (DGA).

RELATED PUBLICATIONS:

- [1] M. Provost, A. Suhm, T. Maindron, K. Raulin, V. Gaud, UV-curable Thin-film Packaging for OLED-based Microdisplays, SID Symp. Dig. Tech 2018
- [2] T. Maindron, T. Jullien, A. André, Defect analysis in low temperature atomic layer deposited Al₂O₃ and physical vapor deposited SiO barrier films and combination of both to achieve high quality moisture barriers, J. Vac. Sci. Technol. Vac. Surf. Films. 34, 031513 (2016).
- [3] J.-Y. Simon, T. Maindron, B. Aventurier, S.M.D. Gatta, E. Viasnoff, T. Jullien, A. Ghazouani, D. Lafond, P.141L: Late-News Poster: ALD-based Multilayer Encapsulation of PIN OLED: On the Stability of the Organic Layer in 85°C / 85% RH Storage Conditions, SID Symp. Dig. Tech. Pap. 44, 1470-1472 (2013)

OLED ON CMOS: WHAT ABOUT THINNING AND CURVING?

AUTHORS:

T. Maindron, B. Chambion, A. Vandeneynde, S. Gétin, M. Provost, A. Suhm, P. Peray, M. Zussy, J. Dechamp (DTSi)

ABSTRACT:

In this work, we use our technical background of CMOS thinning (historically developed for Through Silicon Via technology) to realize curved OLED-based microdisplays. This feature can allow significant innovation on the system/application because it will help to redesign simpler and lighter optical engine systems.

Context and Challenges

For today's near-to-eye technologies, CMOS microdisplay-based systems like glasses or goggles will have to be performant in term of resolution, brightness, contrast but primarily also in term of reduced footprints to look like standard view glasses. Recently advanced fabrication techniques have been developed to provide curved focal plane arrays for CMOS-based image sensors [1] and K. Itogana *et al.*, *Symposium on VLSI Technology (2014)*, B. Guenter *et al.*, *Optic Express* 25 (2017), 13010. In this work we propose to apply such techniques to OLED-integrated microdisplays in such a way that optical engine footprints can be reduced, in the meantime improving the field-of-view of the system as well as the image quality. In this miniaturization context, the packaging strategy becomes crucial and the main issues (OLED fragileness management, stress management, thermal management and thermo-mechanical features) will have to be considered.

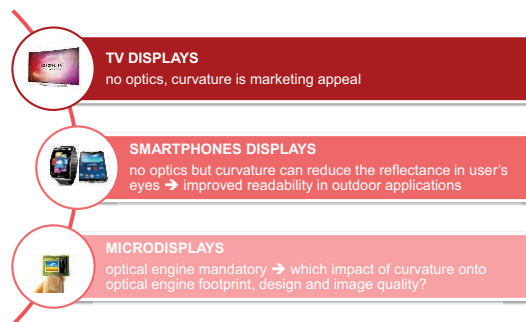


Figure 1: generic concepts of curved displays, following display scale [image source: Samsung, LG and Emagin]

Figure 1 represents a general concept of curved displays, showing that the technological need for such displays increases as display size decreases. In the end, curving microdisplays turn out to be a key feature for microdisplay-based systems while it is purely marketing appeal for large displays such as TV displays.

Main Results

First studies have been conducted onto testing vehicles (no CMOS). Two scenarios have been explored for thinning of the OLED chips: Chip Level Thinning (CLT) as well as Wafer Level Thinning (WLT), with OLED layers deposited before thinning in all cases. The OLED has been protected from thinning process

using a dedicated hard coat layer, made from a sol-gel material (provided by Polyrise Company, Bordeaux). Both scenarios can be implemented with great success.

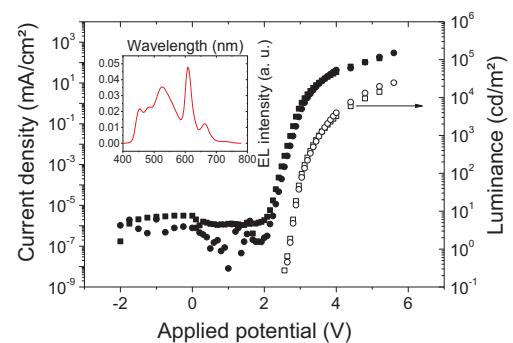


Figure 2: IVL characteristics of a white OLED (a) made onto a thinned Si substrate following WLT process (circles) and (b) following CLT process (squares) with 45 mm radius of curvature; inset: EL spectrum of the white OLED at 2000 cd/m²

The IVL characteristics of a reference OLED made onto a thick Si substrate are identical (not shown here). It is therefore possible to thin down the OLED substrate without altering the fragile OLED architecture, by proper use of a dedicated hard coat layer deposited onto the thin-film encapsulation. The top-emitting white OLED architectures used in this study presents high efficiency (10 cd/A at 5000 cd/m²) and high luminance (10 kcd/m²) in the region < 5V. These characteristics are compatible with a CMOS technology driving characteristics. Figure 3 shows a resulting 0.38" OLED-based microdisplays from MicroOLED company, curved with 45 mm radius.

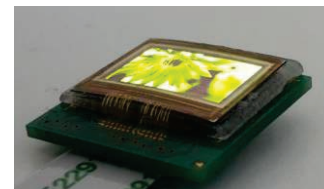


Figure 3: 0.38" OLED-based microdisplays from MicroOLED company, curved with 45 mm radius

Perspectives

The development of a thinning and curving process onto active matrix (CMOS) OLED is ongoing for innovative 1" diagonal chips developed in the framework of the LOMID project (this work is H2020-funded) [2].

RELATED PUBLICATIONS:

- 1] B. Chambion *et al.* 'Tunable curvature of large visible CMOS image sensors: Towards new optical functions and system miniaturization', IEEE 66th Electronic Components and Technology Conference (2016)
- [2] <http://www.lomid.eu/>

TRANSMISSIVE LIQUID CRYSTAL SPATIAL LIGHT MODULATOR (SLM) FOR LIGHT MODULATION USING IN-PLANE SWITCHING (IPS) TECHNOLOGY

AUTHORS:

C. Abélard, B. Racine, U. Rossini, F. Templier

ABSTRACT:

An investigation of IPS-SLM architecture with small pixel pitch (around $5\ \mu\text{m}$) for phase modulation and amplitude modulation application was achieved. The studies were focused on the SLM architecture in order to optimize the performances for specific applications. Most of the transmissive SLM configurations use nematic liquid crystals (LC). We studied in this work the SLM in IPS technology which is well adapted to address pixel at the micrometric scale (around $5\ \mu\text{m}$). SLM can modulate either phase or amplitude of the light, depending of the application. In this work, we studied both, the phase modulation studies resulted from a Vertically Aligned (VA) LC SLM architecture with IPS addressing allowing 2π phase shift and the amplitude modulation studies resulted from an architecture using crossed-patterned electrodes with Homogeneously Aligned (HA) LC allowing a very short response time (around 2 ms).

Context and Challenges

The current SLMs are either reflective or transmissive with nematic LC and use different types of liquid crystal alignment like Parallel Aligned (PAL), Twisted Nematic (TN), and Vertical Aligned (VA). However, today no commercial SLM uses IPS configuration while it allows a better contrast and a viewing angle than other technology. Moreover, driving voltage and response time need to be improved to address specific applications. Due to the reduction of the pixel size, SLM can be more compact and it became usable in specific systems like Head Mounted Display (HMD) or foveated optical systems. An improvement of response time with CMOS compatible voltages could also allow an application for sequential color display application.

The next part will focus on main results on phase and amplitude modulation simulations studies obtained with our IPS configuration system.

Main Results

Several IPS technologies have been investigated for pure phase modulation. It appears that the IPS-VA gives a more homogeneous and higher phase shift than IPS-TN or IPS-HA. However, the phase modulation depends on many parameters such as: birefringence, cell gap, wavelength and electrodes voltage. Moreover, in the IPS configuration, electrodes size and gap are also critical for driving voltage values. In this work we investigated an optimal pixel configuration by changing the geometrical, electro-optical and elastic parameters by simulation using LCDMaster software.

The pixel architecture (figure 1) which has been patented [1] giving the best result is obtained for a cell gap (d) and pixel size of $5\ \mu\text{m}$, a pitch between two electrodes (P) of $2.5\ \mu\text{m}$ and an electrode width of $0.8\ \mu\text{m}$. They are elevated of $d/3$ by an insulator (d_s) and we also add a $0.5\ \mu\text{m}$ insulator below the upper substrate (d_i).

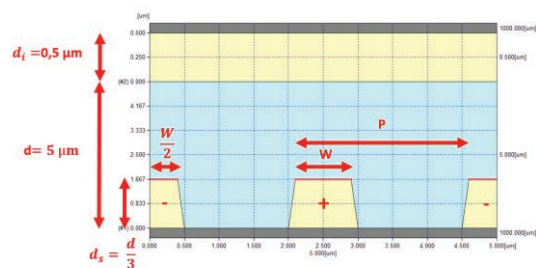


Figure 1: Pixel architecture of the IPS-VA configuration [2]

RELATED PUBLICATIONS:

- [1] C. Abélard, B. Racine, R. Umberto, F. Templier, "A novel IPS-VA pixel architecture for phase modulation and beam-steering application", SID-ME Wearable and projection display, 2017
- [2] Rossini Umberto, "Liquid crystal display comprising erase electrodes" Patent no. WO2012175250

With this architecture, a phase shift of 2π can be reached with a low driving voltage (below 3V).

For amplitude modulation, a IPS-HA configuration (figure 2) was studied as well as the configuration with the cross-patterned electrodes, also patented [2].

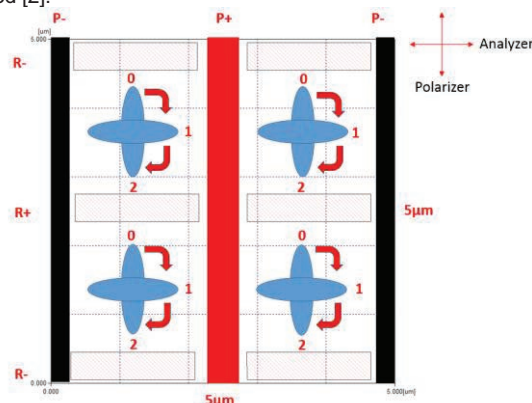


Figure 2: Top view of IPS-HA configuration with crossed-patterned electrodes

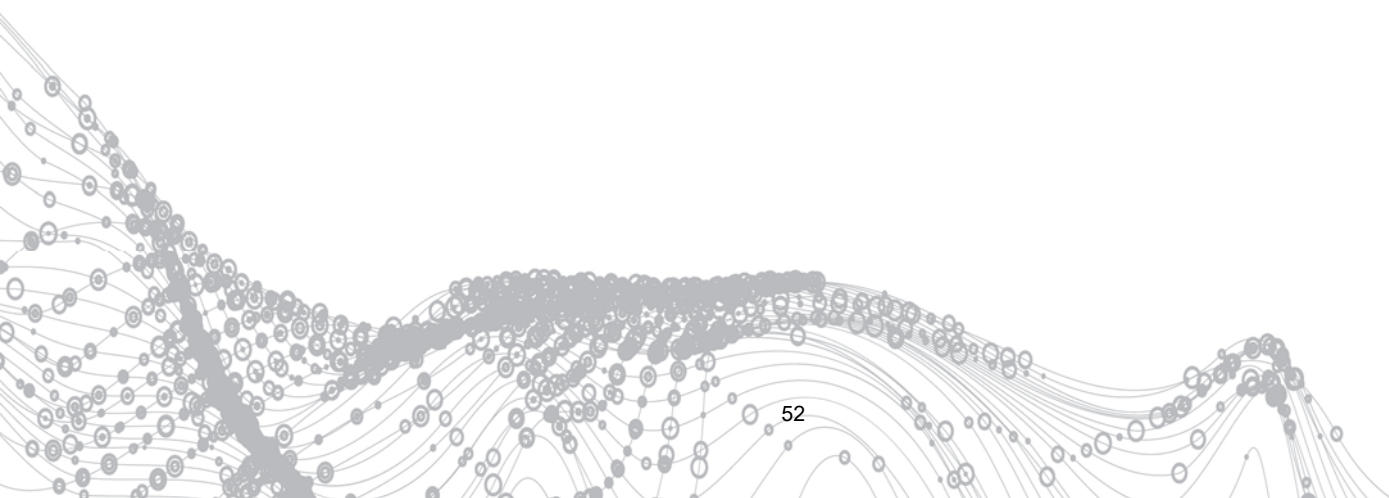
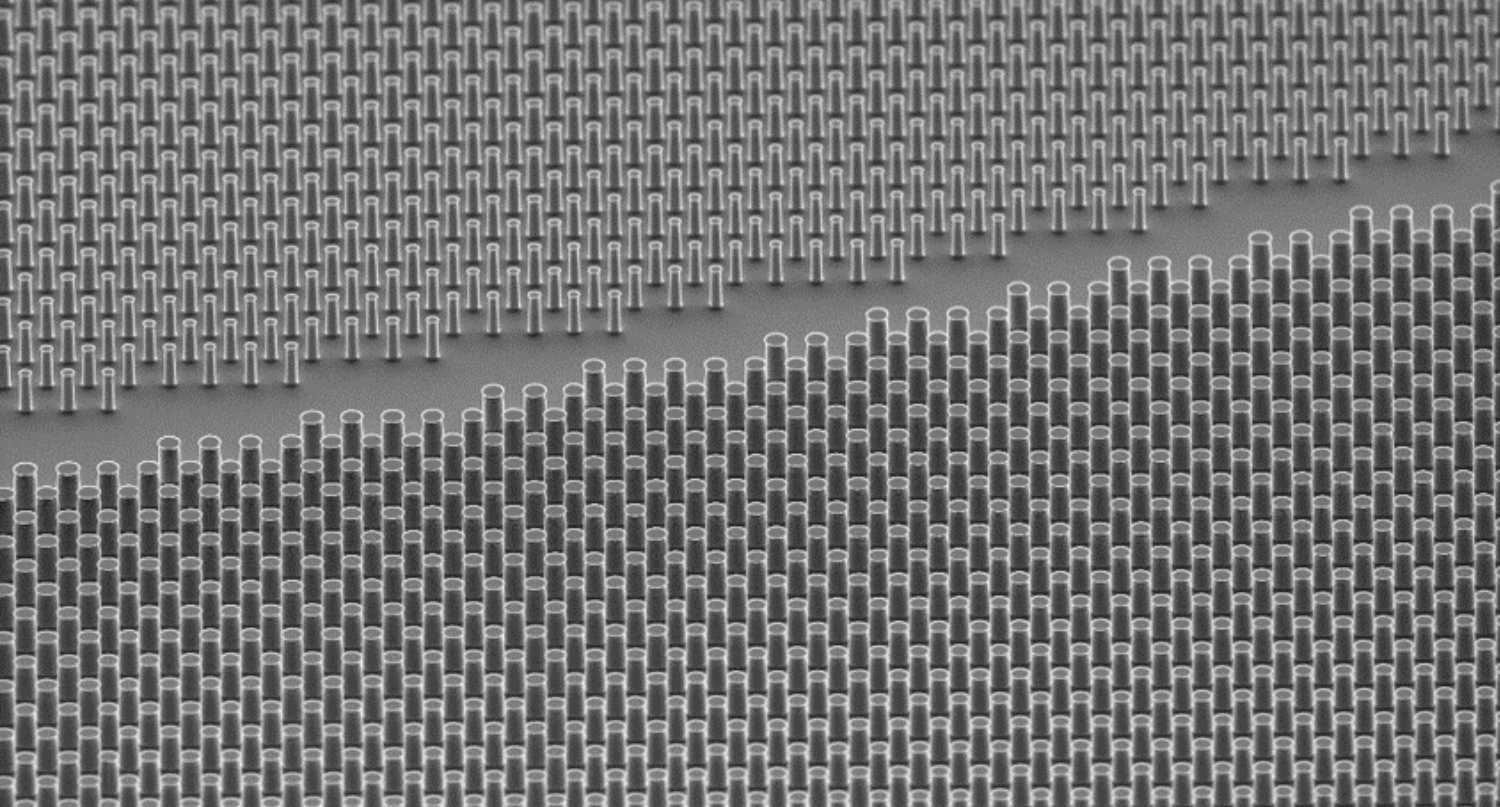
Traditional IPS configurations work only with pixels electrodes (figure 2 : P+ and P-) that move the LC molecules in order to have a bright state in our example (state 1). With this configuration, the LC molecules return to initial state (state 2 in our exemple) by its own mechanical relaxation in around 10 ms. However, a mechanical relaxation slow down the refreshment time of a pixel so we introduced a new design that brings return electrodes (R+ and R-), they induce a electrical relaxation of the LC molecules that reduce the refreshment time to 1ms.

With this configuration it has been proved than small pitch IPS-HA configuration can provide a very fast response time, ten times better than mechanical relaxation.

Perspectives

The studies on amplitude modulation proved the interest of IPS in particular for small pixel pitch. This kind of SLM could be integrated in a sequential color display. These display require a very short response time and could benefit of all the other advantages of IPS technology

The studies on phase modulation configuration has been pushed further by simulating a foveated optical system integrating the newly simulated SLM. Encouraging results have been found in some specific configurations of optical systems. These studies will be implemented on prototype to confirm the simulations.





O8

OPTICS and NANOPHOTONICS

- **Robust automated design/optimization of nanophotonic components**
- **HgCdTe strain-gap topological insulators**

ROBUST DESIGN OF PHOTONIC COMPONENTS

AUTHORS:

N. Lebbe, C. Durantin, K. Hassan, A. Glière, C. Dapogny (LJK), E. Oudet (LJK), J.-A. Désidéri (INRIA)

ABSTRACT:

Whatever the care taken by the operator or the high quality standard of the cleanroom facilities, the production of photonic integrated circuits is prone to manufacturing uncertainties. As a means to overcome this issue, the applied mathematics work presented here aims at anticipating fabrication errors by applying robust design optimization techniques. Two distinct classes of problems, namely (i) those defined by a set of parameters, as well as (ii) non-conventional devices, whose free-form geometries are obtained by shape optimization, are both addressed by the means of multi-objective optimization.

SCIENTIFIC COLLABORATIONS: Lab. Jean Kuntzmann, Chaire OQUAIDO (EMSE), ACUMES (INRIA Sophia Antipolis)

Context and Challenges

Designers of photonic devices increasingly rely on numerical optimization. However, the actually fabricated object may differ significantly from the ideal design. Accounting for manufacturing errors, together with variations of the environmental conditions, is a key issue on the path towards robust industrial deployment.

Main Results

The design of broadband devices is a valid heuristic to search for photonic components which are tolerant to fabrication error. This approach has been previously demonstrated during the design of a silicon-on-insulator adiabatic coupler used as a power splitter [1]. The robustness to fabrication errors has been confirmed experimentally. Since then, a new metamodel based multi-objective optimization method, adapted to the worst-case scenario, has been devised and implemented [2, 3]. The procedure is based on the coupling of genetic and gradient-based methods. First, the NSGA-II genetic multi-objective optimization algorithm is applied on the metamodel prediction of each objective. At each generation, the population is selected, crossed-over and mutated (classical genetic algorithm operations). A clustering procedure then selects a given number of points among the final solutions. The selected points are used as starting points of the multiple gradient descent algorithm (MGDA). The points obtained from MGDA are filtered, based on their prediction error, and then evaluated and added to the training dataset. This sequence is iterated until convergence. A nicely spread Pareto front, which represents the set of optimal solutions among the training dataset, is thus obtained. As can be seen on Fig. 1 (right), a wideband power splitting ratio is attained.

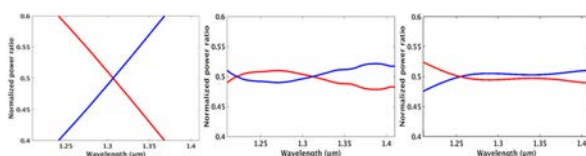


Figure 1: From left to right: simulated power splitting ratio versus wavelength for a conventional design, a single wavelength optimized design and a robust broadband design.

RELATED PUBLICATIONS:

- [1] K. Hassan, C. Durantin, V. Hugues, B. Szelag, and A. Glière, "Robust silicon-on-insulator adiabatic splitter optimized by metamodeling," *Applied Optics*, vol. 56, no. 8, pp. 2047–2052, 2017.
- [2] C. Durantin, K. Hassan, and A. Glière, "Robust optimization of adiabatic power splitters," 12th World Congress of Structural and Multidisciplinary Optimization, Braunschweig, Germany, June 5-9, 2017.
- [3] C. Durantin, "Métamodélisation et optimisation de dispositifs photoniques", Doctorat de l'Université de Côte d'Azur, Nice, France, to be defended 2018/05/28.
- [4] N. Lebbe, C. Dapogny, K. Hassan, E. Oudet, and A. Glière, "Optimisation robuste de forme pour la nano-photonique," presented at the SMAI-CANUM, Cap

d'Agde, France, May 28-June 1, 2018.

An analogous procedure was adapted to the context of topology optimization, where non-parametric shapes, such as the one presented on Fig. 2 (left), are generated. The wavelength duplexer obtained using a MGDA-like algorithm, presents a larger bandwidth than the non-robust one (Fig. 2, resp. right and center).

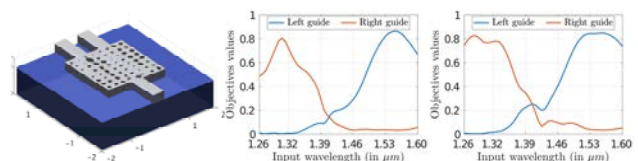


Figure 2: Geometry of a duplexer obtained by topology optimization (left) and spectra of non-robust (center) and robust (right) duplexers.

A new approach, which directly deals with manufacturing errors has also been implemented [4]. This algorithm considers three shapes: the nominal one, as well as the same dilated and eroded by a certain distance. Since the three shapes do not necessarily share the same topology, it is necessary to limit the dilations and erosions up to the skeleton of the nominal shape. A multi-objective optimization is performed, leading, again in the case of a wavelength duplexer, to a shape that is robust to fabrication errors (Fig. 3).

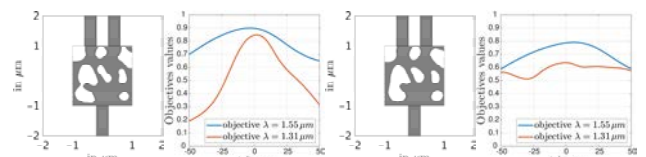


Figure 3: Two shape-optimized duplexers and their sensibility to small homogeneous dilation or erosion. The right one was obtained using a new algorithm, which aims at minimizing the effect of the lithography-etching fabrication errors.

Perspectives

A first set of shape-optimized components will shortly be fabricated by e-beam lithography on SOI substrate. The performances of individual devices, as well as statistics on full wafer variability, will be assessed to confirm the robustness of the design and the validity of our approach.

MBE GROWTH OF HgZnTe/CdTe: TOWARDS ENHANCED STRAIN-GAP TOPOLOGICAL INSULATORS

AUTHORS:

J. Papin, A. Chorier, P. Noël (INAC-SPINTEC), L. Vila (INAC-SPINTEC), J.-P. Attané (INAC-SPINTEC), T. Meunier (I.NEEL-CNRS), P. Ballet

ABSTRACT:

Tensile-strained HgZnTe layers have grown on CdTe(100) and represent topological insulator structures with an inverted band structure inherited from HgTe for zinc fraction lower than about 15% and with a larger strain-induced bandgap due to the increase in lattice mismatch with zinc concentration. MBE growth and material characterization are presented showing excellent crystal quality and surface morphology in the topological range. Low temperature transport of Hall bar devices exhibit electronic mobility close to $100000\text{cm}^2/\text{V.s}$ and clear quantum Hall signatures.

SCIENTIFIC COLLABORATIONS: CEA-INAC-SPINTEC, CNRS - I. NEEL

Context and Challenges

Topological Insulators (TI) are a new class of materials attracting great interest both theoretically and experimentally thanks to their unique electronic and spin properties that arise at their interfaces. With an inverted band structure, the semi-metal HgTe has been identified as a strong TI assuming the opening of a bulk gap. In the general case of 3D-TI, the growth of tensile strained HgTe/CdTe structures naturally opens a gap in the order of 20meV and convincing signatures of topological transport have been demonstrated in such system (C Brüne *et al.*, *Phys. Rev. Lett.* 106, 126803 (2011), and [1-2]). However and despite the predicted robustness of topological states, it is generally found that such small bandgap TI produce unstable results with a clear trend of mixing surface and bulk electronic properties. While the origin is still unclear, crystal defects or material fluctuation such as interface roughness, intermixing or bulk residual doping level represent plausible causes. Increasing the bulk strained gap obviously represents a way to reduce the sensitivity of surface electronic states to any material fluctuation in addition to possibly decouple the surface states from the Γ_8 bulk heavy hole band.

Main Results

Here we present the MBE growth of HgZnTe layers on CdTe(100) substrates. Introducing zinc in amounts lower than 15% would considerably increase the tensile strain in the growing layer while preserving the inverted band ordering. While the critical thickness for plastic relaxation is in the order of 150nm for HgTe/CdTe, it is expected to be significantly reduced when increasing strain i.e. when increasing the zinc fraction. 50nm-thick HgZnTe layers have been grown with different zinc fraction ranging from pure HgTe to about 25% of zinc allowing to continuously follow the increase in tensile strain while checking on bulk or surface relaxation using high resolution X-ray diffraction (HRXRD), see figure 1, and atomic force microscopy. Obviously, increasing the zinc fraction from pure HgTe (black) to 25% (purple) causes a systematic shift to larger Bragg angles witnessing the reduction of the out-of-plane lattice parameter of the tensile-strained layer.

The layer quality is found to be excellent for zinc contents as high as 10-15% resulting in estimated strain bandgap in the order of 70-80meV. For higher zinc fraction, some degradation in the X-rays together with the appearance of dislocation lines in the AFM images suggest partial plastic relaxation.

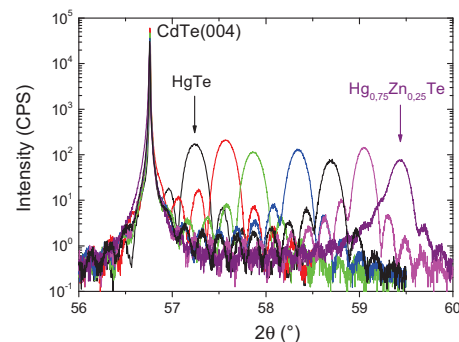


Figure 1: HRXRD (004) reflexion of 50nm-thick HgZnTe/CdTe layers.

The first low temperature electronic transport measurements performed on this particular topological system with Hall bar processed Hg_{0.9}Zn_{0.1}Te/HgCdTe/CdTe structures exhibit electron mobility in the $80000\text{cm}^2/\text{V.s}$ range and clear quantum Hall signatures upon magnetic field, see figure 2. Altogether, material growth and magneto-transport results are very encouraging for promoting this new material as an enhanced bandgap, Hg-based, topological insulator.

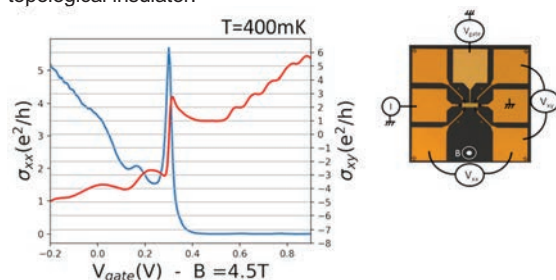


Figure 2: Plot of the low-temperature longitudinal and transverse conductance as a function of gate voltage of a 20nm-thick, $3 \times 40\mu\text{m}$ Hall bar Hg_{0.9}Zn_{0.1}Te sample with a transverse magnetic field of 4.5T.

Perspectives

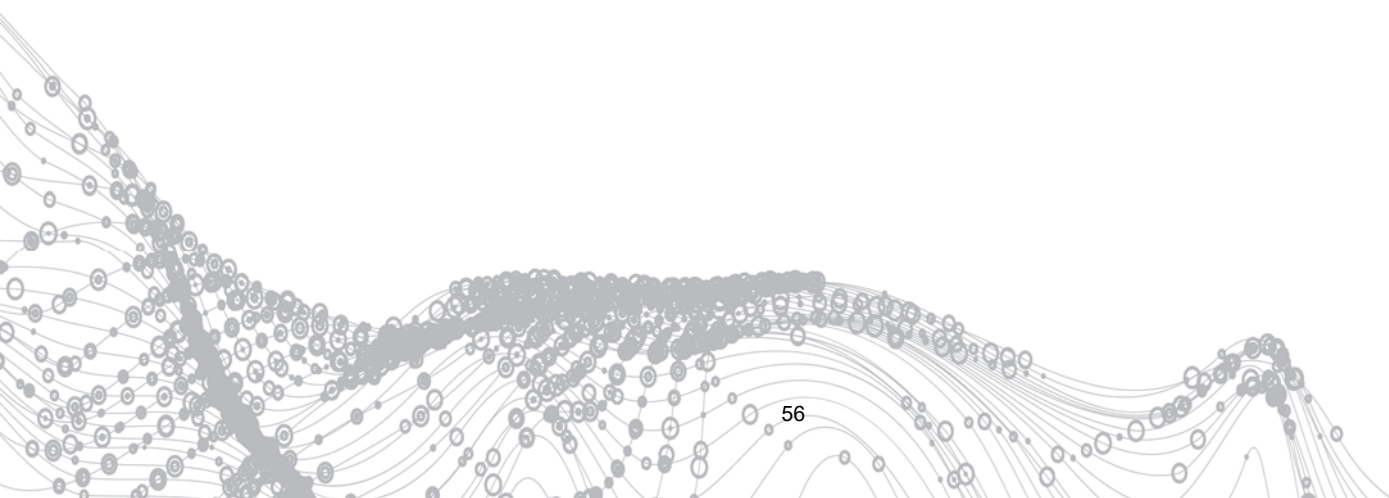
Additional work is needed and currently underway to quantitatively determine the exact gain in strain-gap which is expected to be in the order of 70-80meV compared to the 20meV of current HgTe topological structures. If confirmed, this would lead to a new topological material with enhanced bandgap and as a result enhanced robustness and applicability.

RELATED PUBLICATIONS:

- [1] C Thomas, O Crauste, B Haas, P-H Jouneau, C Bäuerle, LP Lévy, E Orignac, D Carpentier, P Ballet, T Meunier, *Phys. Rev. B* 96, 245420 (2017)
- [2] P. Noel, C. Thomas, Y. Fu, L. Vila, B. Haas, PH. Jouneau, S. Gambarelli, T. Meunier, P. Ballet, JP. Attané, *Phys. Rev. Lett.* 120, 167201 (2018)



CEA-Leti/Denis Morel





O9

PhDs AWARDED IN 2017

- **Bruno DELACOURT**
- **Olivier DUBRAY**
- **Jocelyn DUREL**
- **Julien FAVREAU**
- **Ainur KOSHKINBAYEVA**
- **Ludovic LAURENT**
- **Gautier LAVAL**
- **Jérôme MEILHAN**
- **Yolande MURAT**
- **Dinh Chuong NGUYEN**
- **Aymeric TUAZ**



BRUNO DELACOURT

EXTRINSIC DOPING OF CdHgTe APPLIED TO INFRARED PHOTODIODES

Infrared photodiodes, which are based on narrow gap semiconductors, permit collection of carriers generated by photons impact but also by thermal agitation. This agitation create a parasitic dark current deteriorating device performance. In order to minimize this dark current, the key parameter to maximize is the minority carrier lifetime. In high operating temperature (HOT) context, it open the possibility to increase the operating temperature of photonic infrared detectors. For the mid-wave infrared window, the goal is to work at 150–180 K instead of 80–120 K currently. This would allow significant progress in terms of energy consumption, power and thus autonomy and reliability of the systems. The objective of this thesis is to experimentally determine the theoretical

limits of the minority carrier lifetime in HgCdTe and in a III-V semiconductor. For this, a photoluminescence decay measurement bench as well as a data extraction method making possible to discriminate the recombination mechanisms from the evolution of the signal as a function of the level of carrier injection in the sample were developed. In parallel, a set of characterizations was carried out to assist the development of technologies addressing the HOT context.



OLIVIER DUBRAY

DESIGN AND CHARACTERIZATION OF TRANSMITTER ARCHITECTURES USING SILICON RING RESONATOR MODULATORS FOR HIGH BIT RATE COMMUNICATIONS

Over the past decade, with the diversification of connected devices (PCs, Tablets, TVs and Smartphones), the Internet ecosystem has drastically extended. Today, 80 % of the IP world traffic runs inside the data centers. To address such scaling issues as bandwidth density, energy consumption and cost of the interconnects inside the data centers, the development of new optical transmitters is critical. The purpose of this thesis is to propose and evaluate transmitter architectures built from Silicon Photonics for next 400 Gbit/s data rate standard over up to 2 kilometer-links.

The selected optical modulator is the silicon ring resonator modulator which has substantial benefits: low footprint, low energy consumption and enables dense multiplexing.





JOCELYN DUREL

INTEGRATION OF A HYBRID III-V/SI DBR LASER ON THE BACK-SIDE OF A PHOTONIC DIE

Recently, Silicon Photonics has emerged as a solution for the mass manufacturing of optical transceivers addressing datacenter's needs in terms of increasing data-rate and reduced cost. Several Silicon-Photonics platforms have been demonstrated using standard Si technology. While these platforms differ in many regards, they all lack a solution for a monolithically integrated light source. To solve this problem, the most commonly proposed approach consists in bonding an InP-stack onto a Si-wafer in order to fabricate a Hybrid III-V/Si laser. However, none of those demonstrations have been made with a standard CMOS-BEOL, preventing a proper electronic-photonic integration. To solve the topographical problem induced by the additional layers, a new integration

scheme, called Back-Side, has been developed and is presented in this document. We have proved that, under specific conditions, the grating coupler has the same measured performances in Back-Side and in Front-Side. The implemented laser is based on a hybrid DBR (Distributed Bragg Reflector) III-V/Si cavity. In order to increase the mode confinement in the MQWS (Multi Quantum Wells) and hence ensure a high optical gain, the optical mode is gradually transferred between the III-V waveguide and the silicon waveguide of the hybrid laser by adiabatic tapers, patterned on both sides of the gain zone, to finally be reflected by the mirrors DBR in the silicon. Finally, its manufacturing process is explained before its opto-electronic characterizations are presented.



JULIEN FAVREAU

STUDY AND DEVELOPMENT OF A MID-INFRARED SILICON PHOTONICS PLATFORM: TOWARDS INTEGRATED SENSORS

Nowadays, microelectronic chips and sensors are not simply electronic circuits anymore. They are able to convey both electric and optical signal. As shown by the so-called photonic chips used to transmit data at high speed rate. However, this technology only exploits a very small part of the light spectrum, namely in the near infrared. Exploitation of the whole mid-infrared domain ($\lambda=2-20 \mu\text{m}$) would allow to develop new integrated sensors using molecules specific spectral fingerprints in this part of the electromagnetic spectrum. This thesis deals with the development of integrated optical circuits on silicon capable of handling these wavelengths and compatible with 200 mm clean room fabrication processes. The technology developed in this work, is based on $\text{Si}_{0.6}\text{Ge}_{0.4}$ channel square waveguides in order to obtain compact and low loss optical circuits. First of all, the design of

optical functions required to build circuits is presented. Then, these functions are assembled into circuits which are manufactured and characterized in order to assess performances of the developed technology. Two circuits have been produced: one with standard processes and one with damascene processes. The first one has the advantage of using known processes, whereas the second one allows to make waveguides for different wavelengths on a single chip. These two circuits have been characterized in order to conduct a comparative study between the two fabrication processes. Finally, in order to mature the technology, an in-depth





AINUR KOSHKINBAYEVA
NEW PHOTONIC ARCHITECTURES FOR MID-INFRARED GAZ SENSORS
INTEGRATED ON SILICON

This work focuses on optical multiplexers for mid-IR broadband source in gas sensing application. The design of multiplexer configurations based on two types of diffraction gratings is discussed. Owing to utility of Gaussian approximation of the field and Fourier Optics, we developed a semi-analytical tool allowing to evaluate the responses of array waveguide grating (AWG) and planar concave grating (PCG). This approach also opened the way to implement numerical phase error analysis by introducing normal distribution of errors and to study the correlation between standard deviation of phase errors and the level of crosstalk. FTIR spectroscopy measurement results of 5.65 μm AWGs, built with SiGe graded index core encapsulated in a thick Si cladding on

standard silicon substrate, are compared with the theoretical expectations. We have also performed evaluation of AWG response at elevated temperatures, in the range between 20 °C and 41 °C. The spectral shift showed linear dependence with the temperature, which is in a good agreement with simulation predictions.



JEROME MEILHAN
DESIGN, MODELING AND CHARACTERIZATION OF MICROBOLOMETRIC
DETECTORS FOR SUB-THz IMAGING APPLICATIONS

This PhD dissertation presents the analysis, characterization and optimization of the performances of micro-bolometric imagers in the sub-THz frequency range. This non ionizing span of the electromagnetic spectrum is currently a booming field of research. Development of high-performance and room temperature imagers opens the path towards many applications. One of such promising application is non-destructive screening enabled by the good penetrating power of these radiations through many materials, especially at frequencies lower than 1 THz. Through a radiometric analysis of an active imaging system, we assess the required performances of an imager suited for this application. In this context, we have analyzed the electrothermal performances of the cutting-edge THz imagers based on micro-bolometer developed at CEA-Leti.

Thanks to a detailed model of the bolometer bridge of these detection arrays, we have brought into focus the limiting factors of the current devices. Technological improvement have been considered such as the integration of a new thermometer material. The performance improvements brought by these optimizations have been quantified thanks to the modeling tool we have developed and it is showed that sensitivity close to the pW range can be reached on these imagers. An intensive experimental work have also been carried out in order to assess the sub-THz electromagnetic performances of the micro-bolometer





LUDOVIC LAURENT

HIGH-FREQUENCY-RESONANT ELECTROMECHANICAL NANO-SYSTEMS (NEMS HF): TECHNOLOGICAL BREAKTHROUGH FOR UN-COOLED INFRARED IMAGING

One objective of the microbolometers industry roadmap is to scale down the sensor surface – the pixel pitch – in order to increase the number of imagers fabricated on a silicon wafer. The scaling has been recently slowed down, mostly because of microbolometers self-heating issue and $1/f$ noise which are inherent to the resistive transduction. Our work has focused on a new type of sensor at $12\mu\text{m}$ pixel pitch, which theoretically gets rid of self-heating and $1/f$ noise. In our approach, an absorbing plate is excited at its mechanical resonance through two tiny torsion arms using an actuation electrode placed $2\mu\text{m}$ underneath. Pixel motion is also transduced electrostatically. Since micromechanical resonators feature very low frequency noise, we believe that an uncooled infrared sensor based

on the monitoring of its resonance frequency (which changes with temperature through the TCF) should be extremely sensitive.

We present different models (linear and nonlinear) for the pixel mechanical behavior and compare them to experimental characterization of resonators which were fabricated in dense arrays. We measure the frequency stability of our sensors along with their sensitivity to infrared flux. The best devices show a resolution of $30\text{pW}/\sqrt{\text{Hz}}$, with a response time lower than one millisecond. The scene resolution (NETD) is 2K for an integration time compatible with imaging frame rate. These performances overtake results previously published on this topic with such reduced pixel pitch.



GAUTIER LAVAL

SELECTIVE AREA GROWTH OF GAN PSEUDO-SUBSTRATES ON SILICON FOR OPTOELECTRONIC APPLICATIONS

Light-emitting diodes (LEDs) used in solid lighting systems are made from GaN and its alloys. Although commercial LEDs are mainly developed on sapphire substrate, manufacturers and research laboratories are also interested in silicon substrate, which is cheaper and available in larger diameters. However, its usage raises two issues: the presence of a high dislocation density in epitaxial layers and their tensile stress leading to the formation of cracks. In order to avoid them, solutions exist but require long and complex growth processes resulting in an increase in production costs. The alternative proposed in this thesis is focused on the selective area growth (SAG) of GaN pseudosubstrates on silicon by metalorganic vapour phase epitaxy (MOVPE). Indeed, the SAG through a dielectric mask should make it possible to obtain a good crystalline

material displaying a limited stress (avoiding coalescence) while reducing epitaxy duration. Our work focused on the analysis of the influence of growth parameters (growth conditions, mask design, substrate polarity) in order to understand the involved mechanisms and to control the effect of each of them on the material morphology. The growth of hexagonal [0001] GaN pseudo-substrates on Si (100) was demonstrated by using a textured N-polar AlN layer. Optical and structural characterisations displayed a stress relaxation as well as a good crystalline quality of these structures' surface material. The growth on top of those of



YOLANDE MURAT

NEW STRUCTURES OF ORGANIC LIGHT-EMITTING DIODES FOR SIGNAGE APPLICATIONS AND DISPLAYS

OLED (Organic Light-Emitting Diode) technology has been exploited on an industrial scale for several years, principally in smartphones, TV displays, and similar devices. However, current fabrication processes, such as thermal evaporation under high vacuum, are expensive and cannot be used for low-cost applications (signage, lighting, etc.). This work aims to develop high-performance, stable, low-cost OLEDs. Fabrication by solution processing was chosen to reduce the processing costs in any future commercialization of the work, while the inverted architecture was used to optimize device stability. In this work, ethoxylated polyethylenimine (PEIE) was used to reduce the work function of the transparent cathode. It was shown that higher performances could be obtained with inverted OLEDs

compared to direct devices incorporating the same emissive polymer (Super Yellow). Furthermore, it was demonstrated that a binary blend, (PEIE and a hole blocking material) could be deposited in a single step without reducing the OLED device's performance – greatly simplifying the fabrication process. A TOF-SIMS (Time of Flight-Secondary Ion Mass Spectrometry) study was conducted which demonstrated a vertical phase segregation of the binary blend. Finally, the indium tin oxide (ITO) electrode, which represents at least 25% of the fabrication cost, was successfully replaced with a tin oxide (SnO₂) layer, deposited by ALD (Atomic Layer Deposition).



DINH CHUONG NGUYEN

CONTRIBUTION TO THE OPTIMIZATION OF ELECTROLUMINESCENCE EFFICIENCY IN HIGH POWER LEDs: DECORRELATION OF DIFFERENT COMPONENTS OF THE EFFICIENCY

This PhD. works, which was carried out inside CEA-LETI, aims to dissociate the various mechanisms occurring inside a GaN-based LED employing numerical simulation and experimental characterization. In the chapters 1 and 2, various mechanisms occurring inside a diode/LED are theoretically described. In chapter 3, through numerical simulation, the dominant mechanisms as well as their locations in a VTF ("vertical thin film") LED structure are determined for different voltage ranges. A parametric study follows to assess the interactions between the mechanisms. In chapter 4, the simulations are carried out with an additional field-dependent model for charge carrier mobility. With this model enabled, the simulated LED-electrical-and-optical characteristics approximate the real LED characteristics. Carrier-velocity characterization on p-type GaN, using a

specific sample structure and the resistivity method, is also shown in chapter 4. It can be inferred from the results that under strong electric-fields, the carrier velocity might saturate, or the carrier mobility might decrease. These results strengthen the hypothesis used for the simulations in this chapter 4. The simulations introduced in the chapters 3 and 4 allow the proposition of an equivalent circuit for a GaN-based LED by dissociating the different mechanisms and retaining the dominant ones. This equivalent circuit could help, for instance, identify the different regimes in a real-LED electrical characteristics in order to improve the LED's



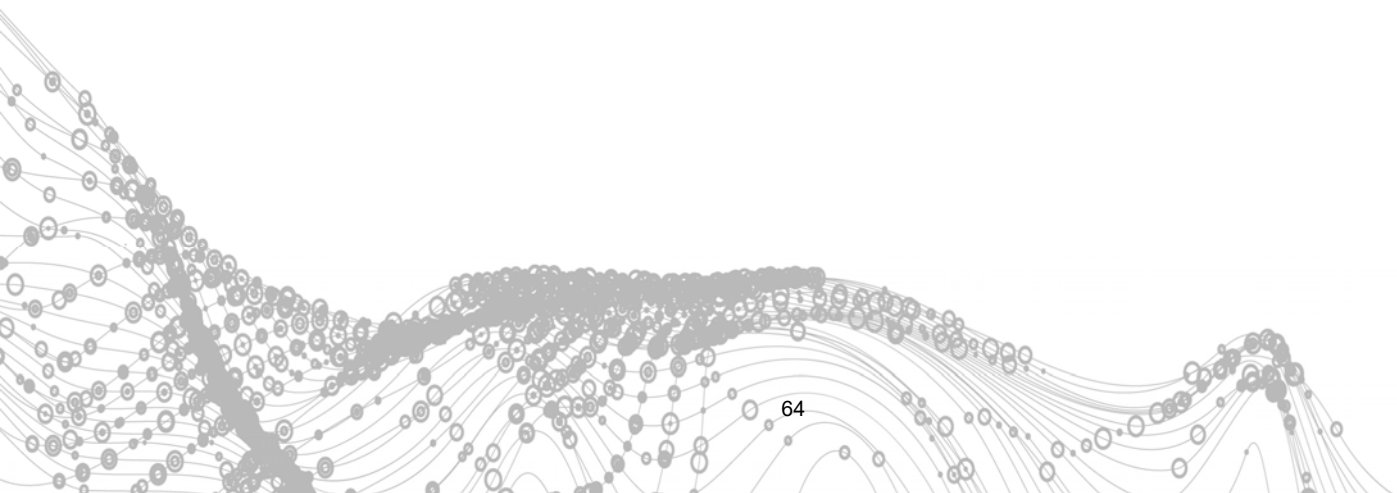
AYMERIC TUAZ-TORCHON

NEW STRUCTURES OF ORGANIC LIGHT-EMITTING DIODES FOR SIGNAGE APPLICATIONS AND DISPLAYS

This thesis concerns the field of HgCdTe infrared detectors for night vision, for which the Infrared Laboratory of CEA -Leti - Minatec is a world leader. The student will participate in the full development of a dual-band detector that simultaneously detects several parts of the infrared spectrum. The active area is a superposition of nanometric layers doped during growth by molecular beam epitaxy, which is then subdivided into photodiode arrays of micrometer size by etching before passivation. Very specific and extremely sensitive investigation techniques, using synchrotron radiation and ion beams will be used to study these structures and determine the local properties of processed materials. In particular, the immediate environment of dopants, local strain generated by etching and atomic

displacements induced by the manufacturing process will be determined.





2017

Annual research report

OPTICS AND PHOTONICS



2017

Annual research report

OPTICS AND PHOTONICS

Contacts

Ludovic POUPINET
Head of the Optics and Photonics division
ludovic.poupinet@cea.fr

Laurent FULBERT
Deputy head of the Optics and Photonics division
Strategy and Programs Management
laurent.fulbert@cea.fr

Alexei TCHELNOKOV
Chief scientist
alexei.tchelnokov@cea.fr



TECHNOLOGY
RESEARCH
INSTITUTE

Commissariat à l'énergie atomique et aux énergies alternatives
Minatec Campus | 17 rue des Martyrs | 38054 Grenoble Cedex 9 | France
www.leti.fr/en

